A study of electron transport processes in cadmium sulphide using the acoustoelectric effect

M. N. Islam

A STUDY OF ELECTRON TRANSPORT PROCESSES IN CADMIUM SULPHIDE USING THE ACOUSTOELECTRIC EFFECT

by

M.N. ISLAM, M.Sc.

Presented in Candidature for the Degree

of Doctor of Philosophy in the University of Durham

MARCH, 1970

ACKNOWLEDGEMENTS

The work recorded in this thesis was carried out under the supervision of Dr. J. Woods and I should like to express my deep gratitude for his inspiration, constant help and encouragement throughout both the course of the research and the preparation of this thesis.

I wish to thank Professor D.A. Wright for permitting the use of his laboratory facilities, the Ministry of Overseas Development, U.K., for financial support and the University of Rajshahi, for granting me leave during the course of this work. I would also like to thank Dr.A.N. Rushby, Dr. K.F. Burr and other members of the group for many useful discussions. The help of the workshop staff headed by Mr. F. Spence in the construction of equipment is gratefully acknowledged. I am also indebted to Mrs. D.M. Armstrong for her careful typing of the manuscript and to Mr. K.M. Elahi for his assistance in drawing the diagrams.

Finally, I wish to thank my wife, Begnm Jamila, for her constant encouragement during my long absence from her and the family.

ABSTRACT

The current saturation associated with the acoustoelectric effect has been investigated in photoconducting crystals of cadmium sulphide. Under normal band gap irradiation the current-voltage characteristic measured under pulsed conditions shows a departure from Ohm's law at a critical field, E_c, of the order of 10^3 v cm^{-1}. The current saturation is associated with the internal generation of acoustic flux which occurs when the electron drift velocity, v_d, exceeds the velocity of sound, v_s, in the crystal. In consequence the critical field for saturation is determined by the drift mobility $\mu_d = v_s/E_c$. The work described in this thesis concerns the measurement of the drift mobility and its relationship to the experimentally determined Hall mobility, μ_H, as a function of conductivity and temperature.

In uniform samples the critical field at room temperature was independent of conductivity over the range 10^{-4} to 10^{-2} $ohm^{-1}cm^{-1}$. The corresponding values of μ_d were all about 300 $cm^2v^{-1}sec^{-1}$ in most of the samples studied and agreed well with the measured values of the Hall mobility. With non-uniform samples, however, the critical field varied strongly with the intensity of incident illumination.

Under saturated conditions potential probe measurements on uniform samples revealed the presence of a stationary high field domain near the positive electrode.

By measuring the drift and Hall mobilities over a range of temperature from 100 to 300^{o}K, the effect of traps on the saturation has been demonstrated. Trapped electrons can participate in piezoelectric bunching provided the trapping time is short compared with the period of the acoustoelectrically amplified waves. Only the shallow traps satisfy this criterion. The work reported here shows that two such traps with ionisation energies of 0·015 eV and 0·037 eV were operative in the sample studied. The capture cross section of the shallower trap was estimated to be about 6×10^{-16} cm^{2}.

Finally the current saturation method has been extended to observe the acoustoelectric interaction of holes in cadmium sulphide under infra-red quenching conditions, and a value of the hole mobility of 48 cm^{2} v^{-1} sec^{-1} has been determined.

INTRODUCTION

Cadmium sulphide is a material which has many interesting properties and which has been studied extensively in connection with the phenomena of photoconductivity and piezoelectricity.

The possible applications of CdS are also numerous and varied. The high photosensitivities that can be achieved make the material suitable for use in commercial photocells and as a very sensitive detector of electromagnetic radiation. Other possible devices based on photoconductive layers include television camera tubes, electrostatic photocopiers, light amplifiers and solar batteries.

Ultrasonic amplification is possible in CdS because the material is photoconductive as well as piezoelectric. Ultrasonic amplification was first discovered in 1961, and this was followed quite recently by the construction of an acoustoelectric oscillator. Further attention has been directed to other possible ultrasonic applications e.g. high frequency transducers, delay lines, etc.

Before a material can find wide-scale application it is usually necessary for its preparation and properties to be understood so that it can be prepared in a reproducible manner. As with all II-VI compounds, cadmium sulphide is difficult to control and although reasonable crystals can be grown their properties are not properly

understood. Thus departure from stoichiometry and the presence of impurities can have profound effects on the electrical and optical properties. A measure of the free carrier mobility is often taken as a criterion of the purity and perfection of a material. The work to be described in this thesis is concerned with the measurements of Hall and drift mobilities in CdS. The drift mobility can be determined from the current saturation which occurs when the applied voltage is approximately 10^3 v/cm. This deviation from Ohm's law is associated with the acoustoelectric effect which is caused by electron-phonon interaction in a piezoelectric photoconductor. McFee has shown that current saturation occurs when the drift velocity of electrons is equal to the velocity of sound in the crystal. The principal quantitative measurement that can be made from I-V curve is that of the drift mobility.

In order to provide a reasonable background against which to consider the results of the various measurements reported in this thesis, some general properties of cadmium sulphide are discussed in Chaper I. Following a brief review of the general and electrical properties in Part A, the effects of defect levels on the optical properties of insulating cadmium sulphide crystals are discussed in Part B.

Chapter II, Part A, provides a brief introduction to the acousto-electric effect, acoustic wave amplification and the effect of traps

on acoustoelectric interaction. This is followed in Part B by a discussion of the phenomena (all acoustoelectric in origin) arising from ultrasonic amplification such as current saturation, current oscillations and high field domain formation. Finally an acoustoelectric oscillator as an active device is described.

The methods of growing single crystals of CdS and the preparation of the samples are described in Part A, Chapter III, while the apparatus which was designed and built for the experimental investigation of the drift and Hall mobilities is described in Part B.

Chapter IV is concerned with some typical room temperature results on current saturation and current oscillation in uniform as well as non-uniform samples. The experimental results on the drift and Hall mobilities are reported for samples of different orientations. The photo Hall effect has been used to estimate the parameters of the active traps in one of the samples.

The investigation of current saturation, and the drift and Hall mobilities at different temperatures is presented in Chapter V. From the theory of the trap controlled acoustoelectric interaction at low temperature the operative traps and their trapping parameters have been estimated.

Finally in Chapter VI, the saturation method has been extended to observe the acoustoelectric interaction with holes under infra-red quenching conditions when the free hole concentration can exceed the free electron concentration.

CONTENTS

PART B PHOTOCONDUCTIVE PROPERTIES OF CADMIUM SULPHIDE

CHAPTER I

CADMIUM SULPHIDE AND ITS PROPERTIES

PART A

1.1 Crystal Structure and Piezoelectricity

Cadmium sulphide can crystallise in two possible tetrahedrally co-ordinated structures.[1,2] The phase in which we are interested is α-CdS with the Wurtzite structure. This may be thoughtof as CdS_4 or SCd_4 tetrahedra stacked in a close packed hexagonal structure. In this arrangement each cadmium ion is bonded to four sulphur ions, one at each corner of a tetrahedron. Similarly, each sulphur ion is bonded to four cadmium ions which lie at the corners of a tetrahedron. The interatomic distance between a cadmium atom and its nearest sulphur neighbours is 2·52Å. The lattice parameters are a = 4·137A and c = 6·716Å[3].

The Wurtzite structure of CdS is illustrated in Figure 1.1a. The lack of inversion symmetry is apparent from Figure 1.1b. The opposite directions of the hexagonal axis are obviously not equivalent. A compressive strain along the hexagonal axis will therefore cause the centres of positive and negative charge in each tetrahedron to move apart along the hexagonal axis. In this way it is seen that a longitudinal strain wave propagating down the hexagonal axis will produce a longitudinal piezoelectric field.

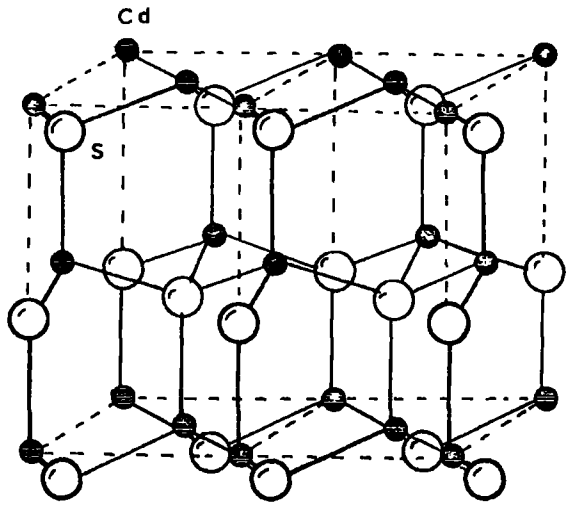

(a)

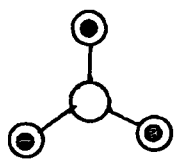

(b)

Fig.1.1. (a) The arrangement of cadmium and sulphur atoms in Wurtzite hexagonal form of CdS.

(b) CdS looking along hexagonal axis.

1.2 Band Structure, Energy Bands and Effective Mass

The conduction band of cadmium sulphide originates from the 5s atomic levels of the cadmium ions. The valence band is split into four sub-bands. The lowest band arises from the s-orbitals of the sulphur ions. The crystal field splitting of the 3p orbitals gives rise to the other two bands, the higher of which is further split into two closely spaced bands, by spin-orbit coupling. Birman[4] has given a picture of the position of the extrema of the valence and conduction bands at K = 0,0,0, which is illustrated in Figure 1.2a.

The separation of various energy bands in CdS at $4{\cdot}2^{o}K$ are shown in Figure 1.2b following Thomas and Hopfield.[5] They provided experimental evidence for the validity of this model (Figure 1.2b) from their measurements of the reflectivity and fluorescent spectra of hexagonal CdS. The band gap at $4{\cdot}2^{o}K$ is shown to be 2·582 eV.

Hopfield and Thomas[6] determined an electron effective mass value $m^{*} = (0{\cdot}204 \pm 0{\cdot}01)m_{e}$, from a study of the exciton absorption and reflection spectra of CdS. Piper and Marple[7] investigated the anisotropy of the absorption due to free carriers in the infrared and concluded that $m^{*}_{11}/m^{*}_{33} = 1{\cdot}080 \pm 0{\cdot}05$. Boer and Dexter[8] measured the anisotropy of the effective mass using a cyclotron resonance technique and found $m^{*}_{11}/m^{*}_{33} = 1{\cdot}12$.

Hopfield and Thomas[6] obtained the value of the effective mass of holes in the valence band as

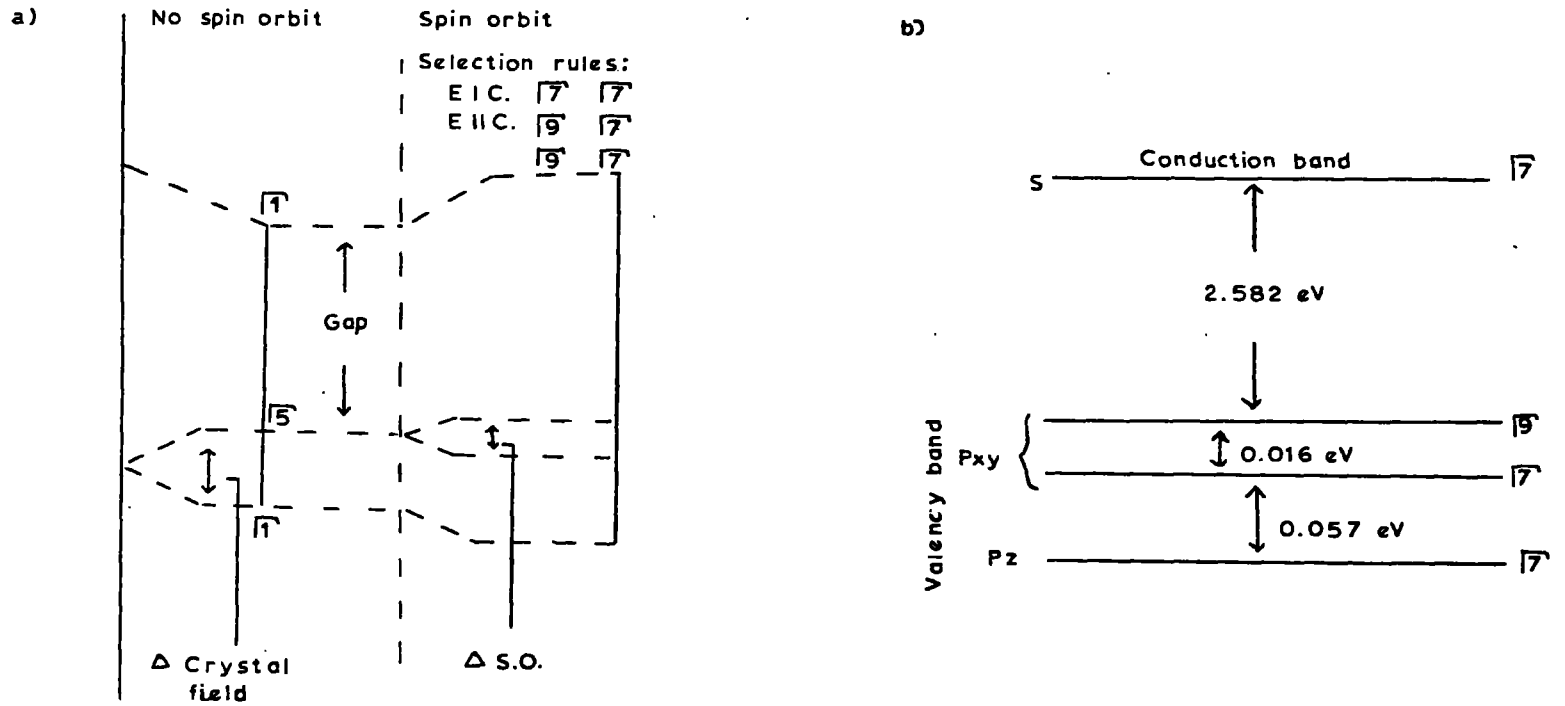

Fig.1.2. (a) Band structure and selection rules for the Wurtzite structures at K=0,0,0. The crystal field and spin orbit splitting are shown schematically. (Birman)[4].

(b) Energy bands for CdS at K=0,0,0 at 4·2°K (Thomas and Hopfield).[27]

$$m_h^* \;||\text{c-axis} = (5 \pm 0{\cdot}5)m_e$$

$$\text{and } m_h^* \perp \text{c-axis} = (0{\cdot}7 \pm 0{\cdot}1)m_e$$

1.3 Electrical Conductivity

In cadmium sulphide which is always found to be n-type, the conductivity can be expressed as $\sigma = nq\mu$ where n is the density and μ the mobility of electrons.

At room temperature single crystals of CdS can have values of resistivity which vary by more than ten orders of magnitude, from 10^{12} to 10^{-1} ohm-cm, depending upon the deviation from stoichiometry and the purity of the samples. With large band gap materials like CdS, the density of electrons in thermal equilibrium will be determined by the impurity content of the sample and by the activation energies of the impurities.

Because of the high photoconductive sensitivity, the electron concentration and hence the conductivity can be varied by several orders of magnitude with photo-excitation. The mechanism of the photoconductive effect is discussed later in this chapter.

1.4 Carrier Mobility and Scattering Processes

The mobility of a current carrier can be defined in such a way that $\sigma = nq\mu$ and $\mu = q\tau/m^*$, τ is the relaxation or mean free time between

collisions. The mobility in fact describes the contribution of the crystal lattice to the conductivity, since n can be variable, but τ and m* depend upon the properties of the crystal.

The processes that can scatter carriers and therefore affect the mobility, include:

a) thermal lattice vibrations,

b) ionised and neutral impurities,

c) imperfections: dislocations, grain boundaries, etc.,

d) other carriers.

a) Lattice Scattering:

(i) Deformation Potential Scattering -

Electrons or holes can be scattered by the deformation potential associated with the longitudinal acoustic lattice vibrations. The deformation potential is proportional to the lattice dilation.

The effective mass method extended to apply to gradual shifts in the energy bands resulting from the deformation of the crystal lattice, is used to estimate the interaction between electrons of thermal energy and the acoustic modes of the lattice vibrations. Calculations by Bardeen and Shockley[9] show that the mobility is given by

$$\mu_a = \left\{ (8\pi)^{\frac{1}{2}}.h^4 \, C_{ii}/(3\epsilon_1^2 \, m^{*5/2} \epsilon^{3/2}) \right\} T^{-3/2} \qquad 1.1$$

where C_{ii} is the average longitudinal elastic constant and ϵ_1 is the

shift of the edge of the conduction band per unit dilation.

(ii) Piezoelectric Scattering -

Piezoelectric scattering arises from the interaction between electrons and the acoustical lattice vibrations via the piezoelectric polarisation field. Piezoelectric scattering can occur only in crystals showing a piezoelectric effect. Hutson[10] writes the piezoelectric mobility as

$$\mu_p = 1{\cdot}44\ k\ (m/m^*)^{3/2}(300/T)^{1/2}\left\{ \Sigma_{mode}(K^2)_{av} \right\}^{-1}$$

$$= A\ (m_e/m^*)^{3/2}(300/T)^{-1/2}\ cm^2/v.sec. \qquad 1.2$$

where A is a constant, which is determined by the piezoelectric and the dielectric constants ($\sim 4{\cdot}10^2$ for CdS). K is the electromechanical coupling factor, and $K = e^2/k\epsilon_o c$, where e is an appropriate piezoelectric constant and c is the appropriate stiffness coefficient.

(iii) Optical Mode Scattering -

The electrons are scattered by the electric potential associated with the polarisation associated with the lattice displacement due to the longitudinal optical phonons. The mobility limited by optical mode scattering according to Frohlich[11] can be written as

$$\mu_o = (16{\cdot}91/\theta^{1/2})(1/n^2 - 1/\epsilon)^{-1}(m_e/m^*)^{3/2} \times (e^{\theta/T} - 1)\ cm^2/v.sec. \qquad 1.3$$

where ϵ is the dielectric constant, n is the optical index of refraction, and θ is the characteristic temperature for longitudinal optical phonons.

b) Impurity Scattering

(i) Ionised Impurities -

When the concentrations of ionised donors or acceptors are high, the electrons suffer Rutherford scattering due to the presence of ions. According to Conwell and Weisskopf[12] the magnitude of the mobility determined by this process is

$$\mu_i = \frac{3{\cdot}2\ 10^{23}\ x^2}{N_i\ \ln(1 + x^2)}\ T^{3/2} \quad cm^2/v.sec. \qquad 1.4$$

where $x = 1{\cdot}8 \times 10^5 / N_i^{1/3}$; N_i is the number of ionised impurities per cubic meter

(ii) Neutral impurities -

Neutral impurity scattering is relatively unimportant and is found to be almost independent of temperature. Erginsoy[13] has calculated the mobility associated with this type of scattering alone and finds

$$\mu_n = \frac{m^* q^3}{20\ N_n \epsilon \hbar^3} \qquad 1.5$$

where N_n is the density of neutral impurities and ϵ is the dielectric constant.

c) Scattering at Dislocations and Grain Boundaries

The scattering caused by low densities of these defects is relatively unimportant. Dexter and Seitz[14] have concluded that, if the dislocation density were as high as $10^8/cm^2$, the effect on mobility should be apparent, and with a density of $10^{11}/cm^2$ dislocation scattering should be comparable to lattice scattering at room temperature. Read[15] has considered the effect of charged dislocations and finds a linear variation of mobility with temperature.

d) Carrier-Carrier Scattering

The scattering of charge carriers by other carriers is difficult to analyse because of the screening effects that occur at the high current densities at which this process is important. When the effective mass of holes is larger than that of electrons, electron-hole collisions can reduce the electron mobility. Electron-electron collisions are more complex; but can generally be neglected.

1.5 Hall Effect

The measurement of the Hall coefficient provides one of the best and most widely used methods of determining the intrinsic mobilities of the charge carriers in solids.[16] Measurements of the Hall voltage and electrical conductivity enable the values of the carrier density, n, and the mobility μ, to be determined and indicate whether electrons or holes are the dominant charge carriers.

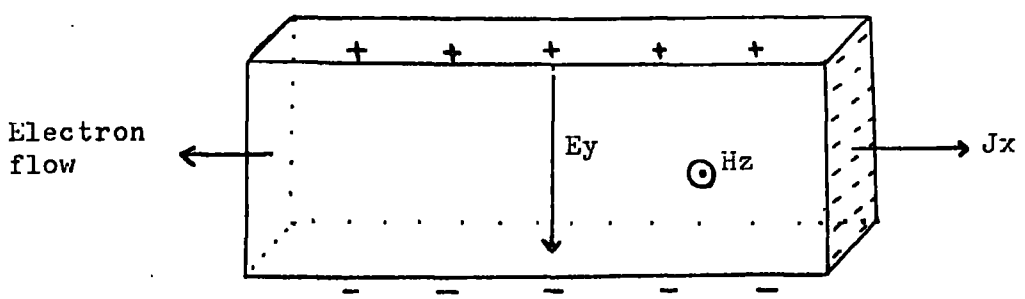

Fig. 1.3. The geometry of the Hall effect experiment.

Consider a rod shaped specimen in a longitudinal electric field E_x and a transverse magnetic field H_z as in Fig.1.3. An electron moving with a velocity v_x is subjected to a downward thrust from the Lorentz force qv_xH_z. In the steady state, a transverse electric field E_y is generated which balances the Lorentz force. Under these conditions

$$qE_y = qv_xH_z \qquad 1.6$$

Expressing v_x in terms of current density $J_x = nqv_x$

$$E_y = -\frac{J_xH_z}{nq} = R_H J_xH_z \qquad 1.7$$

This transverse electric field E_y is known as Hall field. The quantity

$$R_H = \frac{E_y}{J_xH_z} \qquad 1.8$$

is called the Hall Constant. Since $J_n = nq_xv_x$

$$R_H = -1/nq \qquad 1.9$$

and is negative for electrons. A measure of R_H is a measure of the carrier concentration n. This simple value of $R_H = 1/nq$ follows from the assumption that all relaxation times are equal, independent of the velocity of electron. A numerical factor of order of unity enters if the relaxation time is a function of velocity.

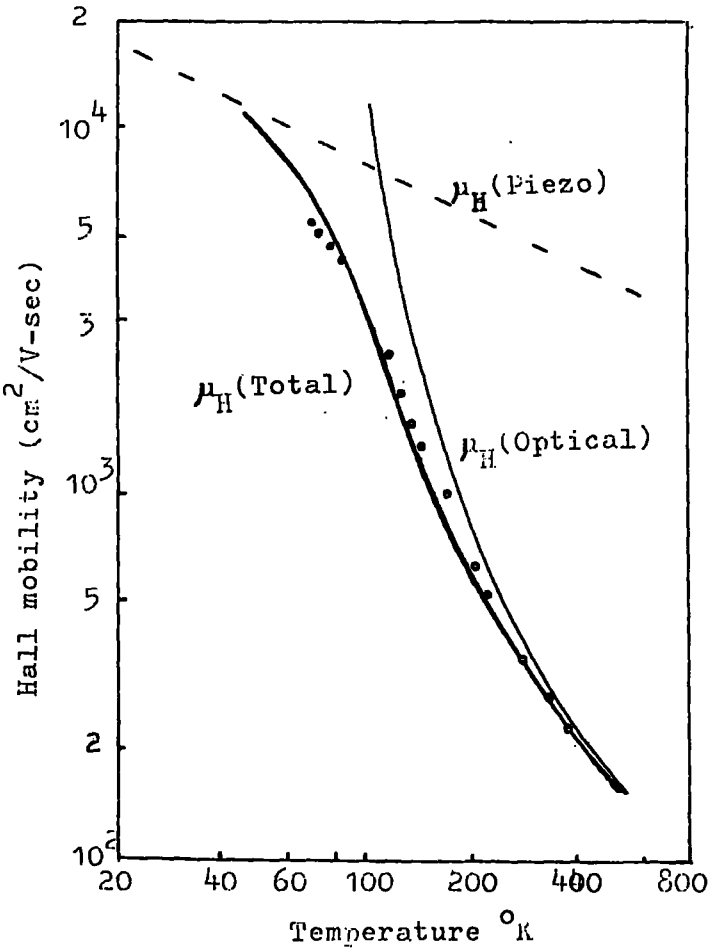

Fig. 1.4. The temperature dependence of the Hall mobility in undoped n-type CdS. (Devlin).[1]

Hall mobility in cadmium sulphide

The electron mobility in cadmium sulphide is found to depend strongly upon the purity of the sample, so that higher and higher values of mobility are continually being quoted, as it becomes possible to produce purer speciments.

The temperature dependence of the Hall mobility ($R_H \sigma$) in undoped n-type CdS is shown in Fig.1.4.[17] The solid curve is the theoretical intrinsic Hall mobility due to piezoelectric and optical mode scattering. In calculating the effect of the two simultaneous scattering mechanisms ($\mu_L^{-1} = \mu_{opt}^{-1} + \mu_{piez}^{-1}$) Devlin[17] took into account the temperature dependence of the static dielectric constant which affects the optical mode scattering (Eqn.1.3) somewhat. He found that a value of m^*/m = 0•2 fitted his data best.

Fujita et al[18] measured the Hall mobility in CdS under pulsed illumination conditions. Their results show no trace of impurity scattering and agreed well with the predicted combined effects of piezoelectric scattering and optical mode scattering. The absence of impurity scattering might be due to the neutralisation of the compensated acceptors by the trapped holes.[18]

PART B

PHOTOCONDUCTIVE PROPERTIES OF CADMIUM SULPHIDE

1.6 Photoconductivity in CdS

Cadmium sulphide is an extremely sensitive photoconductor. The current flowing through a crystal can be increased by a factor of about 10^6 under illumination with light of 1 ft. candle intensity.

The direct effect of illumination is to increase the number of mobile charge carriers in the crystal. If the energy of the incident photon is higher than the energy gap Eg, then each photon absorbed in the crystal will produce a free electron-hole pair.

In highly photosensitive II-VI compounds like CdS electrons are the majority contributors to the photoconductivity. Although electrons and holes are created by absorption of radiation, the holes are rapidly captured at sites where recombination with free electrons occurs at a later time.

1.7 Spectral response

With a pure photoconducting crystal, the dependence of photoconductivity on wavelength will be very similar to the dependence of absorption on wavelength at least on the low energy side of the band gap. Figure 1.5 shows typical absorption spectra (a) and excitation spectra (b) for photosensitive CdS crystals. When the spectral

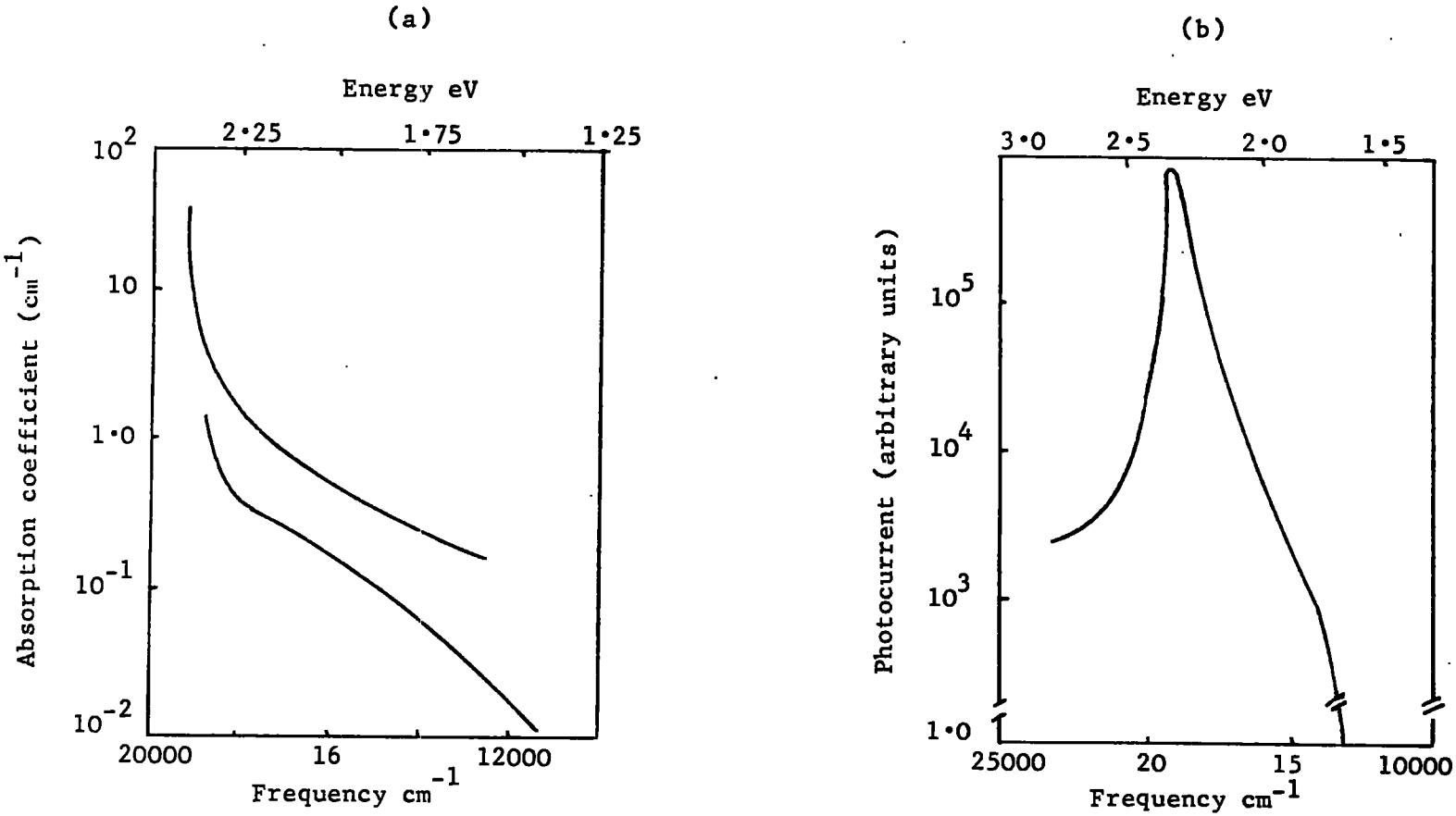

Fig.1.5. (a) typical absorption spectra of CdS at room temperature.
(b) typical excitation spectra of CdS at room temperature (after Balkanski).[19]

response of photoconductivity (Fig.1.5b) is measured[19], it is found that the sensitivity is very high in a narrow region of wavelength near the absorption edge. At shorter wavelengths the sensitivity drops to a constant value smaller than the peak by a few orders of magnitude and at longer wavelengths the sensitivity decreases rapidly to negligible values as the energy of the photons becomes much smaller than the band gap ($\sim$2·4 eV).

The reason for the decrease in photosensitivity with photon energies higher than the band gap is attributed to the difference between surface sensitivity, (the important feature for these highly absorbed photons), and volume sensitivity, (the important feature for the longer wavelength photons which penetrate most of the crystal thickness).

1.8 Free Carrier life-time

The change in conductivity, $\Delta\sigma$, produced by photoexcitation in n-type CdS can be written

$$\Delta\sigma = q\mu\partial n + nq\partial\mu \qquad 1.10$$

the second term on the right of the equation arises from the change in mobility with level of photoexcitation (discussed in section 1.14c). The change in the carrier density ∂n, can be expressed as

$$\partial n = g\tau \qquad 1.11$$

g is the rate of excitation per unit volume and τ is the free electron life time. Substitution of eqn. 1.11 into 1.10 yields (neglecting $\partial\mu$)

$$\Delta\sigma = qg\mu\tau \qquad 1.12$$

The product of the mobility μ and majority carrier lifetime τ, eqn. 1.12, can be regarded as the 'figure of merit' for photosensitivity. It is essentially a material parameter. Since the mobility varies only slightly, whereas the lifetime may vary by many orders of magnitude the majority carrier lifetime is essentially the key parameter for photoconductivity. In pure and perfect CdS crystals, the electron and hole lifetimes are comparable and lie in the range from 10^{-6} to 10^{-8} sec. Such a crystal would be an insensitive photoconductor. However it is possible to change the electron lifetime to 10^{-2} to 10^{-3} sec. and reduce the hole lifetime to less than 10^{-8} sec. by incorporating suitable imperfection centres into the crystal.

1.9 Imperfections in CdS

The general pattern for imperfection behaviour in CdS is that group III and group VII impurities and anion vacancies act as donors, while group I and group V impurities and cation vacancies act as acceptors.

From the measurement of the self diffusion of cadmium in CdS Woodbury[20] proposed that in a pure crystalline material, the sulphur vacancy and cadmium vacancy are the primary defects (Schottky defects). Recently Orr et al[23] have concluded from a study of edge emission in CdS that crystals grown in high pressures of sulphur vapour contain a high concentration of cadmium vacancies (acceptors); and that the

acceptors are automatically compensated by the simultaneous introduction of shallow donors (probably sulphur vacancies) and hence the crystals were always found to be n-type and a p-type sample could not be produced.

1.10 Impurity effects

Many of the potentially important electrical and optical properties of CdS are associated with the presence of impurities and imperfections. The introduction of imperfections may affect one or more of the following properties of the crystal:

a) Photosensitivity - Imperfections which act as recmobination centres decrease the sensitivity. Imperfections which have a high probability of capturing a minority carrier with subsequent small probability of capturing a majority carrier, may increase the majority carrier life-time and hence the sensitivity.

b) Speed of response - Imperfections which act as trapping centres can influence the photoconductive speed of response. The speed of response decreases when imperfections trap the free carriers, since the thermal process is a slow process. Trapped carriers may also reduce the carrier mobility by introducing charged impurity scattering.

c) Spectral response - Since direct excitation from an imperfection centre with a level lying in the forbidden gap requires less energy than excitation across the band gap, the spectral response may be extended to longer wavelengths.

d) Luminescence Emission Spectra - The impurities may provide additional recombination paths. If the recombination is radiative the emission of photons with energies less than the band gap becomes possible via recombination centres with levels in the forbidden gap.

e) Dark conductivity - Donor imperfections increase the conductivity and acceptors decrease it because all cadmium sulphide presently available is n-type.

1.11 Fermi and Demarcation levels

With the crystal under excitation the distance of the steady state electron Fermi level from the conduction band may be calculated from the conductivity and temperature according to the equation

$$E_{fn} = kT \ln \frac{N_c q \mu}{\sigma} \qquad 1.13$$

where T is the absolute temperature, N_c is the effective density of states in the conduction band, and σ is the conductivity. A similar hole Fermi level can be defined in terms of the concentration of free holes.

A defect with a level lying in the forbidden gap can act both as a trap and a recombination centre. The extent to which it acts in one capacity or the other depends on the position of the steady state Fermi levels. Whether a defect acts predominantly as a trap or as a recombination centre depends on the position of its energy level relative to the so called 'demarcation' level rather than the steady state Fermi level.

An electron in a defect level at the electron demarcation level has equal probability of being thermally excited into the conduction band and of recombining with a hole in the filled band. A hole at the hole demarcation level has equal probabilities of being thermally excited into the filled band and of recombining with an electron in the conduction band.

The demarcation level is displaced from the corresponding Fermi level by an energy difference which is usually small. The following expressions relate the demarcation levels with the steady state Fermi levels (E_{fn}, E_{fp})

$$E_{dn} = E_{fn} + kT \ln (N_p/N_n) \qquad 1.14$$

$$E_{dp} = E_{fp} - kT \ln (N_p/N_n) \qquad 1.15$$

where N_p is the density of recombination centres for electrons, i.e. the density of recombination centres which have captured a hole, and N_n is the density of recombination centres for holes.

1.12 Sensitizing Centres

Three important phenomena which occur in photoconducting CdS are discussed in the following section. These are a) impurity sensitization - the increase in photosensitivity produced by the incorporation of impurities; b) superlinear photoconductivity - the increase in photo current with a power of light intensity greater than unity; and c)

infrared quenching of photoconductivity - the reduction in photo current with secondary infrared radiation.

In order to explain these effects it is necessary to postulate that there are two different classes of recombination centres with levels distributed throughout the forbidden gap.[21] They have the following properties:

i) Class I centres have a capture cross section for holes equal to or less than that of class II centres for holes.

ii) Class I centres have a capture cross section for electrons many times (10^5) greater than that of class II centres, once a hole has been captured.

iii) Class II centres are filled with electrons in the dark.

An insensitive photoconductor contains only class I centres. It can be converted into a 'sensitive' conductor by the incorporation of class II centres called sensitizing centres.

Sensitizing centres are expected to be associated with intrinsic crystal defects. The simplest type of crystal defect with the required properties is a compensated cation vacancy or a cation vacancy-impurity complex, either without any trapped holes (doubly negatively charged) or with one trapped hole (singly negatively charged).

a) Impurity Sensitization

The process of sensitization is illustrated in Fig.1.6. The crystal is in a desensitized state when only class I centres are able to function

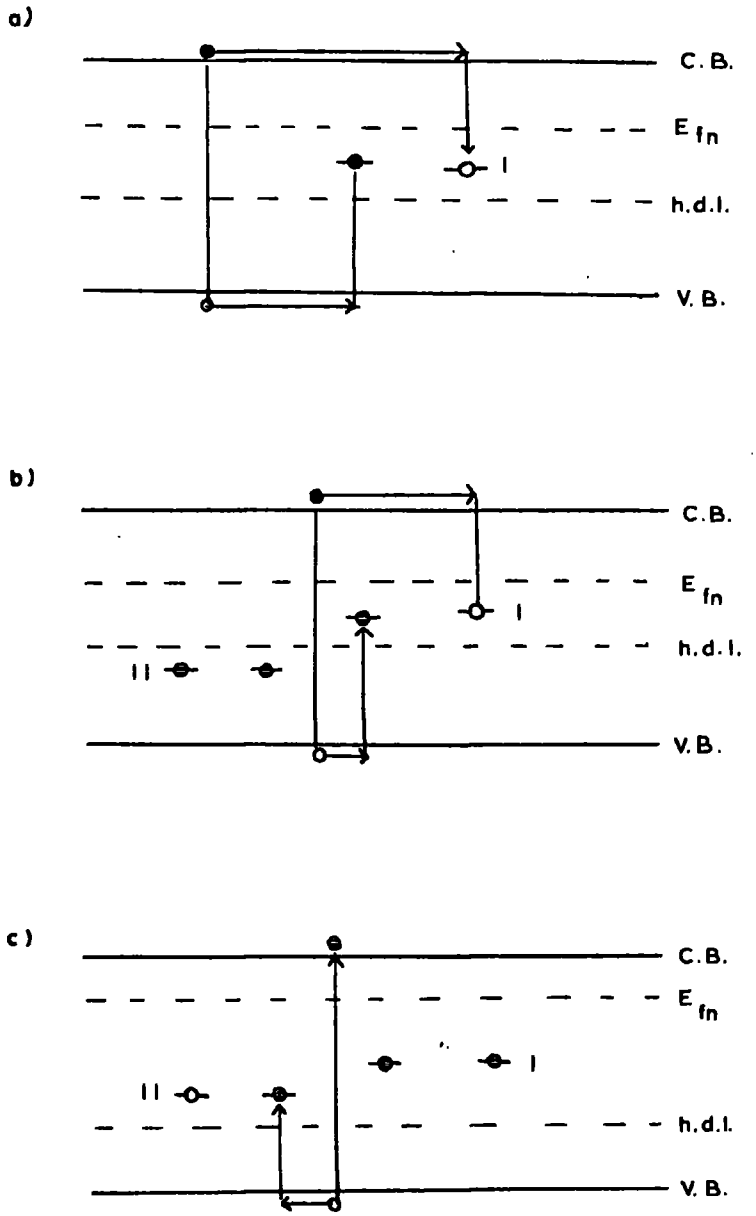

Fig.1.6. Sensitizing process (a) unsensitized (b) sensitizing centres added (c) sensitized and illuminated.

as recombination centres. This is the case in a 'pure' insensitive material, shown in Fig.1.6a, where the presence of the centre I leads to a small majority carrier lifetime for electrons.

If sensitizing centres of type II are added, no effect on the life time is found, as shown in Fig.1.6b, as long as the centres lie below the hole demarcation level. This is the case at high temperatures and/or low light intensities. The centres simply act as hole traps and do not significantly affect the photoconductive gain.

The crystal becomes sensitized as class II centres, are able to function as recombination centres following a shift in the demarcation level. At low temperatures and/or high light intensities the sensitizing centres lie above the hole demarcation level (Fig.1.6c). In these situations holes captured by the sensitizing centres remain there longer before recombination than holes captured by class I centres, because of the small capture cross section of class II centres containing holes for free electrons. As a result, the class II centres become occupied primarily by holes, and if the concentrations of class I and class II centres are much larger than the density of free carriers, the electrons initially in the class II centres will be effectively transferred to the class I centres. Free electrons can then essentially only recombine with holes at centres which have a small capture cross section for electrons. Consequently the lifetime of the electrons is increased and the crystal becomes highly photosensitive.

b) Superlinear Photoconductivity

Samples containing class II centres show a variation of photocurrent with light intensity which is more rapid than linear over a limited range of light intensities. This is referred to as superlinearity.

The occurrence of superlinearity can be thought of in terms of the following model. Consider the case illustrated in Fig.1.6b. When the intensity of illumination is increased, at a constant temperature, the hole demarcation level moves downwards towards the top of the valence band, and as it passes through the class II level these centres become occupied by holes and sensitization occurs. The sharp increase in lifetime of the free electrons which accompanies this sensitization results in the superlinearity of the measured photocurrent. Superlinearity ends when the sensitization process is essentially complete, i.e. when the transfer of holes from the class I to the class II centres is finished.

c) Quenching of Photoconductivity

(i) Thermal quenching - if the temperature of the crystal is raised, while a constant intensity of illumination is maintained, then above a certain temperature the photocurrent rapidly decreases by several orders of magnitude. The threshold for this effect of thermal quenching occurs at progressively higher temperatures as the light intensity is increased.

When the temperature is increased, the hole demarcation level moves towards the centre of the band gap and quenching occurs when the hole demarcation level passes through the class II levels. The centres then effectively come into thermal equilibrium with the valence band and begin to behave as hole traps.

(ii) Infrared quenching - The phenomenon of infrared quenching of the photocurrent is often observed when a photoconductor in the sensitized state is illuminated with secondary radiation in the infrared range (0·8 - 1·8 μm).

In the temperature range below that at which thermal quenching of the photoconductivity sets in infrared quenching of photoconductivity can be caused by the optical freeing of holes.

The mechanism of infrared quenching is illustrated in Fig.1.7. When the electron hole pairs are created by band gap radiation (Fig.1.7a) the photoexcited holes are rapidly captured by the sensitizing centres (Fig.1.7b) because of their large capture cross section for holes.

Optical quenching of photoconductivity occurs:

1. When infrared radiation excites captured holes from the class II centres into the valence band. The resultant free holes in the valance band are then captured by class I centres (Fig.1.7c) with a larger subsequent capture cross-section for free electrons.

2. When infrared radiation excites a captured photoexcited hole from the upper level to the lower level of the sensitizing centres, and this hole is then released thermally to the valence band.

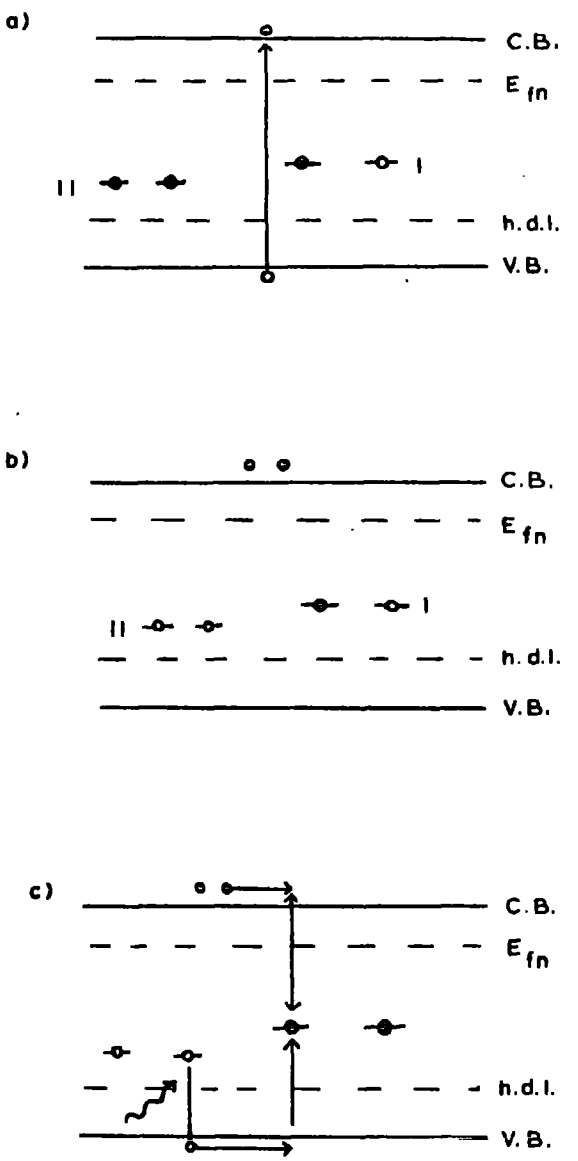

Fig.1.7. Infra-red quenching.

(a) Band to band radiation creates electron-hole pairs

(b) hole captured by sensitizing centres leaving electrons free to give photoconductivity

(c) hole released by infra-red radiation to recombine with and hence remove free electrons, thereby quenching the photoconductivity.

1.13 Recombination Processes

a) Edge emission

The excitation event which leads to the change in conductivity is terminated by the recombination of the photoexcited electrons and holes. In CdS, although direct recombination between free electrons and holes is possible for high carrier densities, it is recombination through an imperfection which always dominates.

The term edge emission is generally employed to refer to the radiative recombination processes which lead to the emission of photons with energies within several tenths of an electron volt of the band gap. In general an edge emission process is observed as a set of lines or bands separated by equal energy increments.

The edge emission of cadmium sulphide excited by mercury radiation (3650Å) at liquid helium temperatures consists of two regions described as the 'green' and 'blue' emissions.[22] The green emission contains a series of overlapping bands, the maxima of which are equally spaced by some 300 cm^{-1} (0·033 eV). ~~apart~~. A typical example of the emission distribution of the photoluminescence of a CdS crystal is shown in Fig.1.8.[23] The green emission can contain two phonon assisted series. The higher energy series has its zero order phonon component centred on 5140Å. The lower energy series has its zero order component located at 5170Å. The series have been estimated as being associated with recombination which occurs with the co-operation of 0,1,2 ....n longitudinal optical phonons.[22]

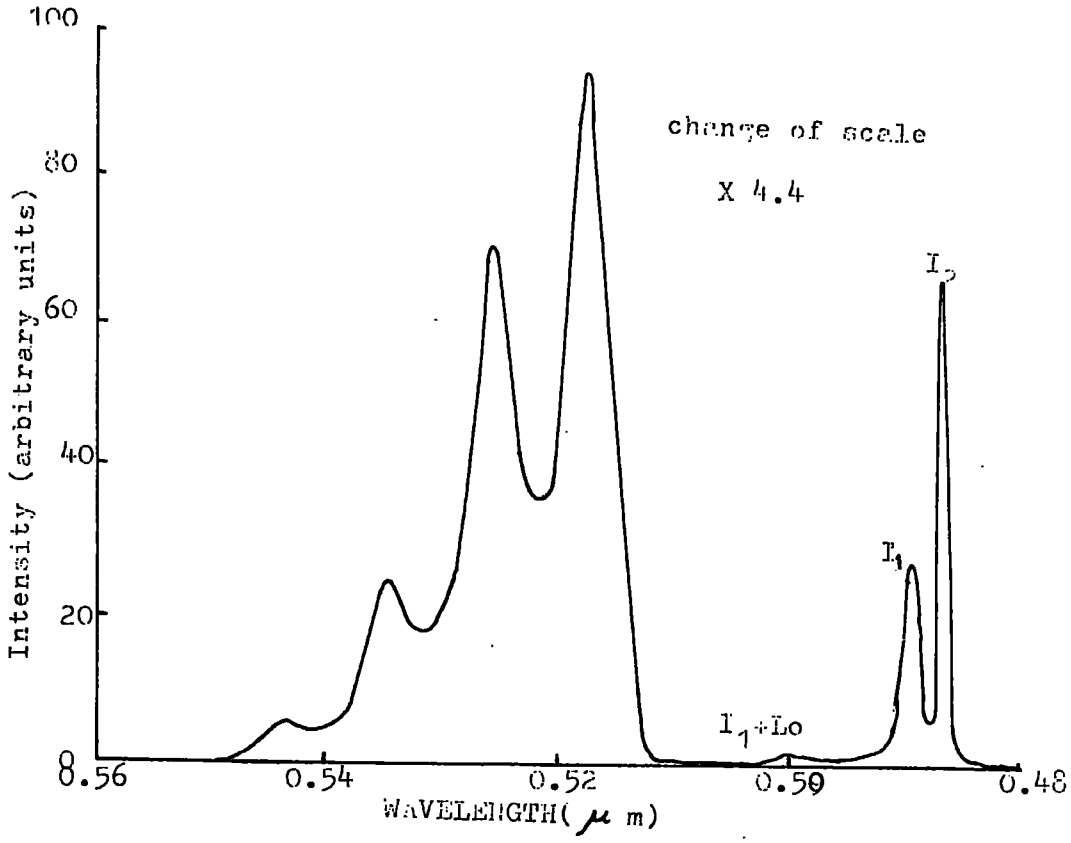

Fig. 1.8. The spectral distribution of the photoluminescence of a CdS crystal grown at 1125°c under a high partial pressure of sulphur Ts= 450°c. (After ORR et al).

Thomas and Hopfield[24] have indicated that the low energy green emission process which is dominant at $4^{o}K$ is associated with the recombination of bound electrons and bound holes. The high energy series which is dominant at higher temperature ($77^{o}K$) was assigned to recombination between free electrons and holes trapped at an acceptor level. Pedrotti and Reynolds[25] confirmed this explanation[24] by studying the spectral position and intensity of the emission as the temperature was changed from $4{\cdot}2^{o}K$ to $77^{o}K$.

Thomas and Hopfield[26,27] have ascribed the blue emission to the recombination of excitons bound to various crystal defects.

Recently Orr et al[23] have measured the green and blue emission at liquid helium temperatures for a number of CdS crystals grown in this department[28] under controlled partial pressures of cadmium and sulphur. Orr et al have concluded that the I_1 and I_2 bound exciton lines which dominate the blue emission are associated with exciton recombination at neutral acceptors (cadmium vacancies) and neutral donors (sulphur vacancies) respectively . The two phonon assisted series which constitute the green emission give an indication of the relative concentration of the same donors and acceptors which are involved in the blue emission.[23]

b) Infrared emission

The edge emission is associated with levels close to the band edges. However, luminescence processes involving levels in the middle of the

forbidden gap can occur and give rise to infrared emission.

In a study of the emission spectra Browne[29] observed banded emission in the range 1·5 to 2·3 μm with three bands centred at 1·65, 1·85 and 2·05 μm in copper doped CdS at 80°K. Bryant and Cox[31] have observed 0·78 μm and 1·06 μm infrared emission bands in undoped and copper-doped cadmium sulphide powders at 90°K.

Potter et al[30] tried to account for the corresponding excitation spectra in terms of two levels which they ascribed to the ground and first excited state of a hole bound to uncompensated, substitutional copper acceptor impurity.

Bryant and Cox[31] proposed a different model for the infrared luminescence and absorption. They consider that substitutional copper gives rise to a single level within the band gap. The infrared emission and excitation observed by them at 90°K was attributed to electronic transitions between a single level, and the various branches of the valence band. They were able to explain their results and most of the other published work with this model.

1.14 Detection of Traps in CdS

There are at least six to eight different trapping levels which are prominent in CdS crystals. This has been demonstrated by Nicholas and Woods.[32] The density, and in some cases even the existence, of some of the traps is determined by the preparative conditions, physical history and possibly photochemical reactions which may occur, see Woods et al.[33]

The following measurements are useful,in providing information about trapping:

a) Variation of response time with light intensity

One major effect of trapping is to make the experimentally observed decay time of the photocurrent much larger than the free carrier lifetime. If no trapping centres are present, then the observed photocurrent will decay in the same way as the free carrier concentration, and the observed decay time will be equal to the carrier lifetime. If trapping centres are present and the density of free carriers is comparable or less than the density of trapped carriers, the thermal freeing of trapped carriers during the course of the decay can sustain the free carrier concentration so that the observed decay time becomes longer than the lifetime of a free carrier.

Any analysis of experimental response curves requires an appropriate model. The simplest model assumes a single trapping level for which retrapping either is or is not important. The decay of photoconductivity is exponential for a model with a single trap level without retrapping. Using this model Nicholas and Woods[32] examined up to six discrete sets of traps in CdS with trap depths ranging from 0·05 eV to 0·83 eV below the conduction band.

b) Thermally stimulated current (TSC)

An important method of detecting and studying trapping in CdS is that of measuring the thermally stimulated current (TSC).

To make TSC measurements the crystal is cooled to liquid nitrogen tenperatures and exposed to illumination which will excite the crystal homogeneously. The radiation is then removed, and the crystal heated at a linear rate in the dark. The magnitude of the thermally stimulated current is proportional to the rate of trap emptying multiplied by the appropriate lifetime for recombination.

The traps may also be detected by studying any luminescence that may be emitted as the electrons return to the valence band via the recombination centres (known as the thermal glow method).

The evaluation of trapping parameters from experimental TSC curve is not straightforward. Nicholas and Woods[32] have given a critical account of ten methods which have been proposed for the evaluation of electron trapping parameters from experimental TSC curves. They found[32] that at least six major trapping levels are common in CdS crystals, although each does not occur in every sample. The levels together with their tentative identifications are as follows:

1. 0•05 eV, double negatively charged sulphur vacancy,
2. 0•14 eV, also associated with sulphur vacancies,
3. 0•25 eV, singly charged sulphur vacancy,
4. 0•41 eV, an unidentified neutral level,
5. 0•63 eV, a single positively charged Cd vacancy,
6. 0•83 eV, is the activation energy for the destruction of a trap complex.

c) Photo-Hall effect

Experiment shows that the magnitude of the Hall mobility can vary with the intensity of photoexcitation. This effect can be used to determine the charge state of traps and to evaluate other trapping parameters.[34] If ionised impurity scattering is dominant, the mobility is inversely proportional to the density of charged scattering centres. Hence it is expected that a change in the density of such centres will lead to a change in mobility. One method of changing the density of scattering centres is to change their effective charge by adding or removing an electron from their environment. Photoexcitation, with its effect on the Fermi level, is one of the means by which changes in the effective charge state of a centre can be achieved.

Consider a donor level lying above the thermal equilibrium Fermi level. It will be ionised at low light intensities and will have a large scattering cross section. As the electron Fermi level rises with increasing light intensity the donors will become occupied, and their charge will be removed so that their scattering decreases markedly. The expression derived by Bube and Macdonald[34] to describe this process is:

$$\frac{1}{\mu_H} = \frac{1}{\mu_\alpha} + \frac{\beta \nu_{th} S_+ N_+}{1 + 2\ \exp[(E_t - E_{fn})/RT]} \qquad 1.16$$

where μ_α is the Hall mobility with all donors occupied (i.e. under strong illumination), β is the proportionality factor between mobility

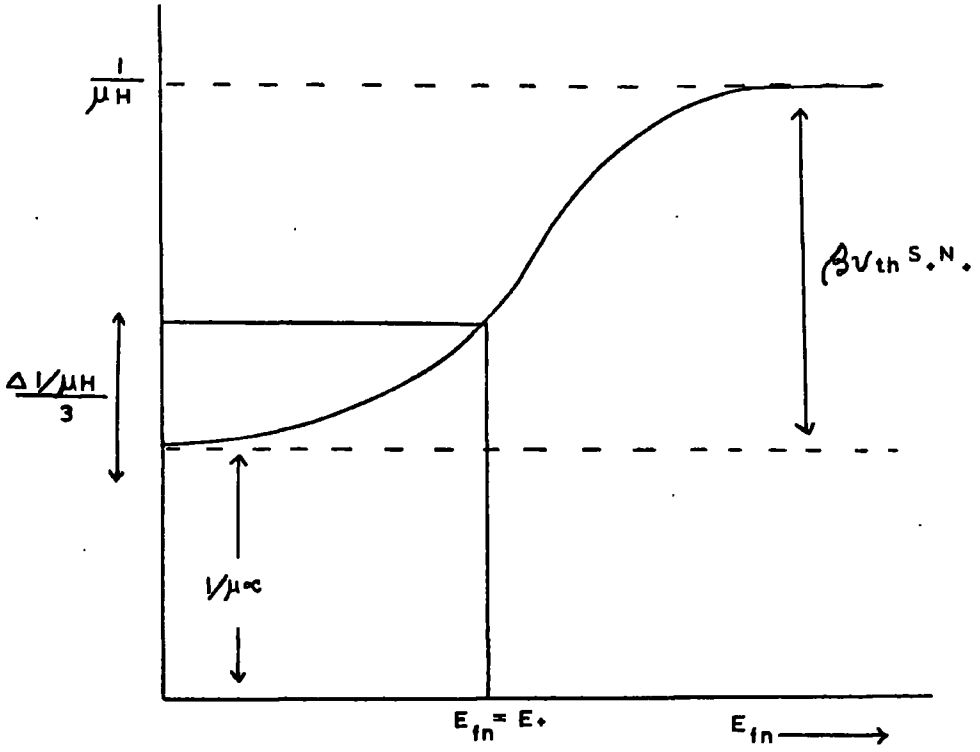

Fig.1.9. Theoretical curve for the dependence of $1/\mu_H$ on the location of the electron Fermi level.

and relaxation time which is equal in magnitude to $5{\cdot}7 \times 10^{-6}$ v sec^2/cm^2, v_{th} is the thermal velocity of the free electrons, S_+ is the donor scattering cross section when ionised, N_+ is the density of donors, E_t is the depth of the donor levels below the conduction band and E_{fn} is the electron Fermi level. Eqn. 1.16 gives $\frac{1}{\mu_H}$ as a function of E_t, E_{fn} can be calculated from the measured conductivity using the relation

$$\frac{\sigma}{\mu q} = n = N_c \exp[E_{fn}/kT] \qquad 1.17$$

where $$N_c = 2\left(\frac{2\pi m^* kT}{h^2}\right)^{3/2}$$

If $\frac{1}{\mu_H}$ is plotted as a function of E_{fn}, a curve of the type shown in Fig.1.9 is obtained. When E_{fn} is much less than E_t, we have $\frac{1}{\mu_H} = \frac{1}{\mu_\alpha}$ When E_{fn} is much larger than E_t, all the scattering terms of Eqn. 1.16 are effective. The difference between $\frac{1}{H}$ for small E_{fn} and large E_{fn} gives $\beta v_{th} S_+ N_+$ directly. If N_+ is known from an independent measurement, for example from thermally stimulated current data, the value of the scattering cross section S_+ can be calculated. At $E_{fn} = E_t$, $\Delta\left(\frac{1}{\mu_H}\right) = (\beta v_{th} S_+ N_+/3)$, this relation allows a value for E_t to be determined.

1.15 Thermoelectric Power Measurements in CdS

Measurements of thermoelectric power can be used to investigate the photoelectronic properties of semiconducting crystals. In CdS both electronic and phonon drag components contribute to the Seebeck

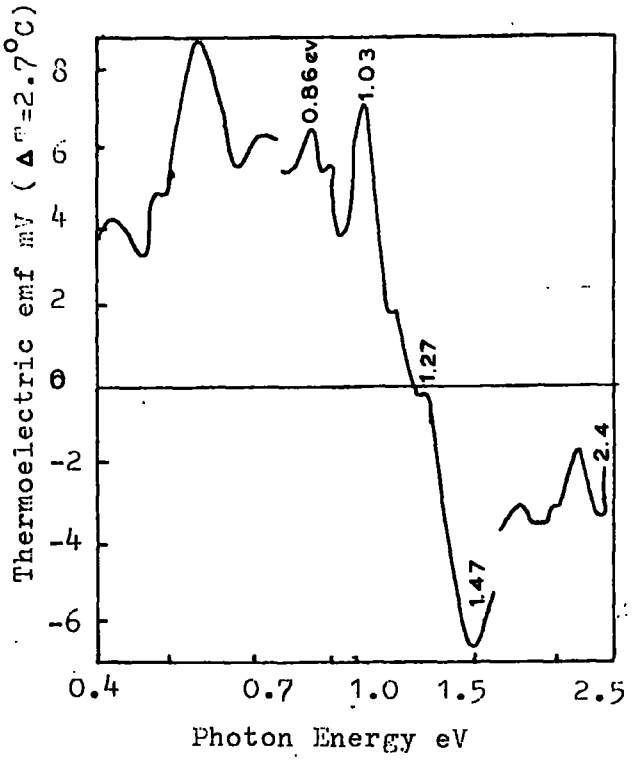

Fig. 1.10. Thermoelectric emf at 300°K as a function of photon energy. (Lawrence).

coefficient.[35] Like the Hall effect, the sign of the Seebeck effect is an indication of the type of charge carrier dominating the conduction mechanism.

The density of current carriers in the conduction band (electrons) or valence band (holes) can be increased by extrinsic photoexcitation, depending on the nature of the transitions involved. Lawrence and Bube[36] have recently measured the thermoelectric power in cadmium sulphide as a function of photon energy of the exciting radiation. The spectrum at room temperature is shown in Fig.1.10. It can be seen (Fig.1.10) that for photon energies smaller than half the band gap the thermoelectric e.m.f. is positive, whereas for photon energies larger than half the band gap the thermoelectric e.m.f. is negative. Lawrence and Bube[36] concluded that the change from positive to negative thermoelectric e.m.f. started at 1·03 eV, which suggests a transition to the conduction band. The abrupt reversal at 1·47 eV, suggests a transition from the valence band.

1.16 Conclusion

Cadmium sulphide has always been found to be n-type, and it is not yet possible to dope CdS in such a way that it becomes p-type. However, infrared quenching can increase the lifetime and concentration of free holes in the valence band and decrease the concentration of free electrons in the conduction band, thereby leading to a preponderance of holes. This effect is used in some of the work to be described later in the thesis.

References

1. W.O. Milligan, J. Phys. Chem., 38, 797, 1934.

2. M. Weinstein, G.A. Wolff and B.N. Das, Appl. Phys. Letters, 6, 73, 1965.

3. S.S. Devlin, J.M. Jost and L.R. Shiozawa, U.S. Dept. Comm. Off. Tech. Serv. PB. Rep. 161,938, quoted by W.L. Roth, II-VI Compounds, Edited by Aven and Prener, 1967.

4. J.L. Birman, Phys. Rev. Letters, 2, 157, 1959.

5. D.G. Thomas and J.J. Hopfield, Phys. Rev., 116, 573, 1959.

6. J.J. Hopfield and D.G. Thomas, Phys. Rev., 122, 35, 1961.

7. W.W. Piper and D.F.T. Marple, J. Appl. Phys., 32, 2237, 1961.

8. W.S. Baer and R.N. Dexter, Phys. Rev., 135, A1388, 1964.

9. J. Bardeen and W. Shockley, Phys. Rev., 80, 72, 1950.

10. A.R. Hutson, J. Appl. Phys., 32, 2287, 1961.

11. H. Frohlich, "Polarons and Excitons" Oliver and Boyd, 1962, page 1.

12. E.M. Conwell and V.F. Weiss Kopf, Phys. Rev., 77, 388, 1950.

13. C. Erginsoy, Phys. Rev., 79, 1013, 1950.

14. D.H. Dexter and F. Seitz, Phys. Rev., 86, 964, 1952.

15. W.T. Read, Phil. Mag., 46, 111, 1955.

16. E.H. Hall, Amer. J. Math., 2, 287, 1879.

17. S.S. Devlin, "II-VI Compounds", Edited by Aven and Prener, 1967 page 581.

18. H. Fujita, K. Kobayashi, T. Kawai and K. Shiga, J. Phys. Soc. Japan, 20, 109, 1965.

19. M. Balkanski and R.D. Waldron, Phys. Rev., 112, 123, 1958.

20. H.H. Woodbury, Phys. Rev., A134, 492, 1964.

21. A. Rose, Phys. Rev., 97, 322, 1955.

22. D.C. Reynolds, C.W. Litton and T.C. Collins, Phys. Stat. Sol., 12, 3, 1965.

23. D.S. Orr, L. Clark and J. Woods, Brit. J. Appl. Phys. Ser.,2, 1, 1609, 1968.

24. D.G. Thomas and J.J. Hopfield, Phys. Rev., 116, 573, 1959.

25. L.S. Pedrotti and D.C. Reynolds, Phys. Rev., 119, 1897, 1960.

26. D.G. Thomas and J.J. Hopfield, Phys. Rev. Letters, 7, 316, 1961.

27. D.G. Thomas and J.J. Hopfield, Phys. Rev., 128, 2135, 1962.

28. L. Clark and J. Woods, J. Cryst. Growth, 3/4, 126, 1968.

29. P.F. Browne, Electronics, 2, 1 and 154, 1956.

30. R.H. Potter, M. Aven and J. Kastner, J. Electrochem. Soc., 109, 1154, 1962.

31. F.J. Bryant and A.F.J. Cox, Brit. J. Appl. Phys., 16, 463, 1965; 16, 1065, 1965.

32. K.H. Nicholas and J. Woods, Brit. J. Appl. Phys., 15, 783, 1964.

33. J. Woods and K.H. Nicholas, Brit. J. Appl. Phys., 15, 1361, 1964.

34. R.H. Bube and H.E. MacDonald, Phys. Rev., 121, 473, 1961.

35. K. Morikawa, J. Phys. Soc. Japan, 20, 786, 1965.

36. R. Lawrence and R.H. Bube, J. Appl. Phys., 39, 1807, 1968.

CHAPTER II

THE ACOUSTOELECTRIC EFFECT IN CADMIUM SULPHIDE

INTRODUCTION

The interaction of charged particles, such as electrons, with waves in solids has been a subject of great interest for the last decade. Further interest has been created by the observation that, under suitable conditions, sound waves in piezoelectric semiconductors could be amplified.[7] The acoustic wave produces an 'acoustoelectric field' by means of the piezoelectric effect and this actuates the motion of electrons in the crystal. When the drift velocity of the electrons is small compared with the velocity of the sound waves, the coupling between the wave and the electrons produces an additional attenuation. However, if a static field is applied to the semiconductor with a value large enough to produce a drift velocity greater than the acoustic velocity, the electrons can give up energy to the sound wave and acoustic amplification occurs.[7]

An important manifestation of the strong electro-acoustic interaction, under the amplifying condition is the 'spontaneous' build-up of acoustic flux,[7] even in the absence of externally induced acoustic waves. It is this spontaneous build up of acoustic flux and the accompanying 'acoustoelectric current' which leads to the well known electrical

phenomena of acoustoelectric interactions, such as current saturation,[14] current oscillations,[14] and the so called high-field 'domain' formation.[15]

Hexagonal II-VI compounds, and cadmium sulphide in particular are useful for examining these effects.[14,15] Cadmium sulphide has large piezoelectric coupling constants[6] together with a reasonable electron mobility, so that strong acoustoelectric effects occur at easily attainable fields ($\sim 10^3$ volts cm^{-1}).

Another advantage of using CdS lies in its photoconducting property. It has been noted that specimen conductivities higher than about 10^{-5} ohm^{-1} cm^{-1} are necessary to observe the effects of electroacoustic interactions.[14,15] In CdS the electron concentration can be adjusted by illumination of the crystal rather than resorting to doping with impurities to achieve the desired conductivities.

Current saturation,[14] current oscillations,[14] and domain formation,[15] which are all acoustoelectric in origin are discussed in part B following the introduction of the acoustoelectric effect and acoustic wave amplification in part A.

PART A

2.1 Definition

The acoustic effects in semiconductors, which differ from those in insulators, are the result of the interaction of sound waves with the conduction electrons.

In cadmium sulphide the most important phenomenon of this type is the acoustoelectric effect,[11] which depends on the density of conduction electrons, which can easily be altered by varying the intensity of illumination.

The term acoustoelectric[1] effect refers to the appearance of a dc electric field along the direction of propagation of a travelling acoustic wave in a medium containing mobile charges.

When a travelling acoustic wave propagates through a semiconductor, a transfer of momentum from the wave to the free carriers can occur. The net momentum is in the direction of propagation of the elastic wave and is balanced by an induced electromotive force. If the ends of the sample are insulated, an electric field 'the acoustoelectric field' is maintained. If the ends of the sample are connected externally through a conductor, a current will flow; such an electric current is called an 'acoustoelectric current'.

It is worthwhile mentioning in passing the phenomenon of 'phonon-drag' (qualitatively equivalent to the acoustoelectric effect) which is the contribution to the thermoelectric power due to the momentum transfer to

electrons from thermal phonons which are streaming down a temperature gradient.

2.2 Acoustoelectric coupling

For the acoustoelectric effect to occur there must be an interaction between the stress wave and the current carriers and a mechanism for momentum absorption and energy loss must exist.

In what follows we shall usually refer to electrons, but similar remarks apply to holes.

The two principal kinds of coupling between u.s. (ultrasound) and free carriers are (a) deformation-potential coupling and (b) piezoelectric coupling. There is also a third coupling mechanism via polar modes.

i) Deformation Potential Coupling

Non-piezoelectric semiconductors react with electrons through the deformation potential. The elastic wave which passes through the crystal produces strain in the lattice. This strain changes the energy of the electron in the conduction band as a result of the perturbation in the lattice and hence the potential changes. This perturbation is known as the deformation potential[2] and can be written as

$$U_d = C_d S \qquad 2.1$$

where U_d is the potential of the electron and C_d is the deformation potential constant.

ii) Piezoelectric Coupling

In piezoelectric materials the propagation of an elastic wave is accompanied by an electric field. Interaction between this electric field and the electrons introduces a coupling between the electrons and ultrasound.

The basic equations of state which describe a piezoelectric crystal in the one-dimensional case are

$$T = cS - eE \qquad 2.2$$

and

$$D = eS + \epsilon E \qquad 2.3$$

The first equation describes the stress T, in terms of strain, S, and the electric field, E. c is the elastic stiffness constant for constant electric field, and e is the piezoelectric constant. The second equation gives the electric displacement, D, in terms of the strain and the electric field, ϵ is the diectric constant.

For an open-circuited piezoelectric solid with low carrier concentration $D \tilde{\simeq} 0$ and hence according to the second equation the magnitude of the electric field produced in a piezoelectric insulator by a strain S is

$$E = \frac{e}{\epsilon} S \qquad 2.4$$

When S represents a sinusoidal acoustic wave $[\alpha \exp j(k_S x - \omega t)]$, this field corresponds to a change in the potential energy of an electron given by

$$U_p = \frac{qe}{\epsilon k_S} S \equiv C_p S \qquad 2.5$$

where q is electronic charge and $k_S = \frac{\omega}{\nu_S}$; ω and ν_S are the angular frequency and velocity of the acoustic wave in the crystal, C_p is the electron-phonon coupling constant.

Comparison of Piezoelectric and Deformation-Potential Coupling

A measure of the relative strengths of the effects associated with the two types of coupling mechanisms is given by the ratio (Eqns.2.1 and 2.5)

$$\left(\frac{C_d}{C_p}\right)^2 = \left(\frac{\epsilon C_d}{qe\nu_S}\right)^2 \omega^2 \qquad 2.6$$

If we compare the piezoelectric semiconductor cadmium sulphide with the nonpiezoelectric germanium using this ratio and the following values for the quantities in Eqn.2.6,

$$C_d \text{ (Ge)} \simeq 10 \text{ eV} \simeq 1{\cdot}6 \ 10^{-18} \text{ joule}$$
$$e \text{ (CdS)} \simeq 0{\cdot}2 \text{ coulomb meter}^{-1}$$
$$\nu_S \simeq 4{\cdot}10^3 \text{ meter sec}^{-1}$$
$$\epsilon \simeq 10^{-10} \text{ farad meter}^{-1}$$
$$q = 1{\cdot}6 \times 10^{-19} \text{ coulomb}$$

then

$$\left(\frac{C_d}{C_p}\right)^2 \simeq 10^{-24} \omega^2$$

At an ultrasonic frequency of 100 GHZ the two types of effects are about equal, but the deformation potential effects in germanium are very small compared with the corresponding piezoelectric effects in CdS at lower frequencies.

iii) Polar Mode Coupling

Longitudinal optical vibrations of the atoms relative to one another (when there are more than one) in a unit cell constitute the polar modes; transverse motion does not produce electric fields.[3] The current densities required to obtain a substantial effect (amplification of sound) were estimated[4] to be of the order of 10^6 amp/cm^2 in polar crystals. However the amplification of ultrasound by optical vibrations has not yet been observed experimentally.

2.3 Carrier Bunching (an effect of coupling)

The effects of the coupling of the ultrasound to the electrons are multifold. We will discuss briefly the effects to be expected before summarising the theory and the resultant experimental work.

We have seen that elastic waves propagate in a solid accompanied either by a deformation potential, or by the piezoelectric effect, the net result is an electric wave(with its accompanying potential)acting on the electrons. If the potential wave was fixed in space and time, the electrons would congregate in the energy 'hollows' corresponding to the minima of potential energy. The electrons would therefore form into 'bunches' along the length of the potential wave separated by distances of one wavelength λ (Fig.2.1) and would tend to diminish the amplitude of the potential in these regions. The accumulation of electrons would stop when the potential became uniform.

Fig.2.1 THE ACOUSTOELECTRIC EFFECT

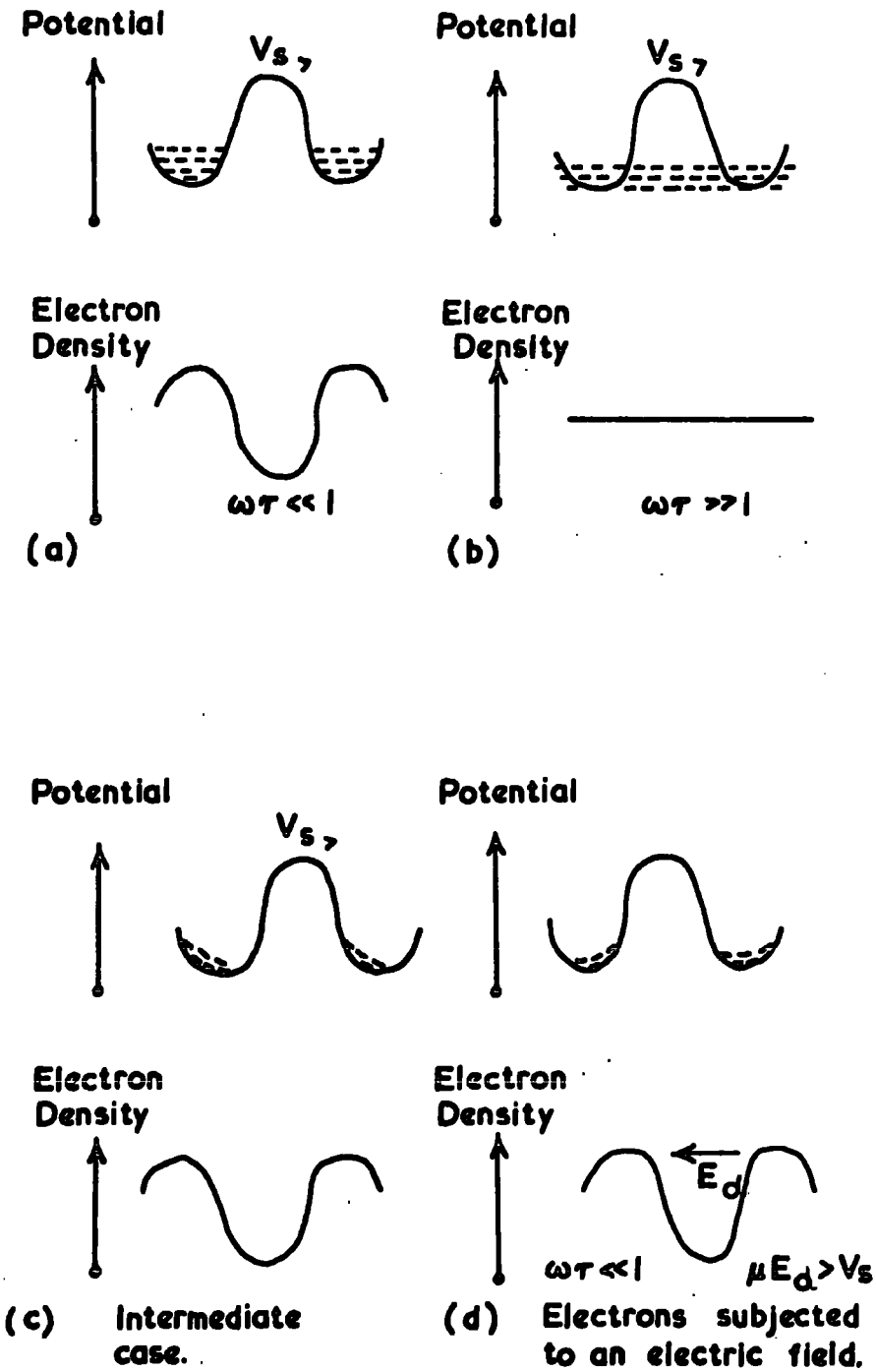

The bunching or rearrangement of the electrons needs a certain time τ to occur, and since the wave is in fact a progressive wave moving along the sample with the velocity of sound, the maxima in the electron concentration are not located exactly at the minima of potential unless the entire electron population moves with precisely the velocity of sound under the influence of an applied drift field. Four cases are illustrated in Fig.2.1. In the first three no electric field is applied.

a) $\omega\tau << 1$, i.e. when the period of the acoustic wave is much larger than the bunching time τ, (or $\tau \longrightarrow 0$). The distribution of the electrons is symmetric with respect to abscissa of minimum energy and the electrons congregate at the potential minima (Fig.2.1a).

b) When $\omega\tau >> 1$, the electrons cannot follow the variations in potential and preserve a uniform distribution (Fig.2.1b).

c) In the intermediate range, the electron distribution will lag behind the potential wave and hence will be dragged along by the wave (Fig.2.1c). This means that energy will be transferred from the wave to the electrons. Consequently the wave loses energy (is attenuated) and the electrons gain kinetic energy. The electric current produced is the acoustoelectric current.[11]

d) Suppose now that an external electric field E_d is applied such as to give the electrons an average drift velocity $v_d = \mu E_d$ in the direction of the wave propagation (μ is the electron mobility).

If $v_d > v_s$ (v_s is the sound velocity), the electrons have a tendency to move more rapidly than the wave and are retarded by the potential wave. This results in an accumulation of electrons on the front of the potential hollows (Fig.2.1d), and the acoustoelectric current changes sign. The average power transferred from the wave will be negative in sign, indicating that amplification will now occur.

2.4 Experimental Observation of Electron-Acoustic Interaction in Cadmium Sulphide

In 1960, Nine[5] reported the observation of ultrasonic attenuation in hexagonal CdS crystals which was very sensitive to changes in the electrical conductivity. Shortly after Nine's result Hutson[6] showed that cadmium sulphide is more piezoelectric than quartz and explained Nine's result on the basis of the coupling of the photoconduction electrons with the acoustic waves. Hutson, MeFee and White[7] (1961) then used the strong piezoelectric coupling in CdS to obtain ultrasonic amplification in the presence of an externally applied drift field.

The experimental arrangement of Hutson et al[7] is shown in Fig.2.2. One microsecond pulses of 15 Mc/s (or 45 Mc/s) produced shear waves in the upper y-cut quartz transducer which passed down through the CdS crystal and were detected at the lower transducer. The CdS crystal was oriented so that the shear wave was piezoelectrically active, i.e. the shear wave propagated in a plane perpendicular to the CdS hexagonal axis with particle displacement along the hexagonal axis. Conduction

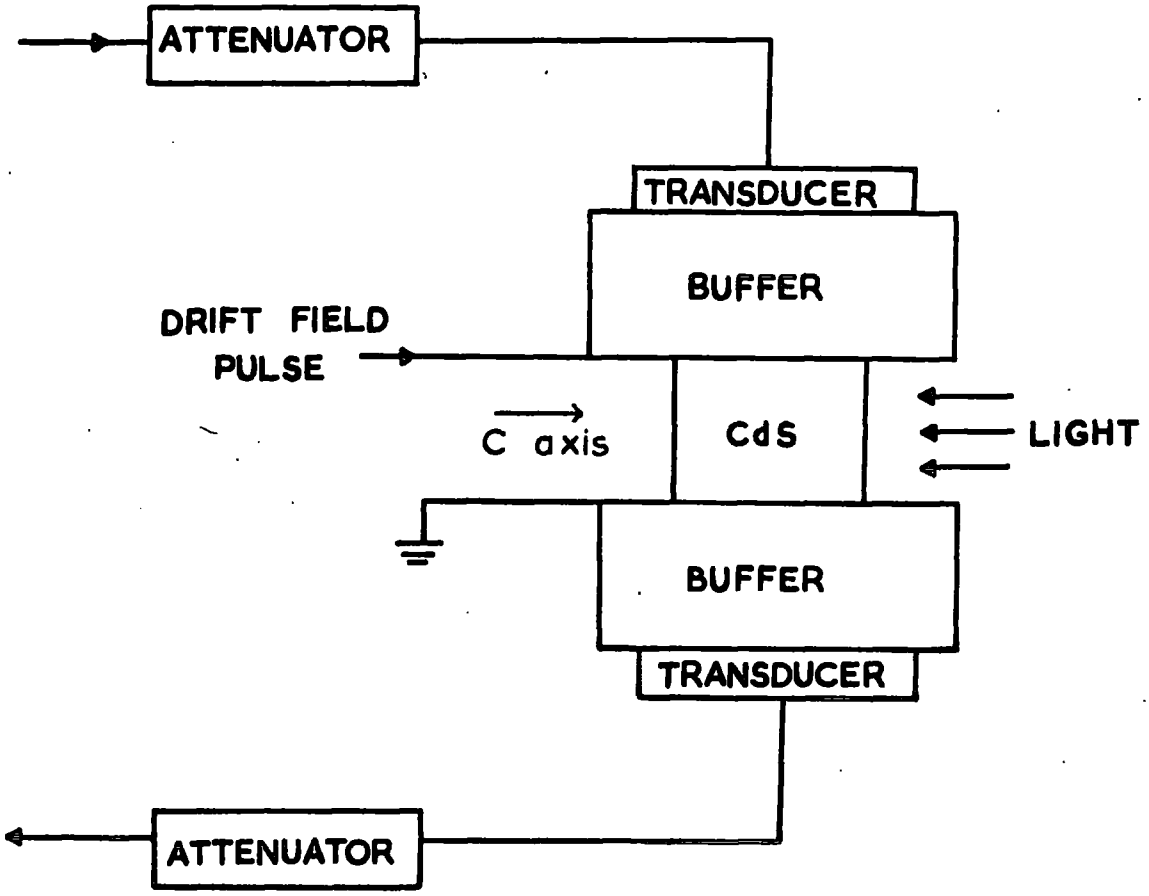

Fig. 2.2

BLOCK DIAGRAM OF THE ARRANGEMENT USED BY HUTSON, McFEE AND WHITE TO OBSERVE ULTRASONIC AMPLIFICATION.

electrons were produced in the sample by illumination with yellow light (5770Å) from a high pressure mercury arc. Under illumination the sample resistivity was in the range of 10^4 to 10^5 ohm cm. In the 'dark' the sample was essentially insulating. Diffused indium contacts were made over the whole of the top and bottom surfaces of the CdS. A drift voltage pulse of approximately 5 microsecond duration was applied between these contacts during the time of transit (~ 4 μsec) of the signal through the CdS.

The observed effects of the electron drift on the ultrasonic attenuation is shown in Fig.2.3a. Positive values of the drift field mean that the electrons are drifting in the direction of sound propagation. For drift fields greater than 700 volts/cm the ultrasonic attenuation becomes negative, i.e. the output signal is larger than the signal obtained in the dark. Zero dB represents the attenuation in the dark. Maximum gains of 25 dB/cm at 15 Mc/s and 55 dB/cm at 45 Mc/s were obtained with a resistivity of 10^4 ohm-cm.

2.5 Theory of Ultrasonic Amplification (small-signal)

The interaction of acoustic waves with mobile carriers will be discussed for the case where $k_s\bar{l} \ll 1$ ($k_s = 2\pi/\lambda$, where λ is the acoustic wavelength, and $\bar{l}$ is the mean free path of the carriers). At ultrasonic frequencies, λ is usually large compared with $\bar{l}$ so that $k_s\bar{l}$ is considerably less than unity. In this case the theory was developed by Hutson and White[8] and extended to the case where external

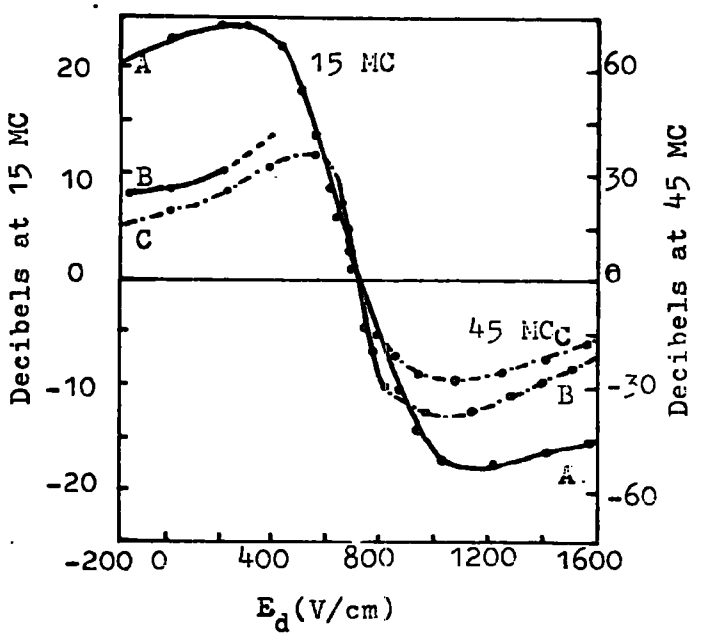

Fig. 2.3a. The observed attenuation in CdS as a function of the drift field . Zero dB represents the attention in the dark.
A : ω_c/ω =1.2 B : ω_c/ω=0.24 C : ω_c/ω =0.21

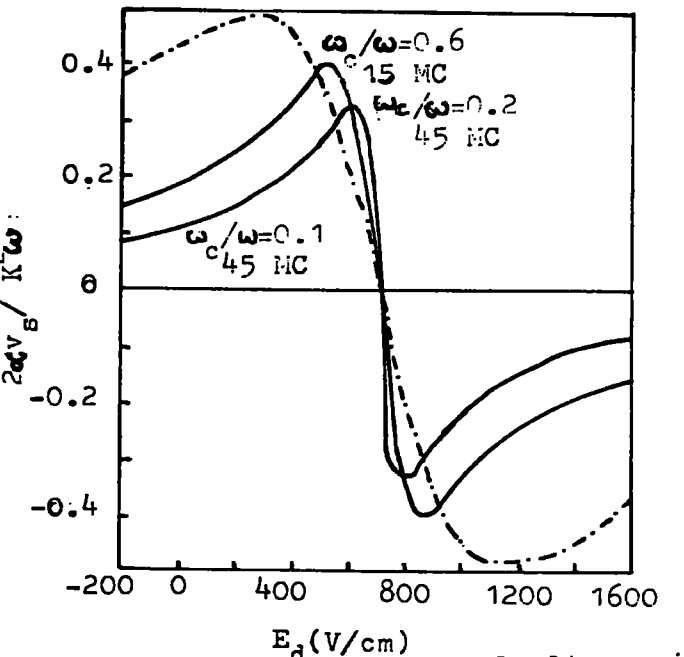

Fig. 2.3b. Theoratical ultrasonic attenuation in CdS as a function of drift field. Plot of $2\alpha v_s/K^2\omega$ from eq.(2.8) as a function of drift field.

(after Hutson et.al)[7].

electric fields are applied by White.[9]

The main object of the calculations was to find the modified elastic constant, which because of interaction with the electrons, will be a function of the properties of the charge carriers (carrier density, mobility and drift velocity).

[For definiteness the carriers will be referred to as 'electrons'. The theory however, applies equally well to mobile holes.]

Consider a piezoelectric semiconductor under an applied electric field E_d, in which only currents and longitudinal acoustic travelling waves in the x direction are taken into account (the one-dimensional case).

The current density (for extrinsic n-type material) can be written as

$$J = \mu q(n + n_s)(E + E_d) + qD \frac{\partial n_s}{\partial x} \qquad 2.7$$

where μ is the mobility and q the charge of an electron; n is the mean carrier concentration, D is the carrier diffusion constant, E is the wave-periodic longitudinal electric field accompanying a travelling wave due to the piezoelectric effect, and n_s is the variation in the density of conduction electrons caused by the acoustic wave.

The small signal theory of acoustic loss or gain was developed using

$$\partial D/\partial x = -qn, \quad \text{Poisson's equation}$$

and

$$\partial J/\partial x = q \frac{\partial n}{\partial t} \quad \text{the continuity equation}$$

to obtain the displacement D in terms of E from eqn. 2.7. This was then substituted in the piezoelectric equation

$$D = \epsilon E + eS$$

to find E(S). This self consistent field was then substituted in

$$T = cS - eE$$

to obtain a complex elastic constant c^*, which describes the anomolous dispersion of the acoustic wave.

Neglecting the term $n_s E$ in the linear (small signal) treatment the attenuation (amplification) factor becomes

$$\alpha = \frac{K^2}{2.\nu_s \gamma} \frac{\omega_c}{1 + (\omega_c/\gamma\omega)^2(1 + \omega^2/\omega_c\,\omega_D)^2} \qquad 2.8$$

where $K^2 = e^2/c\epsilon$ is the electromechanical coupling constant

$\omega_c = \frac{\sigma}{\epsilon}$ σ is the electrical conductivity, to that ω_c is the conductivity relaxation frequency.

$\omega_D = \frac{\nu_s^2}{D}$ is the 'diffusion' frequency; D is diffusion constant

$\gamma = 1 - \frac{\nu_d}{\nu_s}$ is the drift parameter and $\nu_d = \mu E_d$ the Ohmic drift velocity of the carriers.

Note α changes sign when γ changes sign which occurs when $\nu_d > \nu_s$. Since α is an attenuation factor, a negative α describes the amplification of a propagating acoustic wave when the carriers are

drifting in the direction of propagation with a velocity greater than the sound velocity.

It should be noted in the experimental data shown in Fig.2.3a[7] that negative attenuation (amplification) occurs at drift fields greater than 700 volts/cm. If $\mu \sim 300,700$ v/cm corresponds to a drift velocity of 2×10^5 cm/sec, which is greater than the shear-wave velocity of $1{\cdot}75 \times 10^5$ cm/sec in CdS. The curves in Fig.2.3b show the ultrasonic attenuation versus drift field as calculated from eqn.2.8.

The agreement between the theoretical curves of Fig.2.3b and experimental curves of Fig. 2.3a is far from perfect. The theoretical curves are symmetrical about the cross-over field i.e. theory predicts that the maximum gain should be equal to the maximum attenuation. On the other hand, experimentally the maximum gain is found to be considerably less than the maximum attenuation. The discrepancy becomes more marked as the conductivity is decreased (smaller ω_c). Electron trapping[14] and crystal inhomogeneity[7] can lead to reduced gain and cause considerable asymmetry in the gain versus drift field characteristic (trapping effects are discussed in Section 2.7).

2.6 Experimental Observation of Acoustoelectric current in Cadmium Sulphide

Using a general argument based on conservation of energy and momentum between travelling ultrasonic waves and conduction electrons,

Weinreich[12] showed that the local electric field produced by a sound wave is given by

$$E_{ae} = \frac{2\alpha\phi}{qn\nu_s} \qquad 2.9$$

where E_{ae} is the acoustoelectric field, α is the ultrasonic attenuation due to conduction electrons, q is the electronic charge, n the density of conduction electrons and ϕ is the energy density of the ultrasonic wave.

Eqn. 2.9 can be expressed in terms of a current density by multiplying by the conductivity of the sample to give

$$J_{ae} = \sigma E_{ae} = \frac{\mu(2\alpha)\phi}{\nu_s} \qquad 2.10$$

μ is the electron mobility.

Wang's experiment

Wang[10] has measured the acoustoelectric current (Eqn. 2.10) produced in a photoconductive CdS crystal. Wang's experimental arrangement consisted of a shear wave ultrasonic amplifier built in the configuration described by Hutson et al[7] and essentially identical with that shown in Fig. 2.2. 33 Mc/s ultrasonic waves of known amplitude were applied in pulses of 10-μ sec duration. Synchronised drift-voltage pulses of 100-μ sec duration and variable amplitude could be applied across the CdS crystal. Figure 2.4a shows the circuit configuration and the equivalent circuit for the measurement

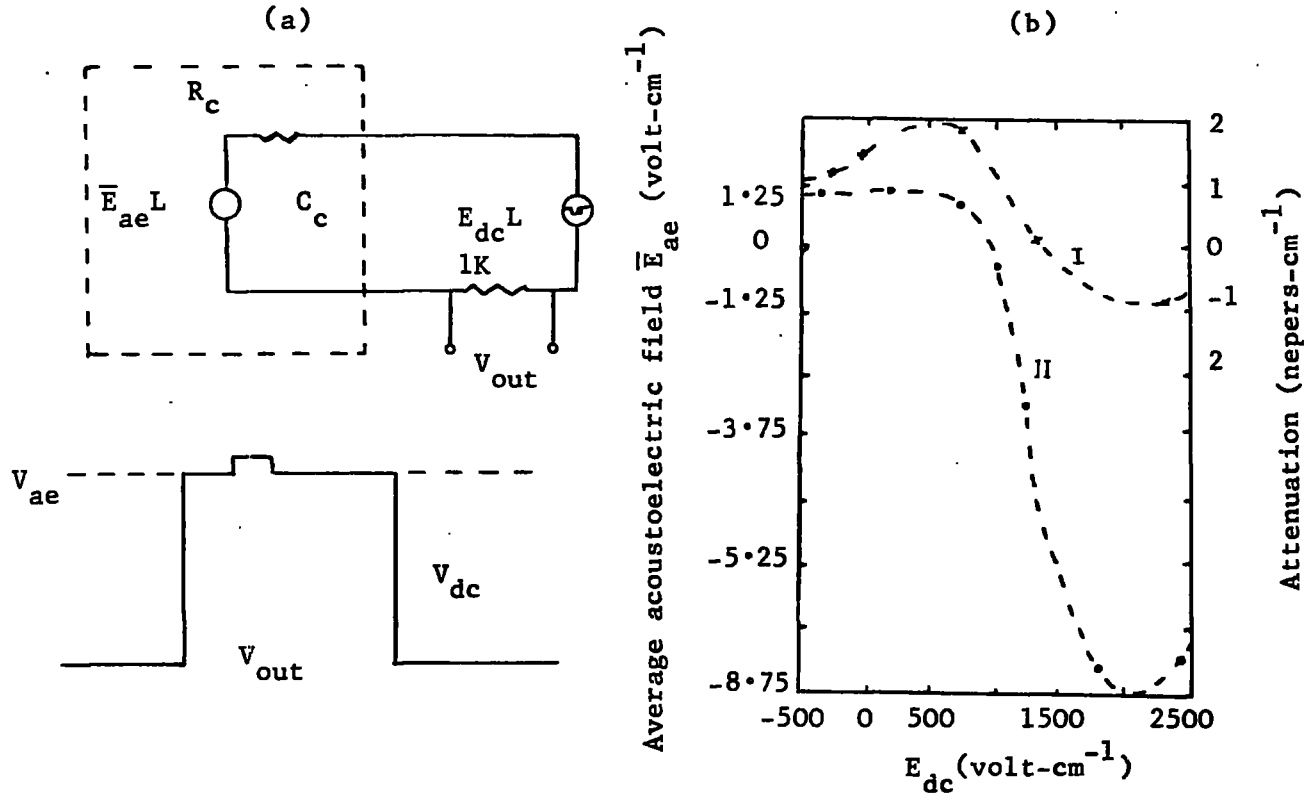

Fig.2.4. (a) Upper: circuit configuration for measurement of average acoustoelectric field $\bar{E}_{ae}$, when the external dc voltage $E_{dc}L$ is applied. L is the crystal length. Portion enclosed by broken lines is the equivalent circuit for acoustoelectric effect. V_{out} is the voltage drop across the measurement resistor of 1K. Lower: observed form of V_{out}. V_{ae} and V_{dc} are the voltage drop caused by $\bar{E}_{ae}$ and E_{dc} respectively.

(b) Curve I: attenuation as a function of external dc field applied.

Curve II: average acoustoelectric field as a function of external dc field applied. Both curves were taken at 8×10^{-5} mho cm^{-1} and acoustic density = 0·6 watt-cm^{-2}. (After Wang).[10]

of the average acoustoelectric field E_{ae} in CdS. Wang also measured acoustic attenuation and the average acoustoelectric field as a function of drift field and obtained the results shown in Fig. 2.4b.

When the drift voltage was zero Wang found that an acoustic input intensity of 1 Watt/cm^2 produced an average acoustoelectric field of approximately 1 volt/cm (Fig. 2.4b) across the crystal. This is to be compared with acoustoelectric fields in the microvolt range produced in germanium[11] by ultrasonic waves of the same intensity. Wang's experiments demonstrate directly that acoustoelectric effects in CdS at ultrasonic frequencies are many orders of magnitude larger than in non-piezoelectric semiconductors like germanium. The important point to notice is that, the ultrasonic attenuation changes sign (to amplification) for sufficiently large drift fields and so does the average acoustoelectric field. This behaviour is to be expected from Weinreich's relation (Eqn. 2.9), which states that the acoustoelectric field is proportional to acoustic attenuation.

2.7 Effect of Bound Electron States (Traps)

i) On acoustoelectric current

In Wang's[10] experiment (Fig. 2.4b) the measured acoustoelectric field was not zero, when the acoustic attenuation was zero, as would have been expected if Weinreich's relation (Eqn. 2.9) were strictly obeyed. The discrepancy should not necessarily be interpreted as

evidence that the relation is not valid when drift fields are applied. According to Southgate and Spector[13] the anomalous behaviour of the acoustoelectric field observed by Wang was caused by carrier trapping. They have shown that the ultimate effect of carrier trapping is to cause the acoustoelectric current to change sign at a drift field lower than that at which the acoustic attenuation changes sign.

In deriving the attenuation (amplification) parameter α (Eqn. 2.8), it was assumed that the only perturbing effect of the acoustic wave was to produce a variation, n_s, in the equilibrium density of conduction electrons. As pointed out by Hutson and White,[8] the acoustic wave will also disturb the equilibrium population of electrons residing in bound states (either donors or acceptors) in the energy gap. Hence, in general, only a fraction f of the acoustically produced space charge, $n_s \exp j(k_s x - \omega t)$, will be mobile, and a fraction (1-f) will be trapped. Hutson and White did not take account of any phase relationship between the mobile and free charge. The phase relationship can be taken into account[13] by considering the fraction f to be complex, i.e.

$$f = f_r + i\, f_i$$

Weinreich's relation (Eqn. 2.9) then becomes

$$E_{ae} = \frac{2\alpha\phi}{nq\nu_s}\left\{ f_r + f_i \left[\frac{(\omega/\omega_D)f_r - (\nu_D/\nu_s)f_i}{1-(\nu_D/\nu_s)f_r - (\omega/\omega_D)f_i}\right]\right\} \qquad 2.11$$

where $\nu_d = \mu E_d$ and the diffusion frequency $\omega_D = \nu_s^2/D$, E_{ae} is the acoustoelectric field.

In the absence of trapping, the real part of $f = f_r = 1$ and the imaginary part of $f = f_i = 0$ and eqn. 2.11 reduces to the ordinary Weinreich relation. When trapping occurs the coefficient of proportionality between α and E_{ae} becomes dependent on both the frequency ω and the electron drift velocity ν_d. This is because both the free and the trapped space charge contribute to the amplification coefficient α, while only the free space charge contributes to the acoustoelectric field. Since only a fraction f of the space charge is free, the relationship between the acoustoelectric field and α depends upon f.

It follows therefore that when trapping occurs, the fields at which α and E_{ae} pass through zero (the cross-over point) will not be identical. The absorption coefficient passes through zero, when

$$(\nu_d/\nu_s)_{\alpha=0} = [1 - (\omega/\omega_D)f_i]/f_r$$

while the acoustoelectric field passes through zero when

$$(\nu_d/\nu_s)_{E_{ae}=0} = f_r/(f_r^2 + f_i^2)$$

when $f_i = 0$, the α and E_{ae} cross-over points coincide. When $f_i \neq 0$ they are displaced from one another.

ii) On acoustic attenuation (amplification)

The agreement between the ultrasonic attenuation as a function of drift field observed by Hutson et al[7] (Fig. 2.3a) and the theoretical ultrasonic attenuation curves[8] calculated from Eqn. 2.8 (Fig. 2.3b) is far from perfect. According to White's theory[8] the maximum ultrasonic gain, α_{max}, should be equal to the maximum ultrasonic attenuation, α_{min} i.e. the attenuation versus drift field curves should be symmetrical about the Cross-over field. Experimental observation[7] on the other hand shows that α_{max} is considerably less than α_{min} and also less than predicted gain. The discrepancy generally becomes more pronounced as the illumination level of the crystal is decreased. Electron trapping can lead to reduced gain and considerable asymmetry of the gain versus drift field characteristics. Uchida et al[13] have generalized the linear theory,[8] to include a finite relaxation time, τ, for the trapping of the electrons into bound states.

Hutson and White[8] amended the expression 2.7 to read

$$J = q\mu(n + fn_s)(E + E_d) + q\,D\,f\,\frac{\partial n_s}{\partial x} \qquad 2.12$$

where f is the fraction of the space charge which is mobile. They considered only those bound states which could attain equilibrium with the conduction band in times short compared with the period of the

acoustic wave. In this case f is a real number between 0 and 1. As can be seen from the expression for current density, 2.12, the drift parameter γ has to be redefined as

$$\gamma = 1 - \frac{f\mu E_d}{v_s}$$

$$= 1 - \frac{v_d(\text{eff.})}{v_s} \qquad 2.13$$

and the diffusion frequency as

$$\omega_D = \frac{v_s^2}{f_D}$$

The effective drift mobility is now $f\mu$. If $f << 1$, E_d will have to be made quite large compared with v_s/μ in order to achieve amplification ($\gamma < 0$).

Uchida et al[13] have extended the treatment of Hutson and White[8] by assuming an arbitrary bound state equilibration time τ. They show that f should have the form

$$f = \frac{f_o - j\omega\tau}{1 - j\omega\tau}$$

$$= \frac{bf_o}{1 + ja}$$

where a is Imf/Ref, and is a measure of the phase difference between the total space-charge bunching and the bound-state bunching; a as well as b, is frequency dependent.

Substituting f into eqn. 2.8, the modified trap-controlled amplification factor becomes

$$\alpha' = \frac{k^2\omega}{2\nu_s} \cdot \frac{\gamma' \frac{\omega}{\omega_c} + a\left(\frac{\omega^2}{\omega_c \omega_D} + \frac{\omega}{\omega_c} a\right)}{\left(\gamma' \frac{\omega}{\omega_c} - a\right)^2 + \left(1 + \frac{\omega^2}{\omega_c \omega_D} + \frac{\omega}{\omega_c} a\right)} \qquad 2.14$$

Here $\gamma' = 1 - \frac{bf_o \mu E_d}{\nu_s}$

and $\omega'_D = \frac{\nu_s^2}{bf_o D}$

If a = 0 α' becomes equal to α. The ratio of maximum amplification to the maximum attenuation as calculated from eqn. 2.13 is

$$\left|\frac{\alpha_{max}}{\alpha_{min}}\right| = \frac{\sqrt{1 + a^2} - a}{\sqrt{1 + a^2} + a} \qquad 2.15$$

and the asymmetry referred to above is apparent.

The parameter a is a measure of the phase angle between the bunches of electrons in the conduction band and the bunching of electrons in the bound states. Uchida et al[13] showed that a tends to become large when the concentration of conduction electrons is small (low light intensity). Their measurements of ultrasonic gain as a function of

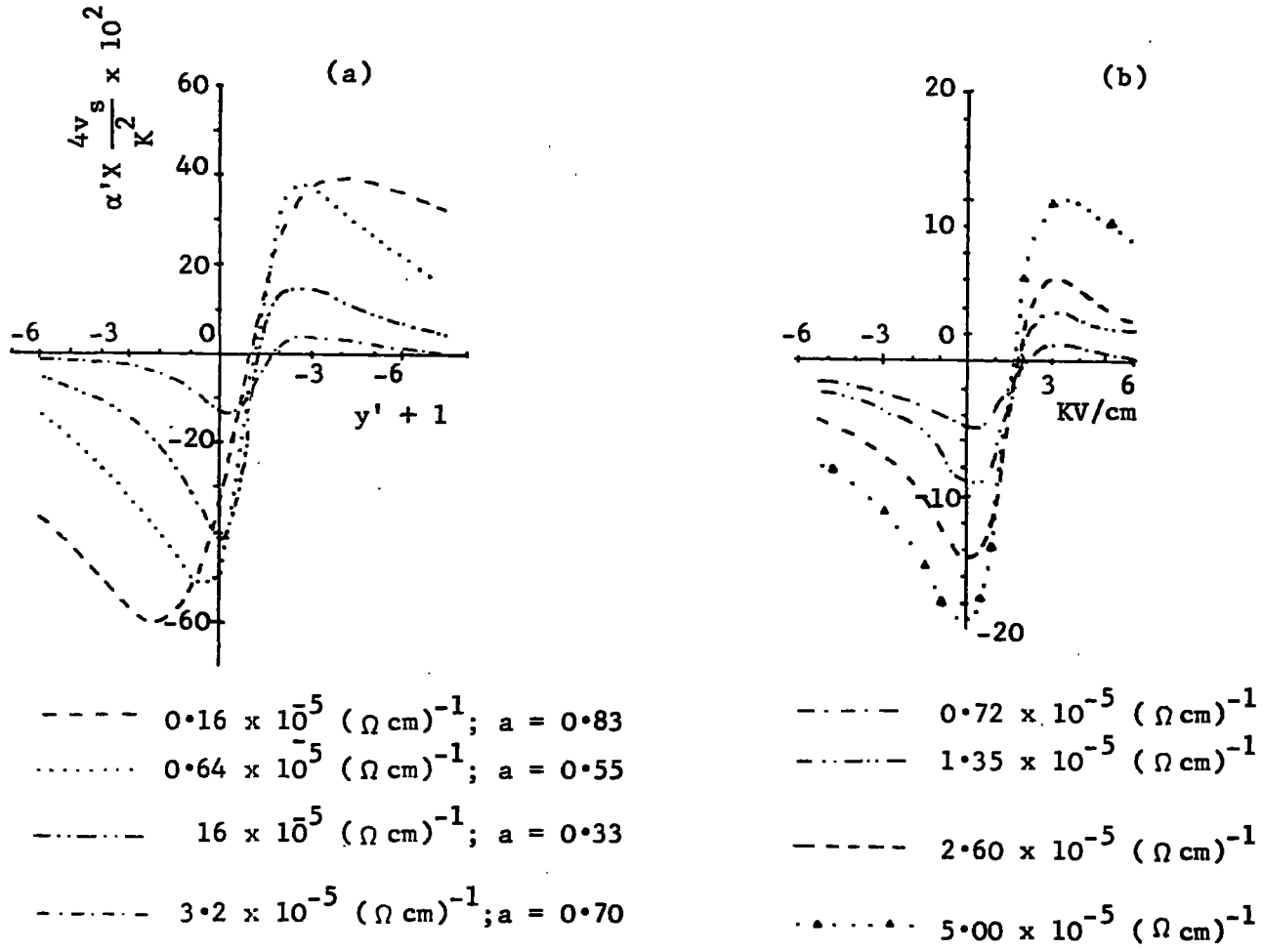

Fig.2.5. (a) Theoretical ultrasonic attenuation in CdS as a function of electron drift field, including the effects of electron trapping by bound states.

(b) Observed ultrasonic attenuation in CdS as a function of drift field. The conductivity is the variable parameter. (after Uchida).[14]

drift field are shown in Fig. 2.5b. The largest gain and the most symmetric curve correspond to the highest conductivity.

For comparison with these data Fig. 2.5a shows curves calculated from eqn. 2.14, which includes the effect of trapping.

The agreement between theory and experiment shows that electron trapping is a major cause of the reduction in the gain and the asymmetry at low carrier concentrations. Trapping also causes the 'cross-over' drift field to increase as carrier concentration decreases (Fig. 2.5a).

PART B

PHENOMENA ARISING FROM ULTRASONIC AMPLIFICATION

Subsequent to the discovery of ultrasonic amplification (discussed in Part A), several new phenomena were observed which are related to acoustoelectric properties of piezoelectric semiconductors. These include:

i) Non-linear electron-lattice interaction[16-18]

ii) Harmonic generation[19-21]

iii) Non-Ohmic behaviour[14]

iv) Current oscillations[14]

v) High-field domains[15]

2.8 Non-linear Effects

Experimental investigation of the amplification of ultrasound by supersonic electrons in semiconductors has shown that if the amplification is large enough certain non-linear phenomena appear. In Part A acoustic wave propagation was solved in a linear approximation (Eqn. 2.8). The linear case $\omega\tau \ll 1$, applies in the case of small acoustic wave amplitudes. In the process of amplification the amplitude of the sound increases by many orders of magnitudes, so that non-linear interaction becomes important.[16]

The source of non-linear interaction in piezoelectric dielectrics is the non-linear dependence of stress on strain and on electric field,

i.e. the violation of Hooke's law. In semiconductors ultrasonic waves interact strongly with the carriers and non-linearities of pure electronic origin are usually more important.

A number of authors[16-18] have given non-linear theories dealing with acoustic waves in piezoelectric semiconductors. According to Gurevich[16] the non-linear amplification factor α can be expressed ($\omega\tau >> 1$) as,

$$\alpha = \alpha_1 \phi(x) + \alpha_2 \frac{1}{L} \int \phi(x)\, dx$$

where α_1 is called the local amplification factor, which is dependent on the local sound intensity only. α_2 is the non-local amplification factor. It depends on the magnitude of the sound in the other parts of the crystal, owing to the acoustoelectric effect and corresponding redistribution of the electric field along the sample. (ϕ is sound intensity and L is the length of the crystal).

Non-linear interactions lead to a restriction on the maximum value of the absolute amplification of ultrasound. Harmonic generation[19-21] formation of high-field domains[15] and instability in the current[14] are all associated with the effects of non-linear electron-acoustic interactions.

2.9 Harmonic Generation

Harmonic generation via the electron sound wave interaction has been observed by several authors.[19-21] It has been shown (Kroger[19])

that the strong acoustic harmonics produced in photoconductive cadmium sulphide are the result of non-linearities in the electron-lattice interaction. The amplitude of the second harmonic was observed to be dependent on the electron density and the applied electric field. The harmonic amplitude was found to increase rapidly as the electron drift velocity exceeded the velocity of sound.

In dielectrics (piezoelectric) the non-linearity of the elastic properties appears in the form of deviations from Hooke's law. The non-linearity produces higher harmonics during the propagation of sound and it may generate 'shock-waves'. Also as the power in the second harmonic is built up, the second harmonic will interact with the fundamental to produce third harmonics, and so on (Hutson[22]).

2.10 Non-Ohmic Behaviour

The observation of current saturation in CdS was first reported by Smith.[14] In general, saturation is observed when a rectangular pulse is applied to the crystal and the series current is monitored on an oscilloscope. With low pulsed voltages the current is proportional to the voltage, so that the sample is Ohmic in behaviour. As the voltage is raised, and provided the electrical field is greater than a critical value, the current pulse is observed to decay in an oscillatory fashion to its saturated value. A typical decaying oscillatory pulsed current under saturated conditions is shown in Fig. 2.7. Fig.2.6 illustrates a typical set of current-voltage curves under the saturation conditions. These measurements were made in the course of the work described in this thesis.

The time necessary for the onset of current saturation after application of the field pulse depends on the magnitude of the conductivity of the specimen and the rise time of the input pulse.[23] In general, the build up time is longer for smaller conductivities and long rise times.

The initiation of current saturation and the accompanying instability in the current are bulk effects, which are independent of contact conditions. This can be deduced from the following facts:
a) changing the electron density will change the total amount of current, but the critical field for current saturation remains constant;

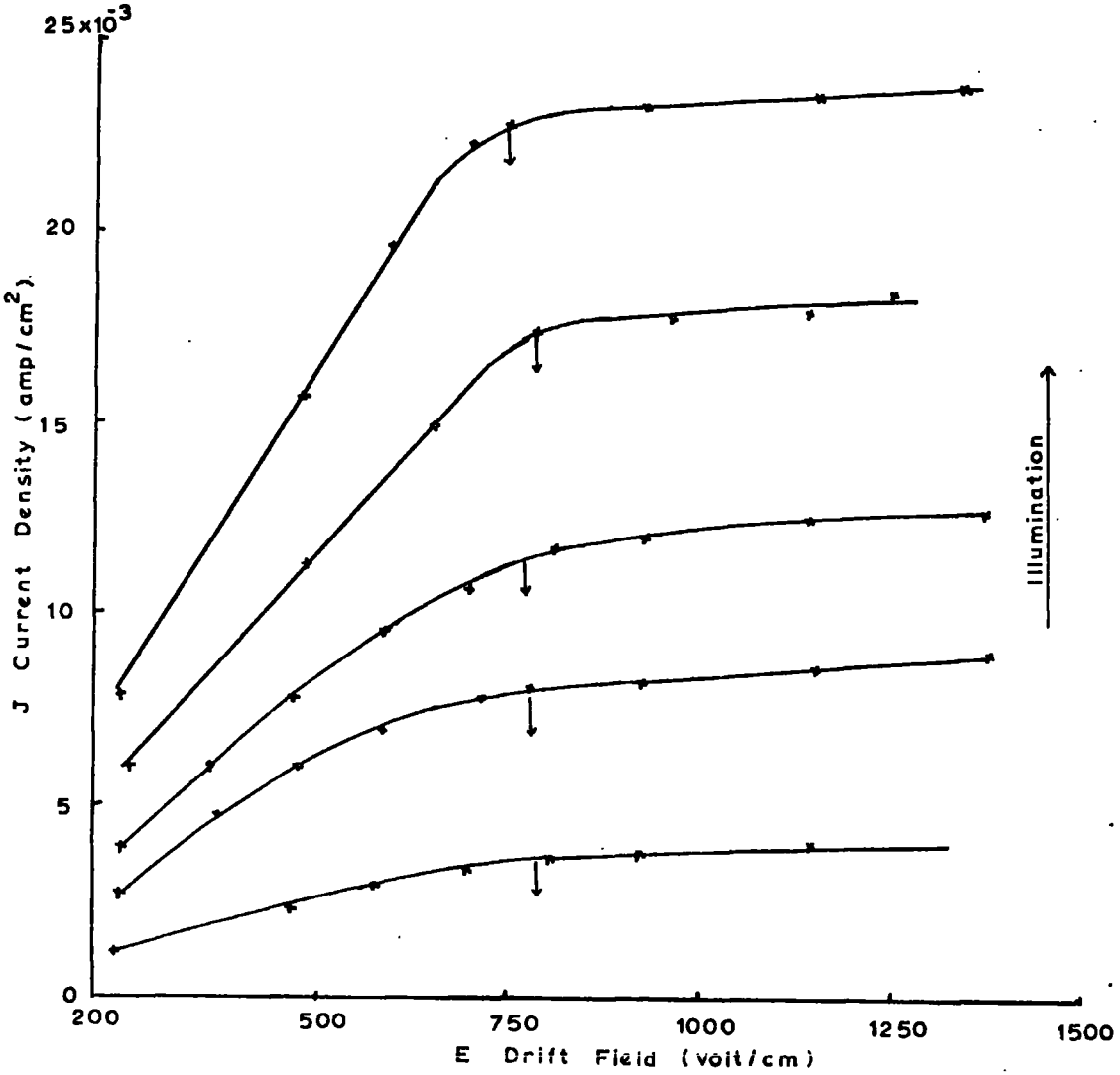

Fig.2.6. Current voltage curves for CdS photoconducting crystal at different illumination level. (Measured in the Department).

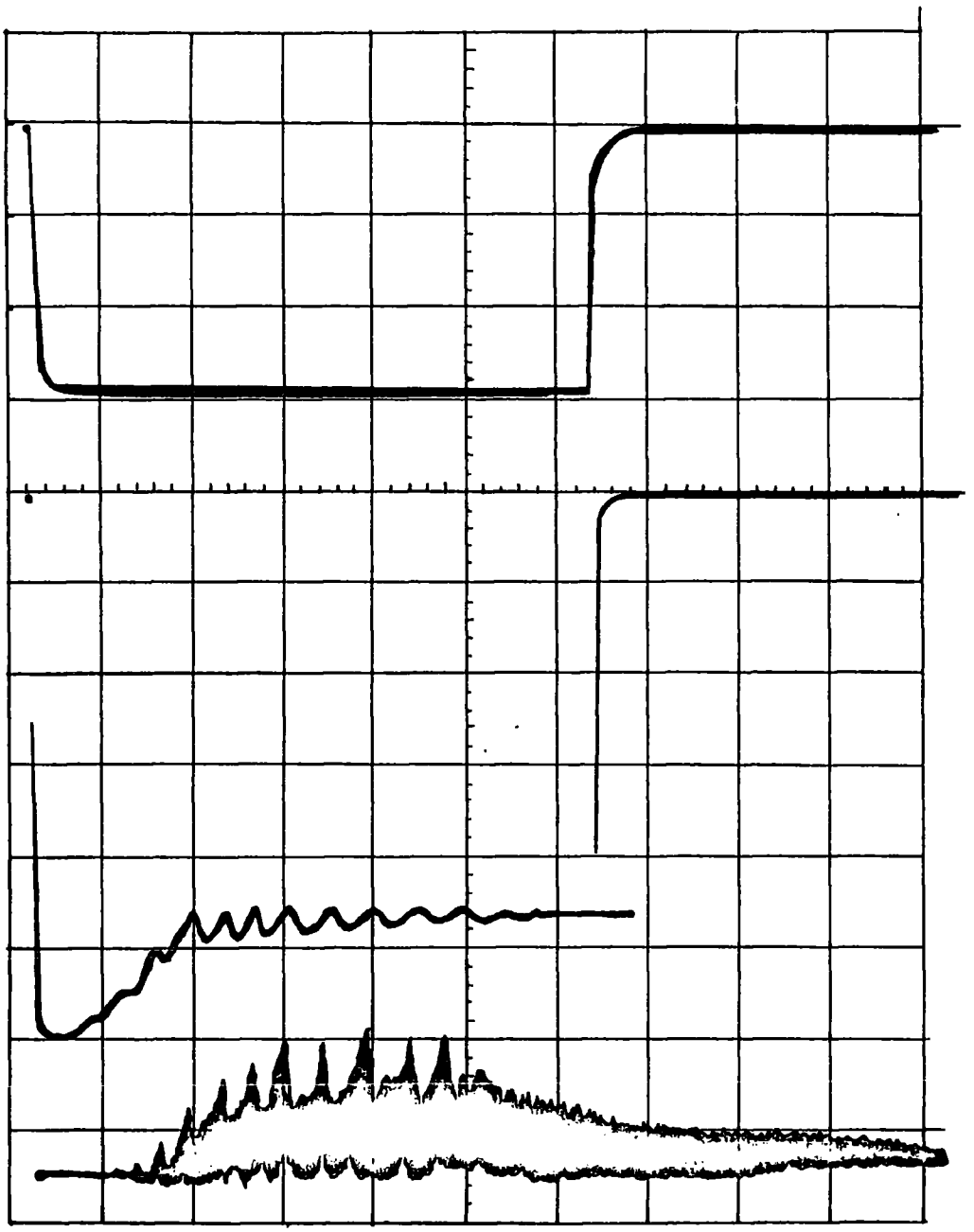

Fig. 2.7 Top trace: Drift voltage applied to CdS sample, [illegible]/div.
Middle trace : Drift current, [illegible]/div.
Bottom trace : Signal from output transducer.
(After McFee)[23]

b) Changing the duty cycle either by changing the pulse length or the repetition rate of both has no effect on the critical field. This eliminates any possible contribution from thermal heating to the saturation mechanism.

c) A comparison of the estimated electron drift velocity at the critical field for saturation with the velocity of the acoustic waves in the crystal provides strong evidence that the saturation effect is acoustic in origin.

The existence of saturation in the current-voltage characteristics of semiconductors is not a new phenomenon, and has been explored previously.[24,25] However, the effect reported previously occurred with electron drift velocities of the order of the thermal velocities of the electrons in the lattice and hence, are referred to as 'hot-electron effects'. They are, in fact, due to electron heating, which is caused by the inability of the relaxation processes to carry away the energy which the electrons receive from the electric field. Such hot electron effects require higher fields than those observed in cadmium sulphide.

Features which distinguish the phonon build up in CdS from 'hot-electron effects'[24,25] can be described as (1) a distinctive threshold drift velocity, above which the current is less than the Ohmic value[14] (2) a marked sensitivity to carrier concentration[26], (3) a response time of the current to the applied voltage (about six orders of

magnitude slower than hot electron phenomena) due to the long build up time of phonons and amplification (4) self-generation of non uniform electric fields[15] (domain formation).

i) Acoustoelectric Explanation of Non-Ohmic Behaviour

Current saturation can be explained in terms of a general discussion of the acoustoelectric effect under the conditions where the drift velocity of the electrons exceeds the velocity of sound.[22]

In piezoelectric crystals like cadmium sulphide the electrons and the acoustic waves are the two interacting systems which exchange energy and momentum. When the electron drift velocity is greater than the velocity of sound, the electrons feed energy into the acoustic waves, and the forward momentum of the electron distribution is thereby depleted. This loss of forward momentum represents an electron flow (the acoustoelectric current) which is counter to the direction of drift.

Hutson[22] has explained current saturation as due to the exaggerated acoustoelectric current[10] accompanying the ultrasonic flux build up under amplifying conditions. This turns out to be useful since it can also explain a more complicated and outwardly different effect noted by Esaki[27] in bismuth. Moore[28] has shown experimentally that both Smith-type[14] current saturation and the Esaki effect[27] (which might be termed voltage saturation) can be observed in the same CdS crystal. Moore's experiment provides evidence for the basically similar nature

of the two phenomena. The acoustoelectric explanation of the non-Ohmic behaviour of piezoelectric semiconductors will be discussed further below.

Wang[10] has measured the acoustoelectric currents produced in a photoconductive crystal of CdS (Fig.2.4). His experiments demonstrate directly that the acoustoelectric effects in CdS at ultrasonic frequencies are many orders of magnitude larger than in non-piezoelectric semiconductors. The measured average acoustoelectric field as a function of drift field shows that the ultrasonic attentuation changes sign (amplification occurs) for sufficiently large drift fields as does the average acoustoelectric field.

According to Weinreich's relation (Eqn. 2.9) the acoustoelectric field is proportional to the acoustic attenuation and acoustic flux density. The spontaneous growth of acoustic energy in CdS under amplifying conditions has been noted by Hutson et al[7] in their original amplification experiment.

One process by which the pulse of acoustic flux may be generated is via an abrupt application of a dc field. The flux density increases as it moves through the crystal. A three phonon process[22] involving the non linear interaction of acoustic waves with electrons (harmonic generation) may be responsible for the establishment of a steady state distribution of sound waves. The effect of the process is that a pair of amplified waves produce a third wave at sum frequency, such that the

sum frequency is higher than the highest frequency for which a linear gain exceeds a linear loss.

The flux may also build up during the process of amplification of the thermal lattice vibrations (phonons) which must be present. The growth of acoustic flux will continue until a non-linear loss mechanism sets in to dissipate the acoustic energy as fast as it is generated.[22]

In view of Wang's measurements, it would be expected that spontaneously generated acoustic waves should be accompanied by measurable acoustoelectric currents. Investigations by McFee[23] have shown that the acoustoelectric current accompanying the spontaneously generated acoustic waves can be comparable to the drift current. In other words, the drift current saturation was found to accompany the spontaneous growth of acoustic energy.

McFee[23] has also shown that current saturation and growth of acoustic energy are strongly correlated. This observation confirms that acoustic wave amplification and build up of acoustic flux are responsible for the current saturation. Figure 2.7 shows, the drift voltage, drift current and the accompanying build up of acoustic waves (as a function of time) in a CdS crystal under amplifying conditions. The strong similarity between the growth of the ultrasonic flux and the decay of the drift current is evident.

The current density in a piezoelectric crystal in terms of the applied drift field E_d and the acoustoelectric field E is (Eqn. 2.7)

$$J = \mu q(n + n_s)(E_d + E) + qD \frac{\partial n_s}{\partial x}$$

where n is the average electric concentration, n_s is the variation in the density of conduction electrons caused by the acoustic waves. Neglecting the diffusion term, i.e. the second term in the right hand side, the dc acoustoelectric current accompanying the steady state acoustic flux arises simply from the term $n_s E$. The current density can be written

$$J = J_o + J_{AE}$$

where $J_{AE} = \mu q n_s E$ is the acoustoelectric component of the current. When the applied field E_d exceeds the threshold value required for amplification the acoustoelectric current is in the opposite direction to the Ohmic current $J_o = \mu q n E_d$ and subtracts from J_o to produce the 'kink' in the current-voltage curve.

ii) Threshold drift field and Crystal Orientation

It has been shown[23] that in CdS the threshold drift field for amplification of a longitudinal wave equals the calculated value v_s/μ_H, when v_s is the longitudinal sound velocity. However, non-Ohmic behaviour and a build up of ultrasonic flux for the same sample begin to appear at drift field which is only about one-half of that at the amplification threshold.

McFee[23], following an idea of Hutson, put forward the following suggestion to explain the apparently contradictory results:

The departure from Ohmic behaviour which is observed is brought about by the amplification of shear-waves instead of longitudinal sound-waves. Although shear waves propagating along the hexagonal axis do not couple with the drifting carriers, 'off-axis' shear waves whose wave vectors make finite angles with the hexagonal axis, will have a finite coupling with the carriers.

Conclusion

McFee's experimental evidence, taken together with Wang's observations, seem to lead quite naturally to the conclusion, that the decay of the drift current under pulsed conditions is simply caused by the acoustoelectric current which accompanies the build up of the ultrasonic flux.

2.11 Other possible explanations

Tsu[29] and Ashley[30] have suggested that 'Cerenkov' radiation will provide an additional mechanism for the loss of momentum of the electrons when the drift velocity exceeds the velocity of sound. This condition would be sufficient for a 'kink' to occur. However, a quantitative evaluation of the intensity of 'Cerenkov' radiation indicates that it is too small to account for the observed change in the apparent resistance by several orders of magnitude.

Prohofsky[31] has put forward a theory of non-Ohmic behaviour that involves the amplification and non-linear piezoelectric interaction of high-frequency acoustic phonons ($\omega\tau > 1$). The theory requires that there be a net gain at room temperature for phonon modes with frequencies in the range 10^{10}-10^{11} cycle/sec. Because of the rapid increase of phonon losses with increasing frequency, it appears doubtful whether net gain could be realised at these high frequencies. On the other hand, net gain has been observed at ultrasonic frequencies.[7] Experimental evidence would therefore seem to favour a theory involving low frequency acoustic waves.

A quantitative solution has been attempted by Grinberg[32]. He assumed in deriving the formula for current voltage characteristic that the amplification of ultrasound is restricted by the saturation in the drift velocity and the excess power developed in the specimen for $v_d > v_s$ goes to produce heat, not to produce ultrasound.

One reason that a complete solution has not been obtained is that waves over a band of frequencies will be involved. Each wave experiences a slightly different gain and has a different reflection coefficient at the crystal boundaries.

2.12 The Second Current Saturation

Rannestad[35] and Uchida et al[36] have observed two levels of current saturation. The second saturation has been attributed to the off-axial amplification of sound waves. If the off-axial mode of amplification were operative, there would probably not be two distinct levels of current saturation. Since the velocity of sound would then vary monotonically from the value corresponding to shear waves to that of longitudinal waves and the threshold for current saturation would vary monotonically.

Diakonov and Ilisavsky[33] are of the opinion that two levels of current saturation are to be expected if the reflected waves are taken into consideration. After the forward flux has grown sufficiently, the amplitude of the reflected waves achieves such a magnitude that the accompanying acoustoelectric current begins to play a significant role. The current would have to be subtracted from the first saturation current. The second level of current saturation would then be observed.

2.13 Current Oscillations

In some CdS crystals in the amplifying state, the initial decay in the current from the Ohmic value to a saturated value reverses and undergo as several or even continuous oscillations in time.[14] This situation is illustrated in Fig. 2.7. The succeeding current peaks are usually lower than the initial peak, which attains the Ohmic value. The amplitude of the oscillations has been observed to decay with time or remain constant, depending on the magnitude of the drift voltage, the level of illumination, the uniformity of illumination, and the homogeneity of the crystal. The oscillations are directly related to the build up of acoustic flux in the crystal and the accompanying acoustoelectric current.

Similar types of current oscillation have been observed in non-piezoelectric crystals of n-type GaAs or InP under electric fields of a few thousand volts cm^{-1}. The drift velocity in these materials becomes about 10^7 cm sec^{-1} for this applied field, which is much faster than the velocity of sound. The drift velocity is comparable to the zero field thermal velocity of $2{\cdot}5 \times 10^7$ cm sec^{-1} so that the electron system will be in a hot electron state.

In piezoelectric crystals like CdS, the magnitude of the acousto-electric field is proportional to the local acoustic flux density.[12] The magnitude of the flux at a given point within the crystal is determined by the acoustic gain, so that there are regions within the

crystal where the incremental increase in the acoustoelectric field will be greater than the incremental increase in the applied field. In such a situation the average current in a piezoelectric crystal can be expressed in terms of both applied field E_d and the acoustoelectric field E as[37]

$$J = \sigma(E_d - E) \qquad 2.16$$

The quantity σ is the low field conductivity. The differential conductivity of the material (slope of the $J - E_d$ curve) is given by

$$dJ/dE_d = \sigma(1 - dE/dE_d)$$

The threshold for the negative differential conductivity is given by

$$dE/dE_d > 1$$

Therefore, the onset of current oscillations can occur at the point where the resultant change in acoustoelectric current is large enough to produce a negative differential conductivity within the sample. The major consequence of the appearance of a differential resistance in the current-voltage curve is to render the material electrically unstable. As a result the material, initially homogeneous, becomes electrically heterogeneous in an attempt to reach instability.[38]

Current oscillations are attributed to the formation, propagation and destruction of acoustoelectric domains.[37]

2.14 High Field Domain and Current Instability

The formation of a high field 'domain' and its movement through the crystal is one of the most interesting phenomena in the phonon amplification process.[15,37,39,40] By acoustic domain one means a relatively narrow region in the crystal with a high localised electric field and elevated intensity of acoustic flux. The initial current decay in CdS followed by current oscillations is related to the formation of high-field domains.

It is known from the work of Ridley[38] that domains may be formed in those materials which exhibit a 'differential negative conductivity'. He has shown from thermodynamic principles that the field inside a material with differential negative conductivity will break into high and low field regions.

In semiconducting crystals, with resistivities of the order of $1 \sim 10$ Ohm-cm. high field domains are formed near the negative electrode and travel with the velocity of sound through the sample. When the domain reaches the anode, the phonon flux in the domain and the space charge on the edges of the domain are absorbed by the anode and the sample returns to the state which existed when the voltage was just applied. The entire process then repeats in a cyclic manner. The period of current oscillation is given by the sum of the domain formation time and domain transit time.[41]

Sometimes the domain is also formed at the non-uniformities due to changes in resistivity along the crystal.[42] In these cases, something electric in origin can be regarded as the domain source, since the domain formation site is independent of any variation of applied field. The local amplification usually occurs in the non-uniform regions. Domain build up is attributed to the non-uniform distribution of the acoustoelectric current due to local amplification of thermal phonons by supersonic carriers.[40]

2.15 Active Acoustoelectric Oscillator

Recently White and Wang[43] observed that an ultrasonic amplifier driven under d.c. conditions could oscillate in a stable high frequency mode. The oscillation corresponded to a very high overtone of the fundamental acoustic resonance of the thin CdS plate (i.e. the 100th harmonic or greater). The oscillation is distinctly different from the oscillations in current which occur in a high gain ultrasonic amplifier with a period corresponding to an electron transit time, and is due to a build up of acoustic flux. This new oscillation has very pure periodic waves which contain either one frequency or several harmonically related frequencies.

In White and Wang's experiment[43] two opposite faces of a thin (0•1 mm) plate of CdS crystal with the c-axis lying in the plane of the plate were polished optically flat and parallel. Very thin indium layers were diffused to provide electrical contacts. Batteries were used as the d.c. source. The oscillations were detected by monitoring the r-f component of the current passing through the crystal.

When a d.c. voltage is applied, a large number of frequencies grow in amplitude. After a period of mode competition, lasting typically 1 m.sec, one mode dominates and stabilises. Under identical setting of voltages and resistivity the crystal can be made to oscillate in the same mode. In a typical crystal with $\sigma = 1{\cdot}5 \times 10^{-5} \text{Ohm}^{-1}\text{cm}^{-1}$ and 0•1 mm thick, coherent oscillations have been observed with frequencies up

to 900 Mc/s. The frequency was found to be stable to several parts per million. Line width was considerably less than one part per million.

If we imagine that a standing wave is a superposition of two waves travelling in opposite direction then the wave propagating in the direction of the drift velocity $v_d = \mu E$ will be amplified, while the wave propagating in the opposite direction is attenuated. The conditions[44] of amplification are that (1) the energy required by the wave during its forward passage exceeds the loss during its passage in the opposite direction and that (2) during its passage in both directions the phase should change by a multiple of 2π. If both these conditions are fulfilled, the wave amplified increases until the non-linear effects (Section 2.9) prevent its further growth.

Device Potentialities

The frequency of the steady state oscillations depends on the applied voltage and sample conductivity and can therefore be changed simply by superimposing the modulating voltage on the bias voltage. Possible use of this property in generating frequency modulated signals has been discussed by Maines and Paige.[45] The frequency shift with the bias voltage, at a fixed conductivity, is observed[45] typically to be of the order of 10 kc volt^{-1}.

In such an oscillating crystal, the current oscillates and the crystal generates a.c. electrical energy. A significant part of the

energy supplied by the driving source is converted into acoustic vibrations. The device may, therefore, find application as an electrical oscillator as well as an acoustic generator. Both these forms of output can be subject to frequency modulation.

Through the conductivity the frequency also depends upon the incident light intensity. Because of the high Q factor of the modes, extremely small frequency shifts can be measured. One can, therefore, use the acoustoelectric oscillator as a transducer for monitoring such shifts.

Single frequency mode of operation at frequencies up to 500 Mc/s has been observed by Maines and Paige.[45] Round-trip gain is predicted[8] to be possible at a frequency up to 3 Gc/s for CdS and 14 Gc/s for ZnO.

Active Device - Audio signals have been transmitted on a 100 Mc/s carrier wave generated by a CdS oscillator and received on a conventional receiver.[46]

References

1. R.H. Parmenter, Phys. Rev., 89, 990, 1955.

2. J. Bardeen and W. Shockley, Phys. Rev., 80, 72, 1950.

3. M. Born and K. Huang, "Dynamical theory of crystal lattices" London, Oxford, 1954.

4. I.A. Chaban and A.A. Chaban, Soviet Phys.-Solid State, 6, 1913, 1965.

5. H.D. Nine, Phys. Rev. Letters, 4, 359, 1960.

6. A.R. Hutson, Phys. Rev. Letters, 4, 505, 1960.

7. A.R. Hutson, J.H. McFee and D.L. White, Phys. Rev. Letters, 7, 237, 1961.

8. A.R. Hutson and D.L. White, J. Appl. Phys., 33, 40, 1962.

9. D.L. White, J. Appl. Phys., 33, 2547, 1962.

10. W.C. Wang, Phys. Rev. Letters, 9, 443, 1962.

11. G. Weinreich, Phys. Rev., 104, 321, 1956.

12. G. Weinreich and H.G. White, 106, 1104, 1957.

13. P.D. Southgate and H.N. Spector, J. Appl. Phys., 36, 3728, 1965.

13. I. Uchida, T. Ishiguro, Y. Sasaki and T. Suzuki, J. Phys. Soc. Japan, 19, 674, 1964.

14. R.W. Smith, Phys. Rev. Letters, 9, 87, 1962.

15. W. Haydl and C.F. Quati, Appl. Phys. Letters, 7, 45, 1965.

16. V.L. Gurevich, Int. Conf. Phys. Sem. Moscow, 1968, p.891.

17. N. Mikoshiba and H. Ozaki, Int. Conf. II-VI Sem. Comp. Brown University, U.S.A., 1967, p.910.

18. P.N. Bucher and N.R. Ogg, Brit. J. Appl. Phys., 1, 1271, 1968; 2, 333, 1969.

19. H. Kroger, Appl. Phys. Letters, 4, 190, 1964.

20. B. Tell, Phys. Rev., 136, A772, 1964.

21. C. Elbaum and R. Truell, Appl. Phys. Letters, 4, 212, 1964.

22. A.R. Hutson, Phys. Rev. Letters, 9, 296, 1962.

23. J.H. McFee, J. Appl. Phys., 34, 1548, 1963.

24. W. Shockley, Bell Syst. Tech. J., 30, 990, 1951.

25. J.B. Gunn, IBM Res. and Developm., 8, 141, 1964.

26. H.R. Carleton, H. Kroger and E.W. Prohofsky, Proc. IEEE, 53, 1452, 1965.

27. L. Esaki, Phys. Rev. Letters, 8, 4, 1962.

28. A.R. Moore, Phys. Rev. Letters, 12, 47, 1964.

29. R. Tsu, J. Appl. Phys., 35, 125, 1964.

30. J.C. Ashley, J. Appl. Phys., 36, 528, 1965.

31. E.W. Prohofsky, Phys. Rev., 134, A1302, 1964.

32. A.A. Grinberg, Sovt. Phys.-Doklady, 9, 301, 1964.

33. A.M. Diakonov and Yu. V. Ilisavsky, Int. Conf. Phys. Sem. Moscow, 1968, p.977.

34. N.I. Meyer and M.H. Jorgensen, Phys. Letters, 20, 450, 1966.

35. A. Rannestad, Phys. Rev., 155, 744, 1967.

36. I. Uchida and T. Ishiguro, Int. Conf. II-VI Compound,Brown University, U.S.A. 1967, p.963.

37. W.H. Haydl, K. Harker and C.F. Quate, J. Appl. Phys., 38, 4295, 1967.

38. B.K. Ridley, Proc. Phys. Soc. (London), 82, 954, 1963.

39. W.H. Haydl and C.F. Quate, Phys. Letters, 20, 463, 1966.

40. A. Ishida, C. Hamaguchi and Y. Inuishi, Proc. Int. Conf. Phys. Sem. Kyoto, 1966, p.469.

41. A. Ishida and Y. Inuishi, Int. Conf. II-VI Compounds, Brown University, U.S.A. 1967, p.971.

42. G.S. Hobson and E.G.S. Paige, Proc. Int. Conf. Phys. Sem. Kyoto, 1966, p.464.

43. D.L. White and W.C. Wang, Phys. Rev., 149, 628, 1966.

44. V.L. Gurevich and B.D. Laikhtman, Sovt. Phys. Solid State, 6, 2299, 1965.

45. J.D. Maines and E.G.S. Paige, Electronics Letters, 3, 459, 1967.

46. Wireless World, February 1968, p.685.

CHAPTER III

EXPERIMENTAL PRELIMINARIES

INTRODUCTION

The current voltage characteristics of a piezoelectric semiconductor show a departure from Ohm's Law at a certain critical field[1] (Section 2.10). McFee[2] has shown that current saturation in cadmium sulphide occurs under the condition $v_d = \mu_d E_c = v_s$, where v_d, μ_d, E_e, and v_s are the electron drift velocity, the electron drift mobility, the threshold drift field and the appropriate velocity of sound, respectively.

Since the electron mobility in CdS is about 250 $cm^2 V^{-1} sec^{-1}$, while the shear wave velocity is $1{\cdot}75 \times 10^5$ cm sec^{-1}, and the longitudinal velocity is $4{\cdot}4 \times 10^5$ cm sec^{-1}, a drift field greater than 700 V cm^{-1} must be applied across the crystal to obtain a 'kink' in the current voltage characteristics.

The current saturation in CdS has been ascribed to the coupling between drifting electrons and ultrasonic waves.[1,2] If strong coupling is to be observed between the electrons and the waves, then the electron concentration must be high. The drift field across the crystal therefore should be in the form of a low duty cycle pulsed voltage, if undue heating is to be avoided. Because the maximum

voltage output from the pulse generator available in the Department was 100 Volts, it was necessary to build a pulse generator.

The drift mobility obtained from a measurement for threshold field for saturation is a measure of the drift velocity under unit applied electric field and is trap controlled. The electron mobility will be reduced if the electrons spend an appreciable time in traps. The Hall mobility $\mu_H = R_H\sigma$ and the corresponding Hall drift velocity $v_{dH} = R_H J$, on the other hand, are thermal equilibrium quantities and are independent of trapping effects.

One of the main objects of the work described in this thesis was to compare the measured Hall and drift mobilities of CdS over the temperature range from 90 to 300^{o}K. This should in principle yield information about the electron trapping processes which limit the drift mobility. The preparation of the samples and apparatus used to obtain the required information is described below.

PART A

CRYSTAL GROWTH AND SPECIMEN PREPARATION

3.1 The Crystals

Most of the samples investigated in this work were obtained from crystals grown in this laboratory by D.L. Clark and K.F. Burr. The samples were cut and ground from large undoped boules of CdS, unless otherwise stated.

A few AEI crystals were also investigated.

Crystal Growth

The method originally employed in this department to grow large CdS crystals utilised a modified Piper Polich[3] technique as described by Clark and Woods.[4] In essence the crystal is grown from the vapour phase in an ampoule which communicates via a constriction or orifice with an outer argon filled jacket.

As indicated by Clark and Woods,[4] nonstoichiometry in the starting charge dominates the growth mechanism in CdS in sealed evacuated tubes, making controlled growth difficult. To overcome these problems Clark and Woods[5] developed a vacuum growth technique where the vapour pressure of one of the components can be controlled independently of the growth temperature. In this method[5] the growth ampoule is provided with a tail which contains a reservoir of either cadmium or sulphur which can be held at a fixed temperature throughout

the growth cycle. Thus rather than allowing the system to establish the partial pressure conditions determined largely by the nature of the charge, a known partial pressure is obtained. The temperature of the reservoir containing cadmium or sulphur is controlled using a thermocouple attached to the tail. The furnace profiles are such that the bottom of the reservoir tail is the coldest part of the whole enclosure. The growth tube is drawn upwards by a rack and pinion drive. During the initial stages of pulling, excess cadmium or sulphur which was added to the charge of CdS sublimes into the tail forming the reservoir from which the required partial pressure can be established. (For a detailed description of the method the reader is referred to reference 5.).

Boules produced by this method[5] are usually yellow in colour, although those grown in the highest pressures of cadmium are slightly darker. Clark and Woods have shown that crystals grown under high partial pressures of cadmium are semiconducting at room temperature with resistivities of the order of 1 ~ 10 Ohm-cm. Crystals grown in the lower pressures of cadmium are photosensitive semi-insulators. Two photosensitive crystals Nos. 78 and 116, which were chosen for the drift and Hall mobility measurements, described in this thesis, were grown in atmospheres where the sulphur pressure was much higher than the cadmium (the sulphur pressures were 98 torr and one atmosphere respectively).

3.2 Sample Preparation

The boules were cut into thick slices containing the c-axis, and then into bars with the long dimension either parallel or perpendicular to the c-axis.

i) Crystal Orientation (X-ray method)

Preliminary examination of the crystal orientation was carried out using the Laue back reflection X-ray technique. This method was also useful in assessing the degree of polycrystallinity of the samples. Many crystals could be cleaved along $(1\bar{2}10)$ planes, when this did not occur a face which was aligned parallel to an (0001) basal plane was identified by the back reflection method. Fig. 3.1 shows a typical back reflection photograph of a CdS crystal with the incident X-ray beam parallel to the c-axis.

ii) Crystal Cutting

The cutting of the preliminary oriented crystal into slices was carried out at 6000 r.p.m. with a 5" diameter (0·015" thick) diamond impregnated disc cooled in a jet of soluble oil. The boule was mounted on a brass block with Lakeside 70C cement; the block being gripped in the rotatable chuck of the automatic cutting machine. Two planes at right angles were then cut through.

iii) Optical Orientation

A final check on the orientation of the sample was carried out with the aid of a polarising microscope. In hexagonal CdS the optic

axis coincides with the c-axis. The sample was placed on the stage of the polarising microscope, between crossed polaroids. The interference figure was observed when highly convergent illumination was used.

Fig. 3.2 shows typical interference figure when the optic axis of a CdS crystal is parallel to the axis of the microscope. (For a detailed description of the theory the reader is referred to reference 6). The centre of the isogyre (cross) in the interference figure marks the position of the optic axis. When the optic axis coincides with that of the microscope, the centre of the isogyre will coincide with the intersection of the cross wires in the eye piece (Fig. 3.2a).

However, if the optic axis is inclined to the axis of the microscope, the centre of the isogyre will be displaced from the intersection of the cross wires (Fig.3.2b). If the centre of the isogyre does not coincide with the centre of the field, the point of intersection of the arms of the cross will move around the centre of the field of view when the stage is rotated and describe a circle before returning to its original position. The intersection of the cross marks the point of emergence of the optic axis, and its deviation from the centre of the field is a measure of the angle between the optic axis and the axis of the microscope.

If the centre of the isogyre did not coincide with the cross wire of the microscope, the lower surface of the crystal was ground off until the centre of the cross did coincide with the cross wires. The

upper surface of the crystal was made parallel by mounting and polishing the sample in an accurately machined steel jig.

iv) Lapping and Polishing

The oriented slices were cut into bars with their long dimension parallel or perpendicular to the c-axis. These rectangular bars were then lapped to final dimensions which were typically 8 x 2 x 2 mm^3.

With two faces cut at right angles, the sample was then mounted in an accurately machined steel jig (using Durofix) which allowed the other faces of the rectangular parallelepiped to be ground. Later the original faces were also ground to remove damage caused during cutting. The grinding was done with a paste of 800 grade carborundum powder on a flat glass plate. Finally the surfaces were polished on a Hyprocel self adhesive disc lap with different hyprez diamond compounds containing 6,3,1 and lastly 1/4 microsize diamond particles.

3.3 Etching

It is well known that mechanical polishing produces damage in the crystal structure of CdS at the surface so that a chemical etch is essential. Prior to etching the samples were rinsed in isopropyl alcohol to remove any polishing solution.

A range of etching solutions was investigated to determine which was the most suitable. The solutions tried included (a) orthophosphoric acid of varying concentrations at different temperatures, (b) a

sulphuric acid potassium permanganate solution at room temperature[7] and (c) chromic acid.[8]

The most successful solution (incidentally it also produced well defined etch pits) was chromic acid at 70°C for about 3-5 minutes. The chromic acid was prepared by dissolving 700 grams of chromic oxide in two litres of distilled water and adding 100 cc. of concentrated sulphuric acid to the solution. After cooling, a small quantity of this solution was diluted three times to obtain the required etchant. The hot solution was progressively diluted before the crystal was removed.

Handling the specimen after etching was reduced to a minimum. The use of tweezers is apt to lead to contamination and significant surface damage.

3.4 Ohmic Contacts

It is well known that indium forms Ohmic contacts on CdS crystals.[9] The basis of the method of applying Ohmic contacts was to evaporate a layer of indium on to the crystal in a vacuum of 10^{-5} torr. It was found that indium does indeed form an electron injecting contact, provided that indium is applied in a carefully controlled manner.

Hall Contacts

Conventional Hall effect measurements on a rectangular parallelepiped Hall sample (dimensions 8 x 2 x 1·5 mm^3) require six Ohmic contacts.

The contact areas were first coated with evaporated indium layers approximately 1 μm thick using high vacuum techniques. Indium was initially outgassed before being evaporated from a molybdenum strip on to the sample via a suitable copper mask. Two small area contacts (about 0·5 mm diameter) were used as Hall voltage and potential probes (spaced 2 mm apart) at each side of the sample. Two current contacts covered the entire end faces of the sample.

Small discs of indium (0·5 mm diameter) were pressed on to the side contacts while an L-shaped indium strip ($\sim$ 5·0 x 2·0 x 0·5 mm^3) was pressed to each end face of the sample. Then the free ends of the L-shaped strips were pressed against a (0·3 mm thick) pyrex cover slip to provide a firm mount for the sample. Wedge shaped indium strips (about 3 mm long) were pressed on to the coverslip with the apex of the wedge just touching the side contacts.

After that the sample with indium contacts was heated in an atmosphere of dry nitrogen on a molybdenum strip heater at about 165^{o}C, just over the melting point of indium, for 1-2 mins. Prior to this the cover slip was cleaned by hydrogen bombardment for about 5 minutes to ensure a good bond with the indium. The net result was a mounted sample with six ohmic contacts. A photograph of a mounted sample is shown in Fig. 5.3a. Enamelled copper wire (35 gauge) was soldered to the ends of the indium strips using a miniature iron. In Fig. 5.3a, the terminals marked I-I were for the applied voltage, v_c-v_c for the

measurement of conductivity and v_H-v_H for the Hall voltage. Also shown are two spare terminals and an indium dot for soldering one of the two copper-constant thermocouples.

The technique described above results in good Ohmic contacts. As a check I-V characteristics were measured with the samples under illumination. A linear relationship was generally found with either polarity of the applied voltage (maximum 10 V d.c.). Although not conclusive these measurements suggested that the contacts were reasonably Ohmic.

Contacts for current voltage measurements

The drift voltage for current voltage characteristics measurements was applied between the large area end contacts of a typical sample dimensions 7 x 2 x 1·5 mm^3. The drift current was therefore parallel to the largest dimension.

Contacts for Potential Distribution Measurements

In order to probe the field distribution along the length of the sample, a row of equally spaced (1 mm apart) small circular layers of evaporated indium dots (about 0·15 mm diameter) was deposited along the length of the sample. All these contacts were made by vapour deposition of indium. The crystal was then heated in an atmosphere of dry nitrogen on a tungsten strip heater. The sample was held at about 165^oC for 1-2 minutes. The evaporated indium then wetted the sample and diffused into the crystal slightly.

PART B

APPARATUS AND EXPERIMENTAL ARRANGEMENT

3.5 Drift-field Pulse Generator

The high voltage pulse generator which was built is basically a simple electronic switch.[10] This switch could be operated up to 4·5 kv d.c. by a low voltage Solartron pulse generator (type GO1101). This latter pulse generator has a continuously variable pulse deviation from 1μsec to 100 msec at a repetition rate between 10 and 5 x 10^5 pulses per second with an amplitude from $\pm$0·5 volt to $\pm$ 100 volts.

A Mullard pentode type EL360 was selected[10] as the switching valve. This has maximum operating parameters of i_a = 4·0A; P_a = 10 watts; v_a = 5 kv; v_{g_2} = 500 v with a 6·3 volt 1·27 ampere heater. The circuit diagram of the high voltage pulse generator is shown in Fig. 3.4. The designed repetition rate was 50 p.p.s. with a pulse duration of 100μsec, i.e. a duty cycle of 0·005. Two 0·1 μF, 8 kv d.c. working capacitors were used in series to protect the Solartron pulse generator. A negative high voltage bias supply (Fig. 3.5b) was used to obtain a negative going pulse across the anode load (the CdS crystal) so that the load current could be displayed conveniently on an oscilloscope. The voltage devloped across the series resistor R by the load current was the quantity actually displayed. The negative high voltage power unit (Fig.3.5b) was capable of delivering 4·5 kv at 10 mA d.c.

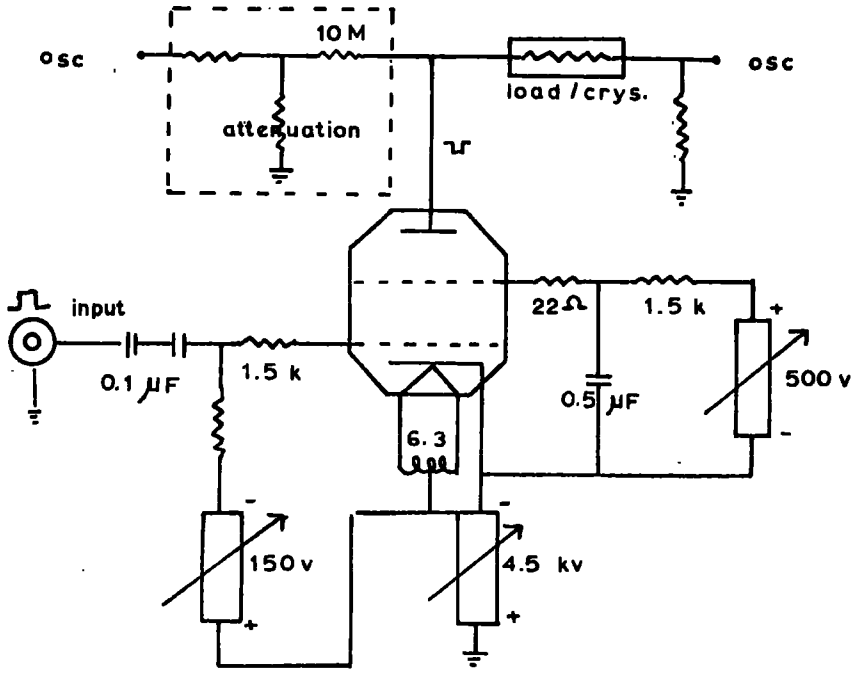

Fig. 3.4 Circuit diagram of the High Voltage Pulse generator.

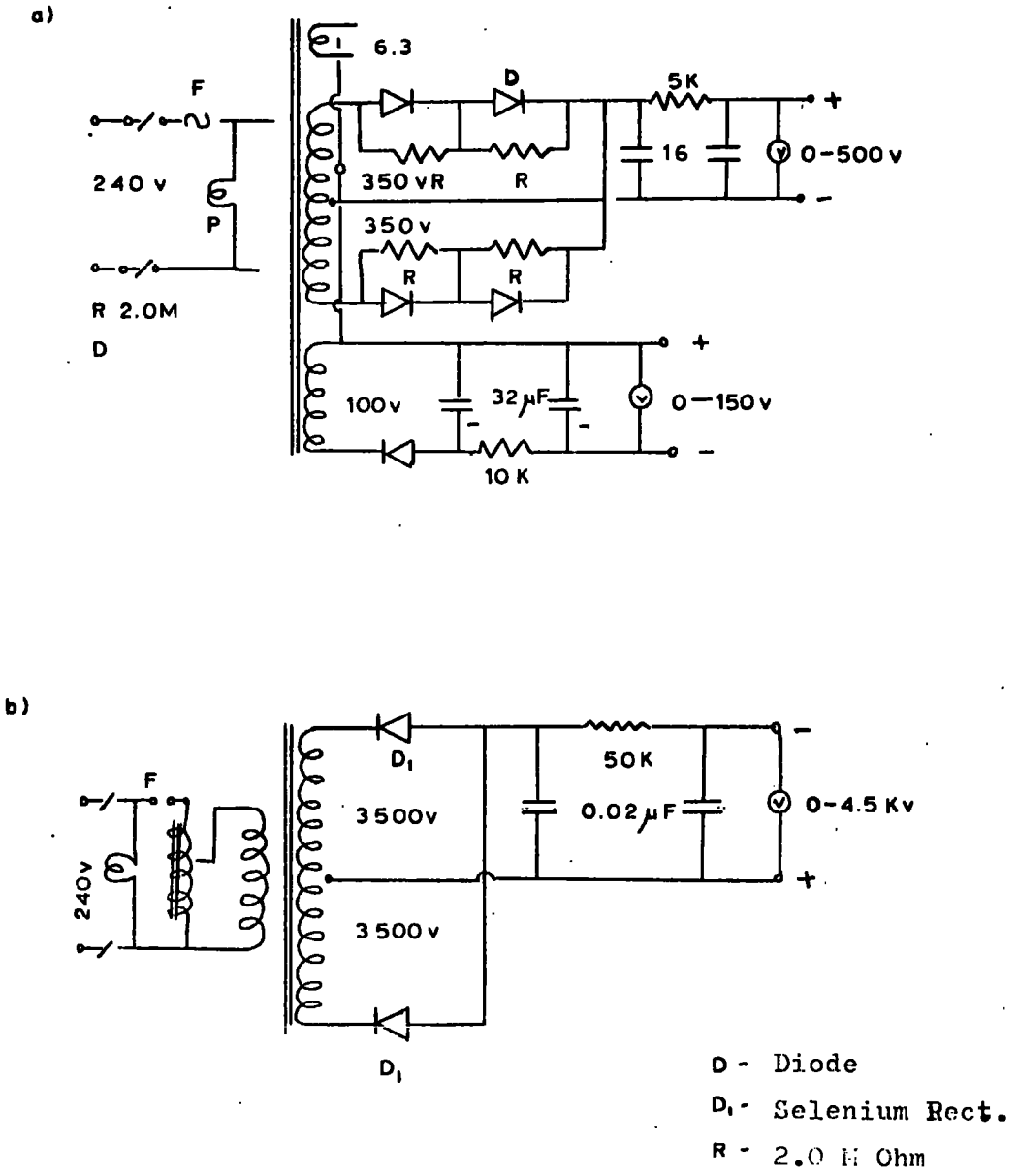

Fig. 3.5 (a) Circuit diagram for screen and control grid supply,
(b) Negative High Voltage (4.5 KV) bias supply.

The control grid and the screen grid bias supply circuits of the EL360 are shown in Fig.3.5a. The grid and screen biases were made adjustable so that the operating characteristics could be changed for very high voltage pulses. In operation the pentode was biased beyond cut-off with 75 volts negative between grid and cathode. The valve was switched on with 100 volt positive pulses applied to the control grid. The screen grid bias was adjusted between 100 and 250 volts depending on the load current.

The maximum pulse output was 4·0 kv at a maximum current of 2 amperes with a duty cycle of less than 0·001. With a load of 100 k ohms the pulse rise time was better than 0·2 μsec and the decay time was of the order of 10 μsec.

3.6 Experimental arrangement to measure the current-voltage characteristics

The experimental arrangement used to measure the current-voltage characteristics in cadmium sulphide is shown in block diagram form in Fig.3.6. A resistor was connected in series with the CdS on the earthy side and the voltage developed across it by the series current in the crystal was measured on a Tektronix 545A oscilloscope with a type 1A1 dual-trace plug in unit. The CdS crystal and the series resistor were connected across the output of the pulser, and the magnitude of the voltage pulse across the combination was measured on the oscilloscope via an attenuator (Fig.3.4).

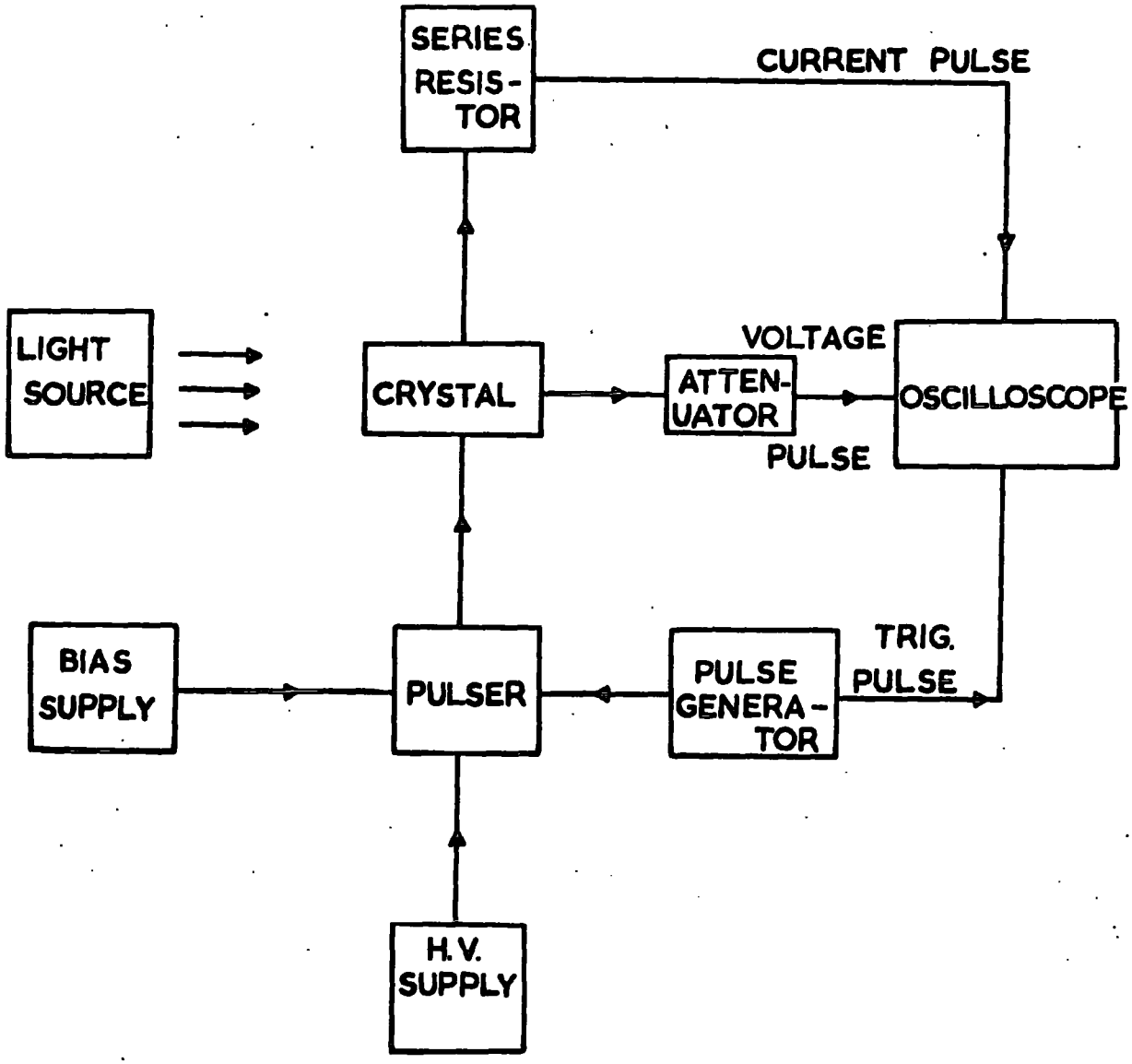

Fig. 3.6 EXPERIMENTAL ARRANGEMENT. (IN BLOCK DIAGRAM)

Between 10 and 50 100v pulses per second with width between 5 and 100μsec were fed to the input of the pulser and the triggering circuit of the oscilloscope (Fig.3.6).

A suitably filtered tungsten lamp was used to illuminate the crystal with visible radiation. The optical system is described in Section 3.8.

3.7 The Cryostat

An all metal cryostat for photo Hall and drift mobility measurements was designed and built in this laboratory. The cryostat was designed so that the Hall sample could be provided with six electrical leads and held at a known temperature in the range 77^{o}K to 400^{o}K, in a magnetic field and under illumination.

A diagram of the cryostat is shown in Fig.3.7. The upper part of the cryostat consists of a nitrogen container N and an insulation space separating the nitrogen container from the outside wall. A nickel silver tube, T , runs through the nitrogen container and contains the exchange gas tube. A multipin socket has been provided on the top of the cryostat for electrical and thermocouple leads to the sample holders. The bottom of the nitrogen container is attached to a nickel silver tube via a copper block C. The lower end of the nickel silver tube is connected to the sample holder. The sample holder can be isolated from the liquid nitrogen container by evacuating the exchange space. In order to heat the sample a nichrome heater H is provided

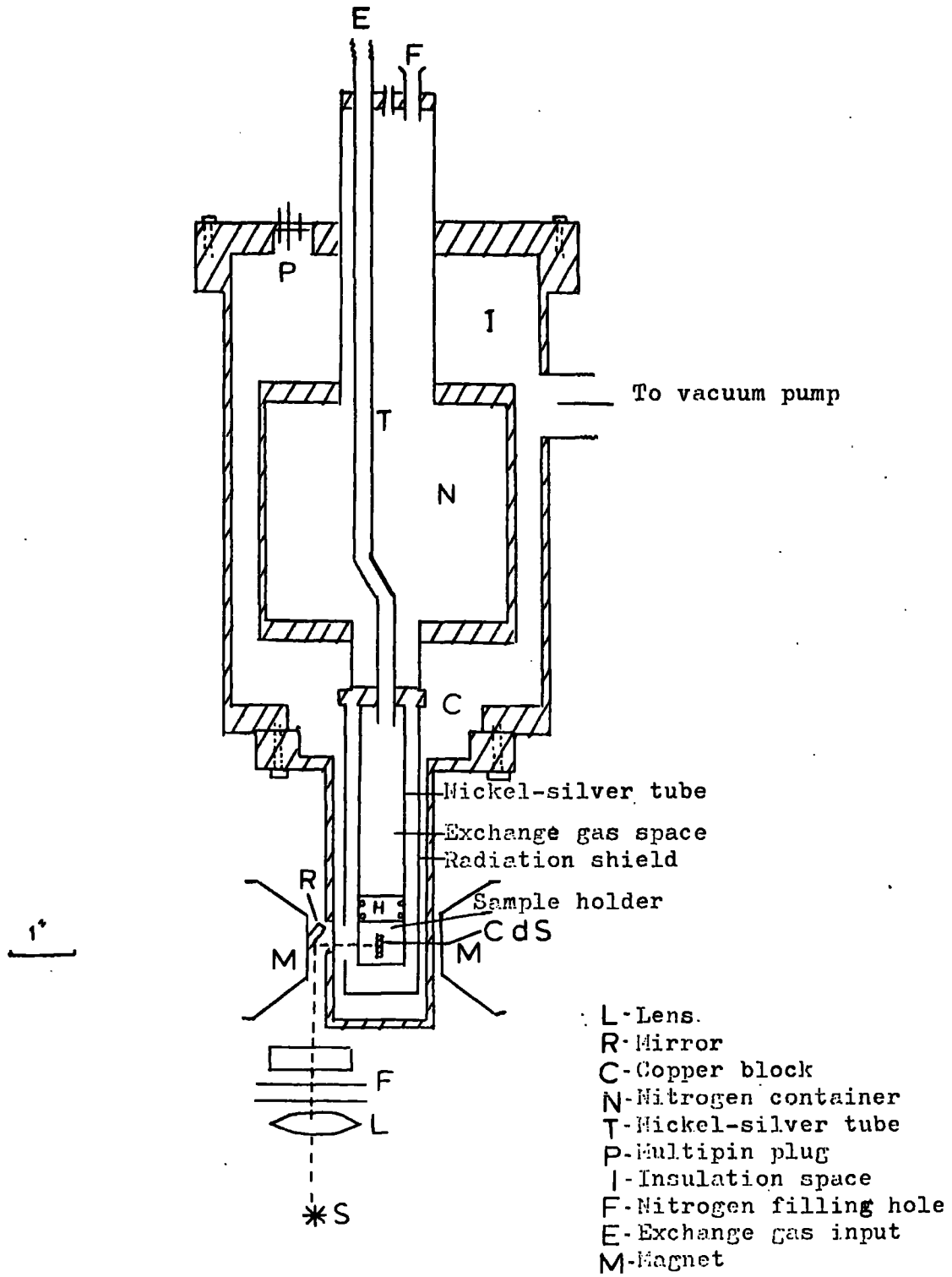

Fig. 3.7. The Cryostat, Magnet, and the Optical System.

which is wound round the shaft of the sample support. The sample holder is surrounded by a detachable copper radiation shield which is connected to the nitrogen container at C. The tail of the cryostat has been fitted with a polished silica window and the inner radiation shield contains a hole to admit light to the sample.

The multipin socket fitted on the top of the cryostat has 12 pin points. Six of these were used for providing electrical leads to the Hall sample, two for the heater (24 V d.c.), and four for 2 copper-constantan (40 gauge) thermocouples. Enamelled copper (35 gauge) wire was used for the electrical leads to the Hall sample. One of the two current leads was insulated with Refrasil and provided with high voltage drift field lead. The junctions of the copper-constantan thermocouples were prepared by spot welding. Two couples were used to monitor the temperature of the sample holder and that of the pyrex cover slip near the sample.2 thermocouples were used to establish the efficiency of the thermal contact between the block and the specimen.

The sample was illuminated with visible and infrared radiation by reflection from a silvered mirror placed on the face of one pole of the magnet adjacent to the polished silica window.

Operation - The cryostat was evacuated to about 10^{-5} torr using an oil diffusion pump backed by a conventional rotary pump. The nitrogen container was filled with liquid nitrogen and the exchange tube was

filled with dry nitrogen. When the desired temperature was reached the exchange gas space was evacuated, thereby reducing the thermal contact and isolating the sample thermally. A heater wound round the copper block enabled any desired temperature to be reached within 5 10 minutes. The rate of temperature change after reaching the required temperature was such that the reading could be taken with no more than $0{\cdot}5^{o}C$ change in the sample temperature over a period of 5 minutes. There was little or no temperature gradient along the specimen because of the large thermal conductivity of the copper support block.

3.8 The Magnet and the Optical System

The magnet was a medium size air cooled electromagnet (2" core dia. tapered to 1") which provided a magnetic induction of about 2,500 gauss at a gap of 5 cm with a current of 2 amperes. The current was supplied to the magnet from a 200 volt d.c. source in series with a suitable rheostat. The magnetic field was measured with Newport (type H) Hall effect magnetometer accurate to 2 per cent.

The optical system is illustrated in Fig. 3.7. The glass lens L allowed the source to be placed well outside the field of the electromagnet M. The mirror R was used to reflect the radiation through a right angle on to the CdS specimen.

To illuminate the sample with band gap radiation a filtered 6V 48 Watt tungsten lamp was used. The specimen was uniformly

illuminated by adjusting the focus of the lamp. Light from the lamp was passed through a condenser lens, a 0·52 μm wide band interference filter and a 1·0 cm path of 10% solution of copper sulphate. The intensity was varied by 3 orders of magnitude using neutral density filters(max. intensity of filtered light ~ 120 ft.c).

To make the measurements under infrared quenching conditions the sample was illuminated with light from a second 48W tungsten lamp which passed through an OX2 chance glass filter (transmission 0·75 to 4·5 μm). 240 V ac passed through a constant voltage harmonic filtered transformer (type CVH125A) was used as a stabilised power source to the lamp transformers.

3.9 The Photo-Hall Measuring Circuit

Hall effect measurements in photoconductors such as cadmium sulphide which are insulating in the dark are difficult to make because of the high impedance and any space charge there may be near non-Ohmic current electrodes. However, in photoconducting samples the carrier concentration can be increased by illumination and the Hall voltage is correspondingly simpler to measure.

Fig. 3.8 shows a schematic diagram of the switching arrangements employed in the photo-Hall measuring circuit. Current from a battery B was fed via the reversing switch R and a calibrated resistor through the specimen (Fig. 3.8a). By adjusting the tappings of the battery and the potential divider, it was possible to adjust the potential

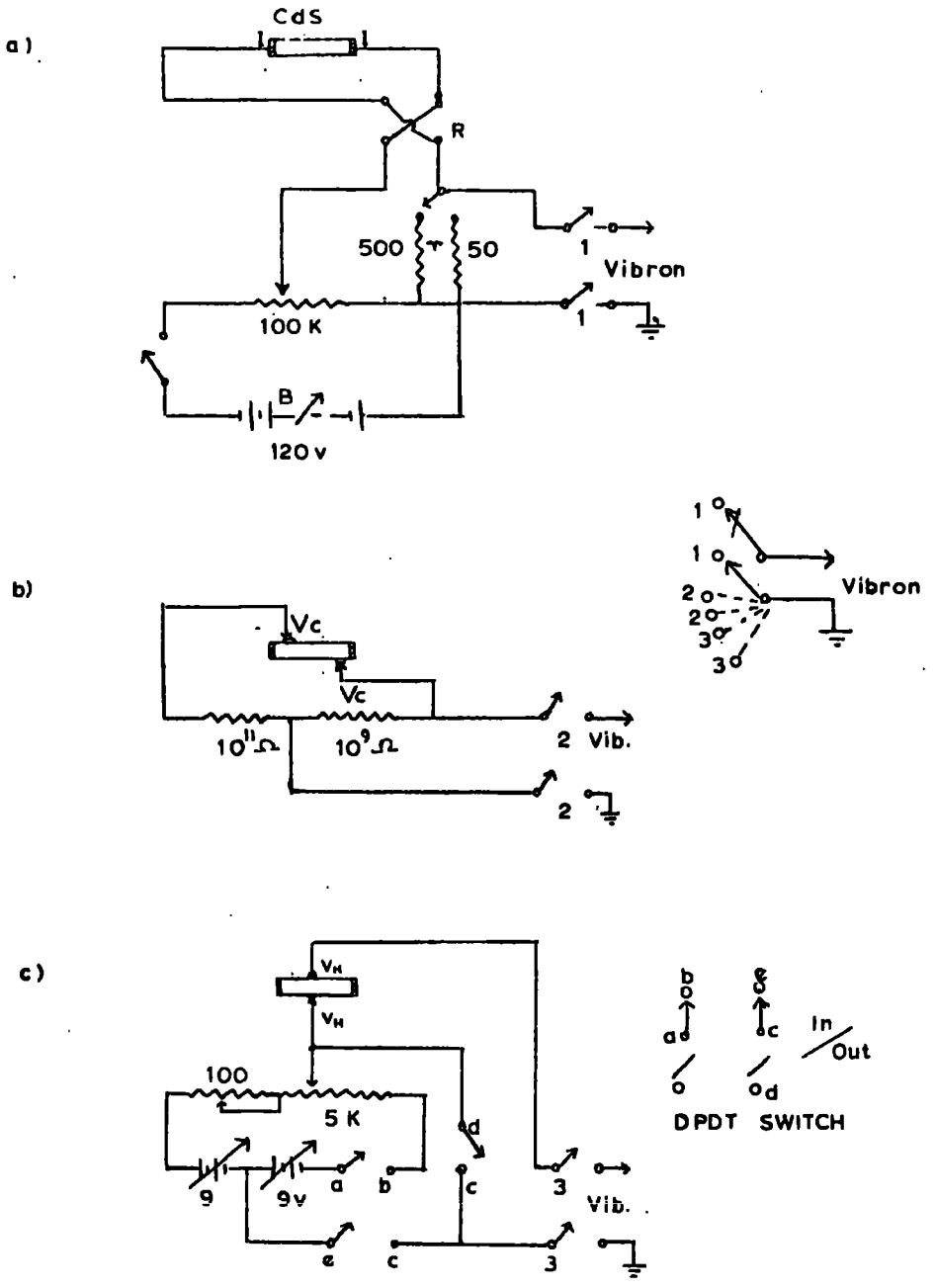

Fig.3.8 Circuit used to measure the Hall effect with vibron electrometer.

(a) To measure current (V_I), (b) to measure conductivity (V_C) and (c) to measure Hall voltage (V_H) including the bucking off circuit.

applied to the specimen from 100 volts to a few millivolts. The current passing through the specimen was determined by measuring the voltage (V_I) across a calibrated resistor.

The conductivity of the specimen was found by measuring the potential drop across the outer pair of the potential contacts. In practice a potential divider with a total resistance of 10^{11} Ω (ratio 100:1) was employed (Fig. 3.8b). The potential divider was necessary as the Vibron electrometer has a maximum input range of 1 volt only.

The central pair of potential contacts was used to measure the Hall voltage V_H. During the specimen preparation the two Hall contacts could not be accurately positioned on an equipotential line opposite to one another, and an appreciable out-of-balance voltage appeared at these contacts with normal current flow in zero magnetic field. This voltage was bucked off with the separate circuit arrangement shown in Fig. 3.8c.

The measurements were made by switching the appropriate voltages to the input of the Vibron electrometer (model 33B-2) with $\sim 10^{14}$ ohms input resistance. The electrometer has five ranges to cover input voltages between 0·2 mV and 1000 mV of either polarity. The accuracy of the indicating meter is better than ±1% of full scale. The same Vibron was used alternately with suitable switching arrangements to measure V_I, V_c and V_H. It was possible to measure Hall voltages for specimens with resistance up to 10^9 ohms with this arrangement.

References

1. R.W. Smith, Phys. Rev. Letters, 9, 87, 1962.

2. J.H. McFee, J. Appl. Phys., 34, 1548, 1963.

3. W.W. Piper and S.J. Polich, J. Appl. Phys., 32, 1278, 1961.

4. L. Clark and J. Woods, Brit. J. Appl. Phys., 17, 319, 1966.

5. L. Clark and J. Woods, J. Crystal Growth, 3/4, 126, 1968.

6. P.F. Kerr, "Optical Mineralogy", McGraw Hill, 3rd Ediction, p.86.

7. J.E. Rowe and R.A. Foreman, J. Appl. Phys., 39, 1917, 1968.

8. L. Clark and J. Woods, J. Sc. Inst., 42, 51, 1965.

9. F.A. Kroger, G. Deimer and H.A. Klasens, Phys. Rev., 103, 279, 1956.

10. N.B. Snyder, M.Sc. Thesis, University of St. Andrews, 1966.

CHAPTER IV

NON-OHMIC BEHAVIOUR AND DRIFT MOBILITY IN CdS AT ROOM TEMPERATURE

INTRODUCTION

The experimental work on which this thesis is based is reported in this and the following two chapters. Before discussing the experiments conducted over a range of temperatures which were designed to elucidate the trapping processes involved, a variety of effects observed at room temperature will be described.

In the first place the non-Ohmic behaviour and the Hall coefficient in photoconducting cadmium sulphide were measured at room temperature. The current-voltage characteristics of CdS crystals with resistivities less than 10^5 Ohm-cm. show a departure from Ohm's law at a certain critical field. It has been shown[1] that current saturation occurs under the condition $v_d = \mu_d E_c = v_s$, where v_d, μ_d, E_c and v_s are the electron drift velocity, the electron drift mobility, the threshold drift field and velocity of sound respectively.

The electron drift mobility μ_d was estimated from the threshold drift field, using the relation $\mu_d E_c = v_s$. The experiment was performed at different conductivities which were produced by changing the intensity of the light falling on the sample. The photo-Hall mobility μ_H was measured using the conventional dc method and its

magnitude was compared with μ_d for different crystal orientations and conductivities.

The spatial distribution of the electric field in the photoconductive samples was also measured in order to investigate the uniformity of the crystals. The effects of inhomogeneities on current saturation and current oscillations have been investigated and are quite important.

This chapter is divided into three parts: in Part A, some typical results of current saturation and oscillations in uniform as well as non-uniform samples are described. Part B, deals with the effects of sample inhomogeneity or current saturation and oscillations, and Part C, is concerned with measurements of the Hall and drift mobilities as a function of conductivity.

PART A

CURRENT SATURATION AND OSCILLATIONS

4.1 Current saturation

The various effects which accompany acoustoelectric saturation in CdS are best illustrated by describing the results obtained in one particular crystal - D116 (dark conductivity $< 10^{-9}$ ohm^{-1}cm^{-1}) in which current saturation was observed.

The sample with dimensions 3·35 x 2·25 x 1·65 mm^3, was cut from the boule with its long dimension in the direction of carrier propagation. The c-axis was at right angles to the long dimension of the sample. Large area ohmic contacts of indium were made to the optically flat small ends and the drift voltage was applied to these in 10 ~ 100 μsec pulses at a duty cycle low enough to avoid heating (about 25-10 cps).

When a pulsed voltage greater than threshold was applied ($>$ 850 volts cm^{-1}) to the uniformly illuminated crystal the transient behaviour was as depicted in Fig.4.1a (at $\sigma \sim 4{\cdot}0 \times 10^{-3}$ ohm^{-1}cm^{-1}). The lower trace shows the waveform of the voltage applied to the CdS crystal and the upper trace the resulting drift current. With voltages less than the threshold ($<$ 300 volts) the current waveform was similar to the voltage waveform, but as the applied voltage was increased, the current waveform became progressively more deformed.

On application of the voltage pulse the resulting drift current (Fig.4.1a, upper trace) initially increased abruptly to a maximum value (Ohm's Law value) and then decayed in about 5 μsec toward a final steady state value, after several cycles of damping oscillations.

Fig.4.1b illustrates the effect on current saturation of changing the sample conductivity from ($6{\cdot}0 \times 10^{-4}$ to $3{\cdot}0 \times 10^{-4}$ $ohm^{-1}cm^{-1}$). With increasing conductivity, the build up time, i.e. the time required for the current to reach a steady state, decreased from ~40 μsec to 15 μsec.

In Fig.4.1c (fifth trace from the bottom) an exaggerated build up time is shown which was larger than 70 μsec at $\sigma \sim 5{\cdot}0 \times 10^{-5} ohm^{-1}cm^{-1}$. The lowest traces do not show any saturation because the applied field was less than critical (400 volts). With increasing applied voltage to 600 volts ($\sim$ 1·5 threshold voltage) the build up time for current saturation decreased to less than 10 μsec, showing a two step current saturation in the upper two curves.

4.2 Current Oscillations

During the experiments on current saturation current oscillations have been observed in many crystals.

(i) Damped Oscillations

The current oscillations in crystal D116(2) which can be seen in Figs.4.1a and 4.1b are damped oscillations. In the illuminated crystal, the current begins to saturate at a certain threshold field and the oscillations are damped within a few (2-3) cycles. The damping of the oscillations can be seen more clearly in Fig.4.2a when the conductivity $\sigma > 3{\cdot}0 \times 10^{-4}$ ohm^{-1}cm^{-1}. Upon application of a pulse voltage (25 μsec 25 cps) higher than 300 volts the current rapidly rose to the ohmic value (see the four lower curves of Fig.4.2a) and was maintained for about 1 μsec. The current then fell rapidly to a saturated value. Approximately 3 μsec after the beginning of the pulse, the current had risen to a second maximum, but did not regain the original value. The current oscillated in this attenuated fashion with each succeeding maximum smaller than its predecessor. The current eventually settled down to a steady state value in $10 \sim 15\mu$ sec.

The Period T of the current oscillation was found to be approximately equal to $\frac{1}{v_s}$ or $\frac{21}{v_s}$ (where 1 is the length of the crystal and $v_s = 1{\cdot}75 \times 10^5$cm/sec) depending on the conductivity of the sample. At conductivities greater than $3{\cdot}0 \times 10^{-4}$ ohm^{-1}cm^{-1} oscillations with

a period about 2 microsec ($\sim$ 500 kc/s) were observed (four lower curves of Fig.4.2a). This was the time required for the sound wave to propagate from one end of the 3·35 mm long sample to the other.

A second mode of oscillation with a period different from the first by a factor of two ($\simeq \frac{2l}{v_s}$) was also observed and became increasingly apparent, as shown in the upper four curves of Fig.4.2a as the conductivity decreased from $3 \cdot 0 \times 10^{-4}$ ohm^{-1}cm^{-1} to $1 \cdot 0 \times 10^{-4}$ ohm^{-1}cm^{-1}. All the curves were obtained with a fixed bias voltage of 400 volts.

(ii) Undamped Oscillations

In some crystals Persistent current oscillations were observed with applied field strengths higher than threshold. The CdS crystal examined was another piece from the same boule D116 [sample D116(3)], with dimensions $6 \cdot 7 \times 2 \cdot 2 \times 1 \cdot 2$ mm^3. The electric field was applied along the long dimension which in this sample was perpendicular to the c-axis. Ohmic contact was made with indium to the parallel polished faces of the crystal.

Upon application of a pulsed voltage (40 μsec 25 cps) greater than 500 volts ($\sigma = 4 \cdot 0 \times 10^{-4}$ ohm^{-1}cm^{-1}) the oscillatory behaviour of the current was as shown in Fig.4.2b. The amplitude of the oscillation was found to increase with increasing field (Fig.4.2b) and reached a maximum value of about 40% of the total current (Fig.4.2c) at 800 volts. Further increase in the drift voltage led to a decrease in the amplitude of oscillations. The period was 3·3 μsec, which is

approximately equal to the shear wave transit time between electrodes spaced at 6•7 mm apart.

The potential distribution under uniform band gap illumination (tungsten light passing through a 0•52 μm interference filter) is shown in Fig.4.7a (the technique of measurements is described in sec.4.6). The curve (Fig.4.7a) illustrates that there was a continuous variation of resistivity along the length of the sample. When the polarity of the applied voltage was such that electrons drifted from the low resistive to the high resistive end of the bar, continuous oscillations were observed as shown in Fig.4.2c. However, on reversing the polarity (low resistive end positive) no oscillations occurred.

4.3 Observation of acoustic flux under saturation conditions

Current saturation has been observed when the drift velocity exceeds the velocity of sound. Hutson[2] has shown by an extension of the small signal theory of acoustic wave amplification[3] that current saturation may be interpreted in terms of the acoustoelectric current accompanying the ultrasonic flux.[4] The acoustoelectric current flows in the reverse direction[5] to the drift carrier current (ohmic current).

The generation of acoustic flux has been observed under saturation conditions in our crystals. The experimental configuration used was similar to that of Hutson et al[4] (as shown in Fig.2.2, Chapter Two), with the exception that no input transducer was used. Crystal D111 (dark resistivity 10^7 ohm cm) was selected for this experiment as a sample with a reasonably large cross-section and good photoconductivity ($\sigma \sim 10^{-3}$ ohm^{-1} cm^{-1} with max light) could be obtained from the boule. The crystal, with dimensions, 10 x 10 x 2 mm^3, was oriented for longitudinal wave propagation. The c-axis of the crystal was perpendicular to the 10x10 mm^2 faces of the crystal which were polished flat and parallel. Evaporated indium (about 2 μm thick) was used to bond a fused silica disc (5 mm diameter and 2mm thick) on to each face. A fused silica buffer was used to provide electrical insulation between the drift voltage and transducer output. An x-cut 1·0 cm dia. quartz transducer (20 Mc/s longitudinal wave) was bonded with salol (phenyl-salicylate) on to the top of the silica disc. The principal advantage

of salol is that a very good ultrasonic bond can be obtained at room temperature. Salol is a highly suitable bonding material for both shear and longitudinal waves at room temperature.[6] Two indium contacts were provided for the application of drift field. The transducer output was led away via thin (35 gauge) enamelled copper wires connected to each surface of the transducer by a small dot (0·2 mm dia.) of silver dag.

The crystal was uniformly illuminated with light from a tungsten lamp passing through 5200Å filter (to reduce the resistivity to about 10^3 ohm cm). A pulsed drift field (30 μsec, 25 cps) with positive polarity toward the transducer end was applied between the indium contacts, and the current was monitored across a series of resistance. The output of the transducer was connected to a 545 A Tektronix oscilloscope.

At zero field the transducer output was about 5 mv. On increasing the applied field (below threshold) the current through the crystal increased, but the transducer output remained unchanged at about 5 mv. On increasing the drift field beyond 200 volts ($\sim$ 1000v cm^{-1}), the current pulse increased abruptly to an initial maximum value, and then decayed toward a final steady state value within a few cycles of damped oscillations. At the same time the output from the transducer showed a sudden rise in amplitude to about 100 mv. The nature of the output flux was similar to those observed by McFee[1] (see bottom trace

of Fig.2.7, Chapter Two). As the transducer used in our experiment was tuned to 20 Mc/s, only a narrow portion of the complete spectrum was observed. No correspondence between the observed flux and oscillation in the current could be detected.

On reversing the polarity of the drift field so that the transducer side of the crystal was negative no flux was observed under current saturation conditions.

The feature to be emphasized is that the acoustic flux builds up only under current saturated conditions and only in the direction of the drifting electrons.

4.4 Discussion

When the illuminated photoconducting crystals were subjected to electric fields beyond a critical value two prominent effects were observed in the external circuit.[7] (1) The current departed markedly from Ohm's law and saturated almost completely and (2) low frequency current oscillations which were either damped or continuous appeared.

Acoustic flux has been observed under current saturation conditions (Sec.4.3). The mechanism of current saturation and oscillations may be understood in terms of the generation and amplification of acoustic flux[4] and the accompanying acoustoelectric current flowing in the reverse direction.[5]

Damped Oscillations - The current saturates after several cycles of damped oscillations as shown in Fig.4.1a, 4.1b and 4.2a. The time to reach the saturation level (the build up time) is found to be dependent on the conductivity and applied electric field.

Immediately after applying the external voltage, flux is uniformly generated across the crystal. The flux propagating in the direction of electron flow will be amplified[3] and on reaching the anode will be reflected and move against the electron drift. If the amplification of the flux during its travel with the drift substantially exceeds the attenuation suffered during its travel against the drift plus the losses incurred upon reflection at the crystal boundaries, a build up of ultrasonic flux will occur and the flux will reach its saturated value after

several round trips through the crystal.

At higher conductivities and/or applied fields the amplification is higher[3] and the build up of acoustic flux will be completed in a shorter (build up) time (upper curves, Fig.4.1c).

Undamped Oscillations - Persistent current oscillations as shown in Fig.4.2b and 4.2c were obtained with crystal D116(3). The potential distribution along the length of the crystal is illustrated in Fig.4.7a. The curve demonstrates that the crystal has a continuous variation of resistivity along the length. The period of the oscillations (3·3 μsec) is approximately equal to the time for a single transit between the electrodes (6·7 mm) for shear waves (v_s = 1·75 x 10^5 cm sec^{-1}).

When the high conductivity end (left in Fig.4.7a) was made negative and fields beyond threshold were applied, the flux at the cathode region moves with the accelerating electrons (due to increased field intensity) and is amplified. The flux build-up will then be complete on reaching the anode.

On reversing the polarity, the flux in the cathode region (now at the high field region) moves into a region of decelerating field and reaches a point where the field strength is lower than threshold. From this point onward the flux is attenuated instead of being amplified and no flux build up can occur.

Period of Oscillations - Two modes of oscillation could be obtained in sample D116(2) as shown in Fig.4.2a. Oscillations with the longer period (upper curves) were obtained on decreasing the crystal conductivity from about $3 \cdot 0 \times 10^{-4}$ ohm^{-1} cm^{-1} to $1 \cdot 0 \times 10^{-4}$ $ohm^{-1}cm^{-1}$. The crystal which was 3·35 mm long was oriented for shear waves and the periods obtained were approximately 2 and 4 μsec. This demonstrates clearly that at higher conductivity (but with fixed field intensity) the flux build up takes place in a single transit (due to higher amplification) and at lower conductivity (lower amplification) the flux builds up over a round trip. Similar results were obtained on changing the field only (with fixed light intensity).

PART B

EFFECTS OF CRYSTAL INHOMOGENEITY

4.5 Threshold field for current saturation

Details of some of the crystals used to make the experimental observations of non-ohmic behaviour are summarised in Table 1. The orientation and the conductivity of a sample in the dark and under illumination are included.

TABLE 4.1

Details of the CdS crystals used

Crystal No.	Dimensions mm			Orientation	Conductivity $ohm^{-1}\ cm^{-1}$	
	length	width	thick-ness		dark	max. illumination 120 ft-c
D78(1)	8·77	2·57	1·66	$\sim 20^{o}$ off c-axis	$< 10^{-9}$	$\sim 10^{-3}$
D116(1)	7·3	2·1	1·25	$\parallel$	$< 10^{-10}$	$\sim 10^{-2}$
D111	7·2	2·0	1·5	$\perp$ r	$< 10^{-9}$	$\sim 10^{-3}$
D116(2)	3·35	2·25	1·65	$\perp$ r	$< 10^{-9}$	$\sim 10^{-3}$
D116(3)	6·7	2·2	1·2	$\perp$ r	$< 10^{-10}$	$\sim 10^{-3}$

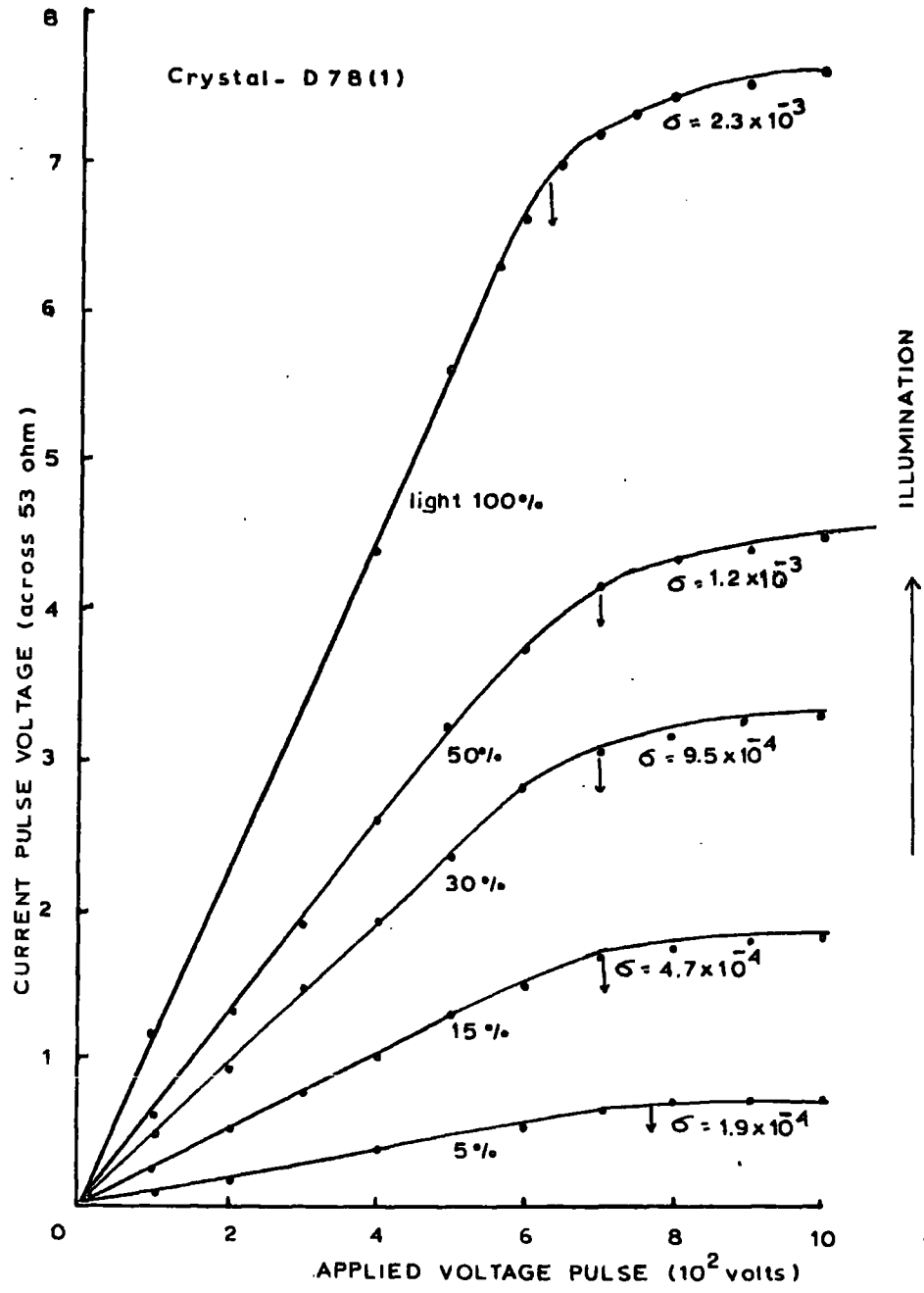

Fig.4.3. Current-voltage characteristics of photoconducting cadmium sulphide as a function of light intensity for crystal D78(1).

Fig.4.3 shows the drift current as a function of drift voltage for crystal D78(1). The drift voltage was applied (in 30 μsec pulses) along the length (8·77 mm) of the sample. With drift voltages less than 700 volts (drift field ~ 800 v/cm) and $\sigma = 2{\cdot}3 \times 10^{-3}\,\text{ohm}^{-1}\text{cm}^{-1}$ for example the drift current was a linear function of the drift voltage (ohmic region). A departure from ohmic behaviour was evident at drift voltages greater than 700 volts. Figure 4.3 shows the I-V curves obtained for pulse widths between 20 and 60 μsec with the intensity of illumination as a parameter. The threshold drift fields E_c measured at the 'kink' in the current voltage characteristics were somewhat dependent on the photo induced conductivity σ. E_c increased with decreasing conductivity as did the build up time. Below $\sigma = 5{\cdot}0 \times 10^{-5}\,\text{ohm}^{-1}\text{cm}^{-1}$, current saturation was not observed with input voltages up to 2500 volts. No saturation was obtained at any conductivity when the width of the voltage pulse was less than the build up time. At low conductivities no appreciable flux build up can occur because of the low acoustoelectric interaction when so few charge carriers are present, then no current saturation is detectable.

4.6 The effect of crystal inhomogeneity

The variation of the threshold field with photo induced conductivity and the production of current oscillations are strongly influenced by non uniformities in the sample. Inhomogeneous crystals have been studied to elucidate some of the effects.

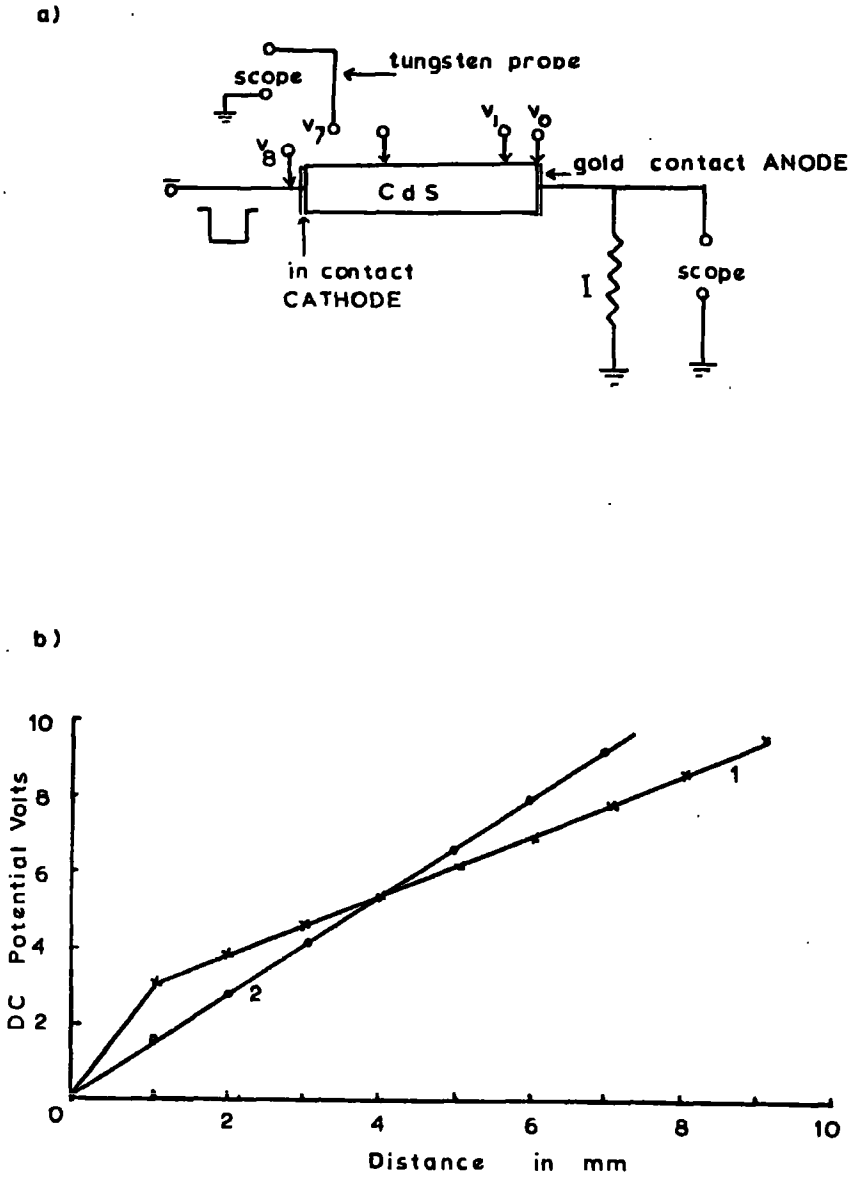

Fig.4.4. (a) Experimental arrangements for measuring potential distribution by pulsed method.

(b) Potential distribution in (1) non-uniform and (2) in uniform sample, respectively, for crystal D116(1).

The uniformity of our samples was measured with a potential distribution technique. Inorder to probe the potential distribution, indium contacts were placed at 1 mm intervals along the length of the sample. All the contacts were made by vapour deposition of indium followed by a short heat treatment to diffuse the indium into the surface as described earlier.

The measurements of the electric field distribution at room temperature, were carried out using an indium tipped tungsten probe mounted on a micromanipulator. The arrangement shown in Fig.4.4a allowed the voltage difference between any two contacts to be displayed on the oscilloscope (the pulsed method) or measured with a Philips PM2440 microvoltmeter (the dc method).

From a knowledge of the potential distribution in a sample one can determine whether non-ohmic behaviour is controlled by the bulk material or by the electrical contacts. Moreover, even if the saturation is controlled by the bulk, it is important to know whether there is an anomalous potential distribution in the sample or not. A spatial inhomogeneity of the electric field in some of the sample was formed, even in the conduction region where Ohm's law was obeyed for either polarity of the applied voltage.

(i) The effect on threshold field (at different conductivities)

The effect of crystal inhomogeneity on the threshold field has been studied, particularly in sample D116(1). The sample, with dimensions of

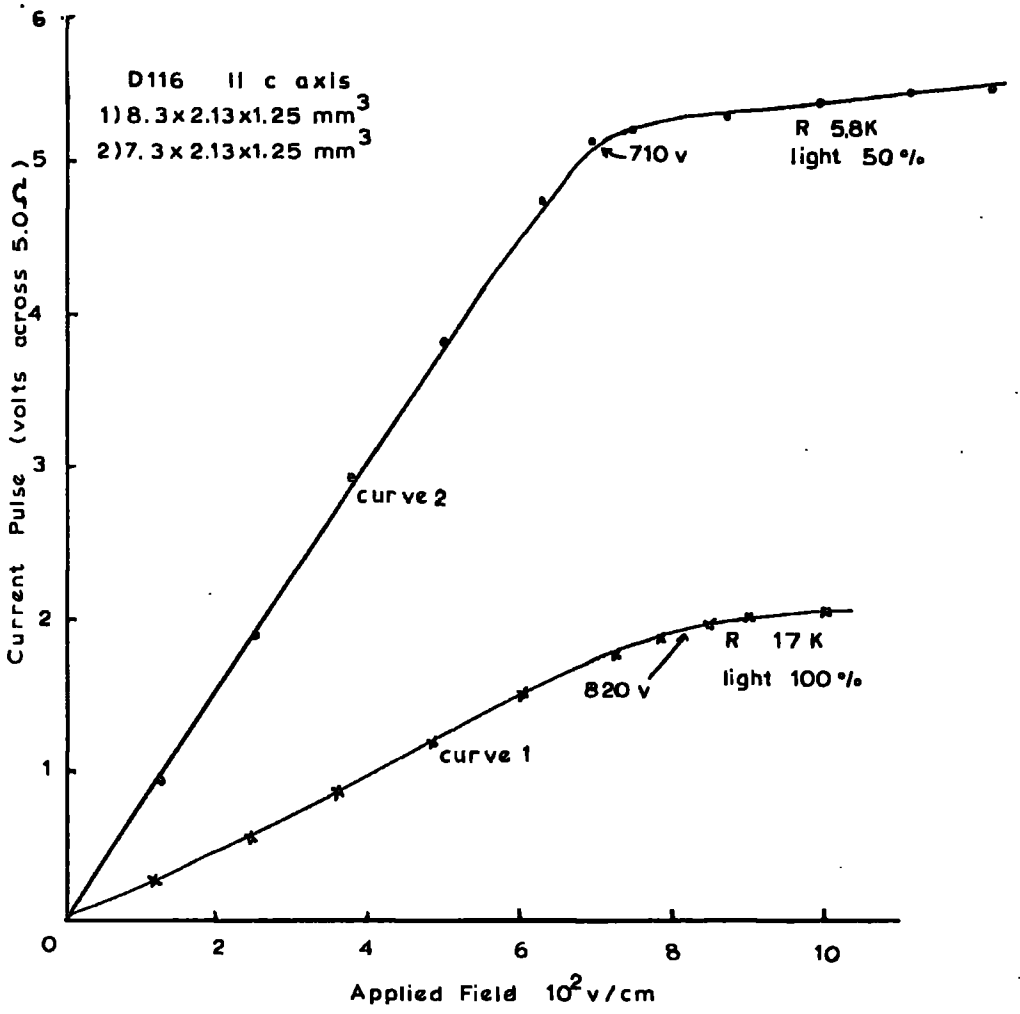

Fig.4.5. I-V curve characteristics
(1) for non-uniform sample and (2) for uniform sample D116(1).

$8{\cdot}3 \times 2{\cdot}1 \times 1{\cdot}25\ mm^3$ was uniformly illuminated with light from a tungsten lamp passing through a wide band $0{\cdot}52\ \mu m$ interference filter. A potential of 10 vdc was applied along the long dimension (8·3 mm) which was also the c-axis of the crystal. Fig.4.4b curve 1 shows the measured electric field distribution as a function of distance from one end of the sample. Reversal of the field direction and varying the intensity of illumination did not change the potential distribution appreciably. The measurements showed that a 1 mm length of one end of the sample had a high resistivity.

Fig.4.5 curve 1 shows the current-voltage characteristic for this (non-uniform) crystal measured with the maximum intensity of illumination available. Curve 1, Fig.4.6 shows the critical drift fields for current saturation as a function of conductivity σ. The threshold field E_c increased steadily throughout the range of decreasing conductivity. The value of E_c increased from 780 v cm^{-1} at $\sigma = 1{\cdot}8 \times 10^{-3}$ $ohm^{-1}cm^{-1}$ to 1150 v cm^{-1} at $\sigma = 4{\cdot}0 \times 10^{-5} ohm^{-1}cm^{-1}$.

At this stage, 0·3 mm was removed from the inhomogeneous end (1 mm) of the sample and the contacts reapplied. Under maximum illumination E_c was found to be reduced to 750 v cm^{-1} ($\sigma = 2{\cdot}3 \times 10^{-3} ohm^{-1}cm^{-1}$). E_c remained fairly constant for values of σ up to $2 \times 10^{-4} ohm^{-1}cm^{-1}$ and then increased to 1000 v cm^{-1} at $\sigma = 3{\cdot}2 \times 10^{-5} ohm^{-1}cm^{-1}$. The sample was still inhomogeneous.

Next a further 0·7 mm was removed from the non-homogeneous end of the sample to reduce the total length to 7·3 mm. Excellent saturation

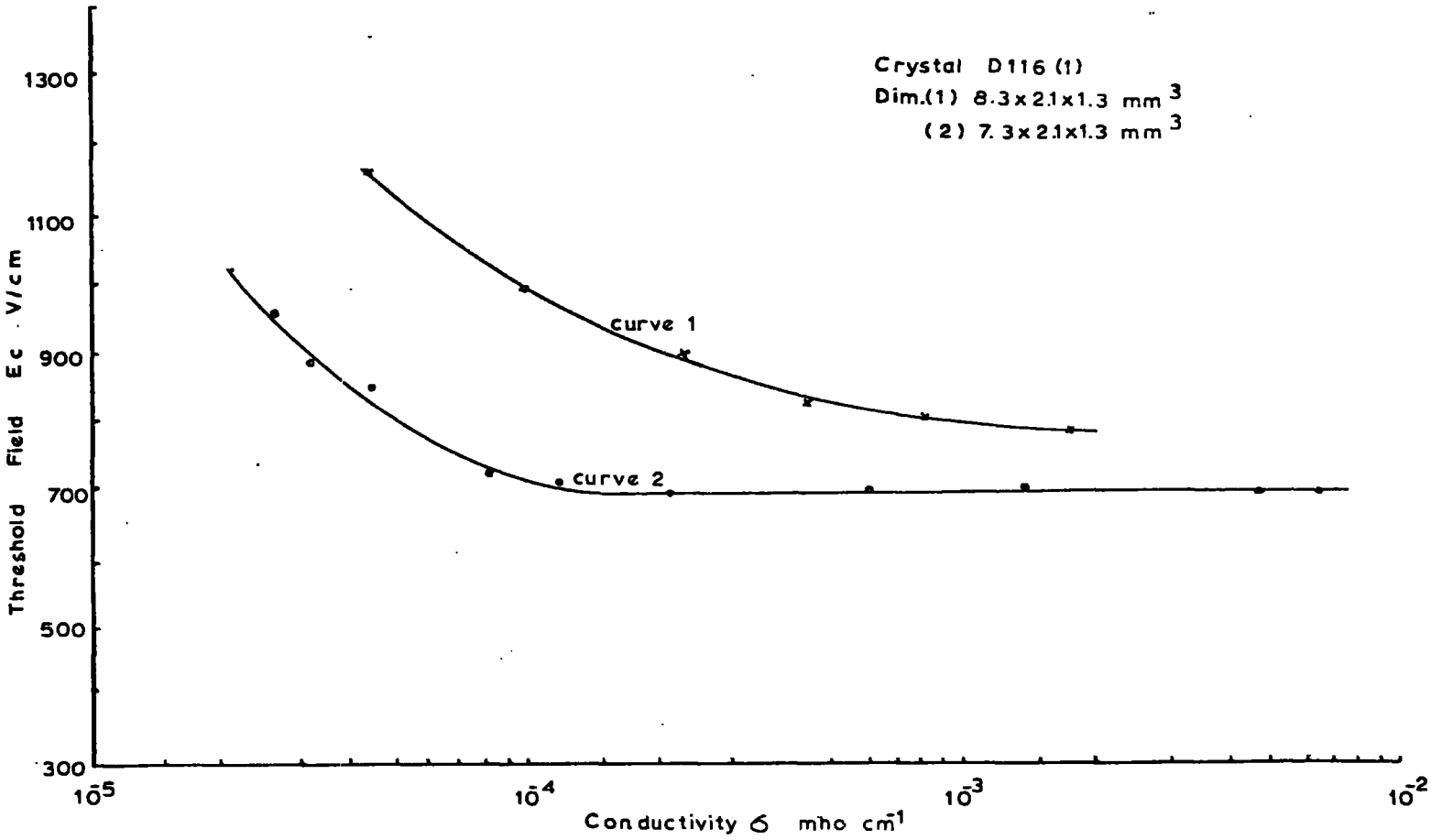

Fig.4.6. Threshold field E_c as a function of conductivity σ for crystal D116(1). Curve 1 for non-uniform resistivity; curve 2 for uniform resistivity.

was then observed. A typical example is shown in curve 2, Fig.4.5 which was obtained with the sample illuminated with half the maximum available light intensity. Curve 2, Fig.4.6, shows that the value of E_c at high light intensities was now reduced to 700 v cm^{-1}, and that E_c remained constant as the conductivity was decreased to 10^{-4} $ohm^{-1}cm^{-1}$. Under these conditions the potential distribution along the length of the specimen was almost uniform as indicated by curve 2, Fig.4.5.

(ii) Effect on current oscillations

The curve in Fig.4.7a shows the potential distribution of crystal D116(3) under uniform illumination (tungsten light passed through a 0·52 μm interference filter). The curve illustrates that there was a continuous variation of resistivity along the length of the sample. With the polarity of the applied voltage, such that electrons drifted from the low resistive end (cathode) to the high resistive end of the bar (6·7 mm long) continuous oscillations were observed (as shown in Figs. 4.2b, 4.2c) at an applied voltage greater than 500 volts (700 v cm^{-1}) when $\sigma = 4{\cdot}0 \times 10^{-4}$ $ohm^{-1}cm^{-1}$. No oscillation was observed on reversing the polarity of the applied field. This result is discussed in Section 4.4.

(iii) Inhomogeneity above the threshold

The potential distribution above threshold was measured under pulsed conditions only to avoid undue heating of the crystal. The

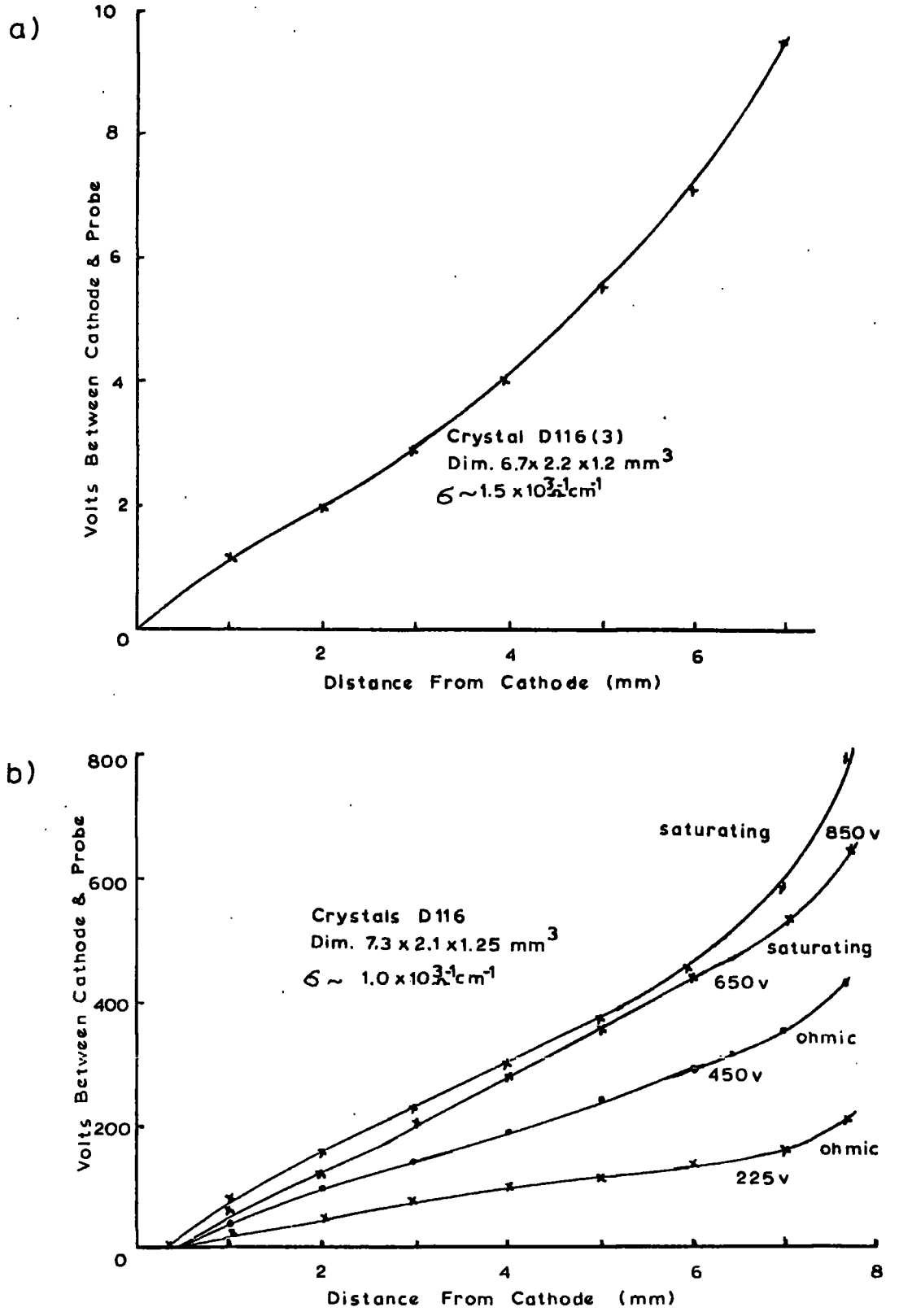

Fig.4.7. (a) Potential distribution in a non-uniform sample D116(3)

(b) Potential distribution in a uniform sample in ohmic and saturating conditions for crystal D116(1).

arrangement used is shown in Fig.4.3a. The potential distribution was measured in both the ohmic and saturation regions of the I-V characteristics.

Fig.4.7b shows the measured electric field distribution in sample D116(1) as a function of distance from the cathode. The direction of electron drift was from left to right. The sample was uniformly illuminated and the current saturated above 550 volts. The lower two curves (Fig.4.7b), corresponding to 225 volts and 400 volts applied represent the field distribution in the sample under ohmic conditions. The upper two curves, corresponding to 650 volts and 800 volts respectively, represent the field distribution under saturation conditions. The field near the positive electrode becomes higher as the applied field increases above the threshold as demonstrated by the upper two curves in Fig.4.7b.

4.7 Discussion

A typical current-voltage characteric in photoconducting CdS (crystal D78(1)) is shown in Fig.4.3. The conductivity was varied by varying the intensity of illumination. The significant fact common to all these I-V curves is the abrupt discontinuity in slope at a critical field E_c. The change in crystal conductivity only changes the saturated photocurrent but the field for saturation remains almost unaltered. At lower conductivities (lower two curves, Fig.4.3) the current saturation is rather weak, ('kink' in the 1-V curve). This demonstrates weak carrier-acoustic wave interactions at lower conductivity.

The principal quantitative measurements which can be made from an 1-V curve is that of the drift mobility. This is found from the critical field showing the onset of current saturation.

(i) Effect of inhomogeneity

The method of calculating the drift mobility assumes that the potential distribution along the specimen is uniform. Non uniformity in the sample leads to a higher critical field (and lower apparent drift mobility) as shown in Fig.4.6.

The variation of E_c, with the conductivity for crystal D116(1) is shown in curve 1, Fig.4.6. Curve 2, shows the variation of E_c for the same crystal after removing 1 mm from the inhomogeneous end (see Section 4.6(i)).

A variation of E_c with conductivity has been reported by Ishida et al.[8] who attributed the changes in E_c to (a) electron trapping effects and (b) an increase in mobility at high light intensities which is caused by a reduction in ionised impurity scattering.[9] However, present observations (Fig.4.6) demonstrate that a variation in E_c with conductivity can be caused by inhomogeneity in the sample.

(ii) Threshold field at low conductivity

Even in the homogeneous sample, the threshold field increased rapidly (curve 2, Fig.4.6) for values of conductivity below 10^{-4} mho cm^{-1} and saturation became progressively less pronounced. The potential distribution was still substantially uniform. At conductivities below 10^{-5} mho cm^{-1} no saturation was observed at all.

Current saturation due to the build up of acoustic flux occurs when the amplification in the drift direction exceeds the loss in the opposite direction. It can be shown[1] (from the linear theory of ultrasonic amplification[3]) that the threshold condition for net round trip gain (neglecting losses due to reflection at the sample boundaries, and trapping effects) is

$$v_d = \mu_d E_c$$

$$\therefore \quad E_c = \frac{v_s}{\mu_d} \left[1 + 4\left(\frac{\omega_c}{\omega_D}\right)\right]^{\frac{1}{2}} \qquad 4.1$$

where $\omega_c = (\sigma/\epsilon)$, $\omega_D = (v_s^2/D)$, σ, ϵ, and D are the dielectric relaxation frequency, diffusion frequency, conductivity, dielectric constant and diffusion constant respectively. In the sample (D116(1)) used, $v_s = 2{\cdot}0 \times 10^5$ cm sec^{-1}, $\omega_c = 1{\cdot}2 \times 10^{12}\sigma$ sec^{-1} and $\omega_D = 6{\cdot}0 \times 10^9$ sec^{-1}, $\mu_d = 300$ $cm^2v^{-1}cm^{-1}$ at 300^oK. Thus eqn. 4.1 becomes

$$E_c = \frac{v_s}{300}[1 + 8{\cdot}0 \times 10^2\sigma]^{\frac{1}{2}}$$

$$= 700[1 + 8{\cdot}0 \times 10^2\sigma]^{\frac{1}{2}} \qquad 4.2$$

The theoretical threshold fields E_c predicted by eqn.4.2 would be expected to remain constant as the conductivity is reduced below 10^{-2} mho cm^{-1}. According to eqn.4.2 E_c should increase for values of σ higher than 10^{-2} mho cm^{-1}. This is the reverse of what we have observed. Hence there would appear to be a discrepancy between the present observation and theory. In our experiments no change in photo Hall mobility was observed in crystal D116(1) even at 10^{-5} mho cm^{-1} (Fig.4.8). In our experience (based on the measurements made on a number of different crystals) it would seem that the increase in E_c at lower conductivities ($< 10^{-4}$ mho cm^{-1}) is a basic feature of the acoustoelectric interaction which is not taken into account in the argument which leads to eqn.4.2. The following interpretation is proposed to explain the effect.

Current saturation occurs as long as there is a net round trip gain. The acoustic wave amplification increases with increasing electron drift velocity i.e. with applied field ($v_d \geq v_s$) until the gain reaches a maximum at about twice the velocity of sound ($v_d \simeq 2v_s$). Further increase in electron drift velocity decreases the amplification factor. The amplification also decreases with decreasing conductivity ($\sigma < 10^{-4}$ mho cm^{-1}).[12] At lower conductivities (below about 10^{-4}mho cm^{-1}) the low amplification can be compensated by a gradual increase in the electron drift velocity which is achieved by increasing the applied field (hence a high E_c). However, at still lower conductivities ($\sigma < 10^{-5}$ mho cm^{-1}), further increase in electron drift velocity (beyond about twice the velocity of sound, corresponding to 1400 v cm^{-1} in Fig.4.6) would lead to a reduction in the amplification factor (and the net round trip gain necessary for current saturation could not be achieved.

(iii) Non uniformity under saturated conditions

Voltage probe measurements on a uniform sample D116(1) under saturation conditions (upper two curves, Fig.4.7b) show a stationary high electric field (high field domain)[10] near the anode, while over the remainder of the sample, the field distribution is fairly uniform. This demonstrates that the acoustic flux grows along the length of the specimen and becomes maximum at the anode end. In this way a high

resistivity region is formed because of the large reverse acoustoelectric current associated with the flux.[5]

Comparison of the upper two curves (Fig.4.7b) shows that raising the applied voltage further beyond the threshold voltage mainly serves to increase the field in the high field domain. When the direction of the drift was reversed so that electrons flowed from right to left, in Fig.4.7b, it was found that the high field appeared near the left hand end of the sample. With this type of non uniformity near the anode the current saturated after 2-3 cycles of damped oscillations.

PART C

ELECTRON DRIFT MOBILITY AT ROOM TEMPERATURE

4.8 Photo Hall mobility

The photo Hall mobility was measured using the circuit arrangement shown in Fig.3.8 (Chapter III). The specimens No. D78(1), D116(1) and D111 (see Table 1, Section 4.5) were provided with three pairs of contacts, one pair at the ends to enable current to be passed, a pair of potential probes along the specimen and a transverse pair near the centre to measure the Hall voltage. A direct current (a few micro-amp to a few mA) was passed through the specimen and the resistance and hence the conductivity was found by measuring the current, and the voltage between the potential probes. All the measurements were made with a high impedance Vibron electrometer (input resistance $\gtrsim 10^{14}$ ohms).

A magnetic field of 2·4KG with a gap of 5 cm between the pole pieceswas used. Two sets of readings were made for either direction of the magnetic field and with either direction of the electric field. The resultant readings were averaged to eliminate possible sources of error [11] from thermoelectric and thermomagnetic effects.

Experimental results

The measured photo Hall mobility μ_H as a function of conductivity σ for three samples is shown in Fig.4.8. Curve 1, obtained from crystal D78(1), shows a steady decrease in the Hall mobility from 360 $cm^2v^{-1}sec^{-1}$ at $\sigma = 4{\cdot}0 \times 10^{-3}$ mho cm^{-1} to 240 $cm^2v^{-1}sec^{-1}$ at $\sigma = 10^{-5}$ mho cm^{-1}. Curves 2 and 3, for samples D116(1) and D111 respectively show that the Hall mobility μ_H was independent of conductivity.

Variation of μ_H in Crystal D78(1)

The observed decrease in electron mobility μ_H with decreasing conductivity for sample D78(1) can be interpreted in the manner proposed by Bube and MacDonald.[9]

Measurements made on crystal D78(1) at room temperature showed a variation in conductivity from $6{\cdot}2 \times 10^{-3}$ to $6{\cdot}1 \times 10^{-7}$ mho cm^{-1} when the intensity of photoexcitation was reduced from a maximum (100%) to 5×10^{-4} (0·0005%) of the highest light intensity available (120 ft-c). The Hall mobility increased from 180 $cm^2v^{-1}sec^{-1}$ to 370 $cm^2v^{-1}sec^{-1}$ as the electron concentration n increased from $2{\cdot}1 \times 10^{10}$ to $1{\cdot}0 \times 10^{14}$ cm^{-3}.

Bube and MacDonald[9] have shown that a variation in Hall mobility can be interpreted in terms of a change in the occupancy of the imperfection centres. The occupancy of the imperfection centres is determined by the location of the quasi Fermi level. The electron Fermi level E_{fn} can be calculated from the expression

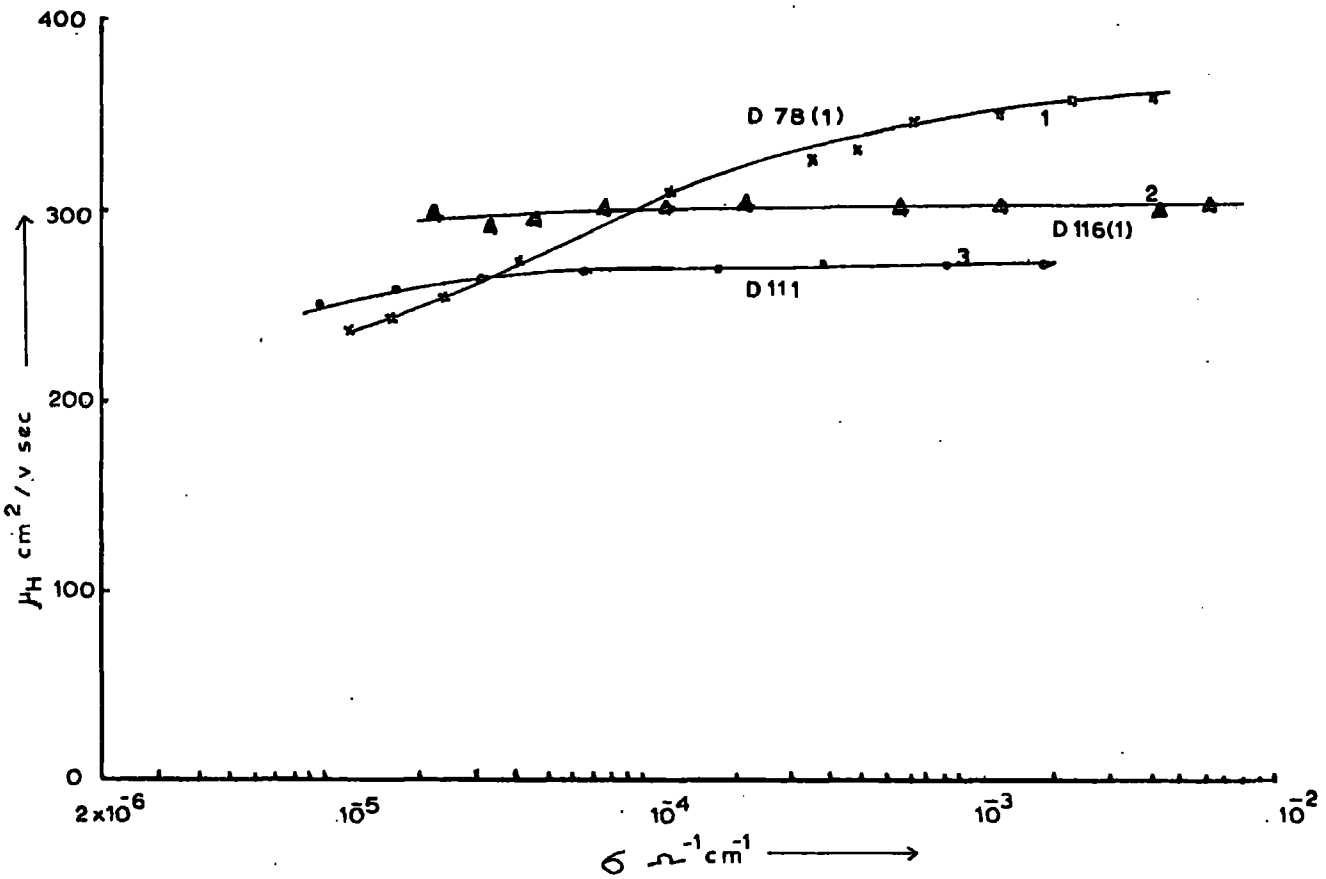

Fig.4.8 Hall mobility μ_H as a function of conductivity σ for (1) crystal D78(1), (2) crystal D116(1) and (3) crystal D111.

$$n = N_c \exp \frac{-E_{fn}}{kT}$$

or $$E_{fn} = kT \ln \frac{N_c}{n}$$

where N_c is the density of states in the conduction band = $2{\cdot}14 \times 10^{18} cm^{-3}$ for CdS at room temperature ($300^{o}K$, $m^{*} = 0{\cdot}2$ Me).

The electron Fermi level lies between 0·249 ev to 0·46 ev for electron concentrations between $1{\cdot}0 \times 10^{14}$ and $2{\cdot}1 \times 10^{10}$ cm^{-3}.

The imperfection centres responsible for the observed variation in electron mobility with photo excitation are positively charged centres (ionised donors) which lie above the electron Fermi level in the dark. As the Fermi level rises with increasing photo excitation, these centres become filled with electrons, their charge is removed and their scattering decreases strongly. The effect of the photoexcitation on the electron mobility is described by the equation[9]

$$\frac{1}{\mu_H} = \frac{\beta}{\tau_o} + \beta v S_+ N_+ [1 + 2 \exp \{ (E_+ - E_{fn})/kT \}]$$

where β/τ_o represents the scattering due to all processes other than ionised impurity scattering. v is the thermal velocity of an electron, S_+ is the scattering cross section of the positively charged donor, N_+ is the density of donors and E_+ is the depth of the donor level below the conduction band.

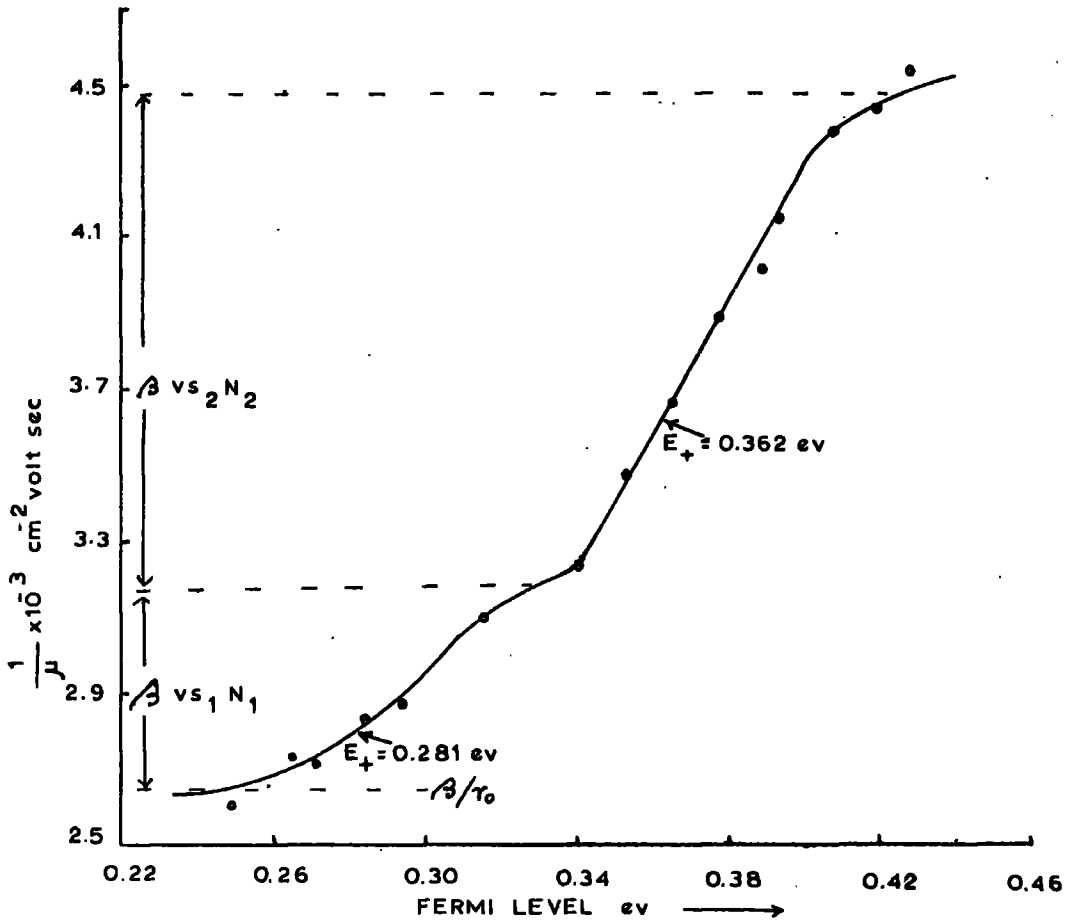

Fig.4.9. Reciprocal Hall mobility ($1/\mu_H$) as a function of the location of the electron Fermi level to obtain E_+ for crystal D78(1).

According to the above equation, a plot of $1/\mu_H$ against E_{fn} should lead to an S-shaped curve from which the energy level of the scattering centres can be calculated by determining the point at which $1/\mu_H$ changes by one third of the difference between the values of $1/\mu_H$ at the extreme limits of the S-shaped curve.

Fig.4.9 shows a plot of $1/\mu_H$ as a function of E_{fn}. Two almost S-shaped curves in agreement with the prediction of above equation were obtained. The curves can be interpreted in terms of the existence of two traps with depths of 0·281 and 0·362 ev. The shape of the curve shows that the two traps were positively charged in the dark.

4.9 Comparison of the Drift and Hall mobilities

When non-ohmic effects caused by the acoustoelectric interaction are observed, the carrier drift velocity at the onset of the non-ohmic conduction is equal to the velocity of sound ($v_d = v_s$).

The threshold field for current saturation E_c as a function of conductivity in the range 3×10^{-5} to about 10^{-2} mho cm^{-1} is shown in Fig.4.10 (lower two curves) for two uniform samples D78(1) and D111. Crystal D111 was oriented perpendicular to c-axis while crystal D78(1) was randomly oriented. The threshold field for current saturation E_c as a function of conductivity σ between $2{\cdot}5 \times 10^{-5}$ and 10^{-2} mho cm^{-1} for crystal D116(1) is shown in curve 2, Fig.4.6.

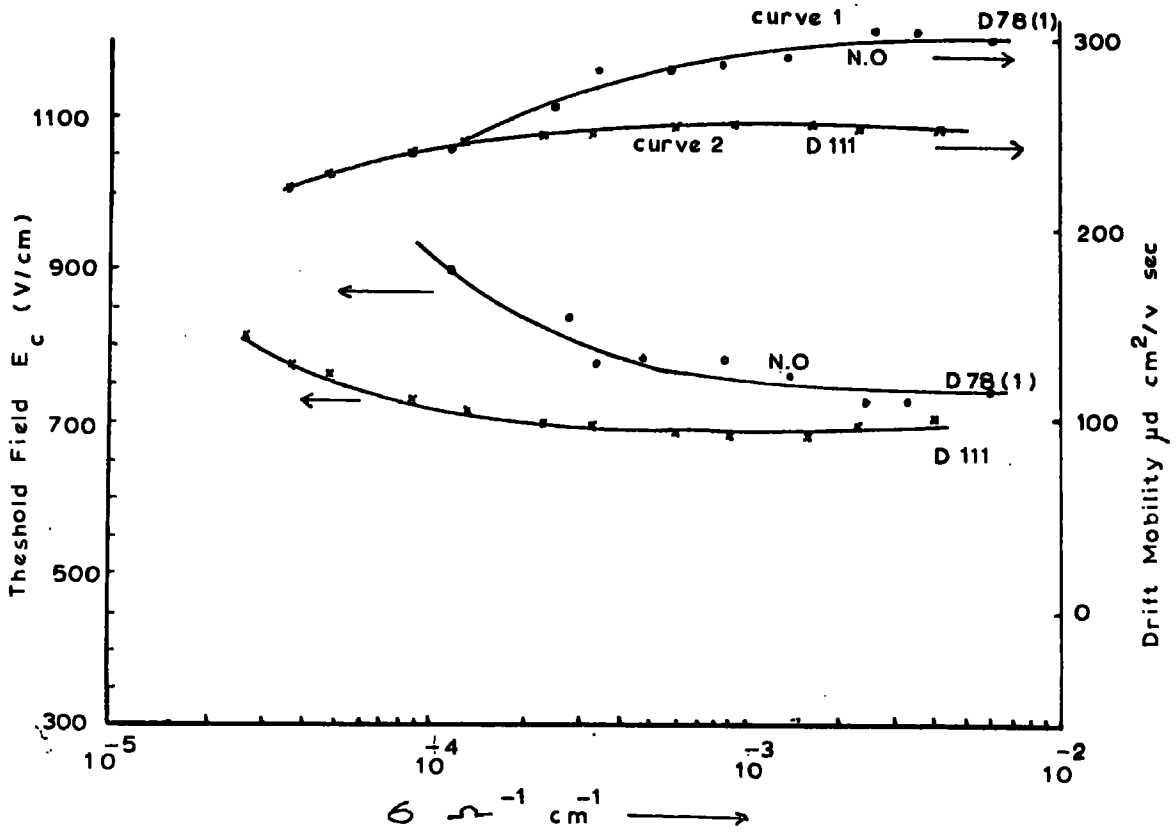

Fig.4.10. Threshold drift field E_c and drift mobility as a function of conductivity σ for two samples.

The values of electron drift mobility estimated from the condition of equality of the appropriate velocity of sound are shown in Fig.4.10 for crystal D111. The electron drift mobility of 258 $cm^2v^{-1}sec^{-1}$ in crystal D111 (oriented perpendicular to c-axis) was obtained by using a shear wave velocity of $v_s = 1{\cdot}75 \times 10^5$ cm sec^{-1}. The value of 258 $cm^2 v^{-1}sec^{-1}$ is in good agreement with the measured Hall mobility of 272 $cm^2 v^{-1}sec^{-1}$ (see Fig.4.8) for conductivities between 10^{-4} and 4×10^{-3} mho cm^{-1}.

The value of electron drift mobility for sample D116(1), (oriented for longitudinal sound waves) estimated from E_c (curve2, Fig.4.6) was about 630 $cm^2v^{-1}sec^{-1}$ if the longitudinal sound wave velocity ($v_s = 4{\cdot}4 \times 10^5$cm sec^{-1}) was used. This value of drift mobility was about twice the value obtained from the measured Hall mobility of 300 $cm^2v^{-1}sec^{-1}$ (see curve 2, Fig.4.8). This discrepancy between the Hall and drift mobility can be resolved if the interaction with off axis shear waves is considered. If the electrons couple with off axis shear waves, as pointed out by McFee[1], departures from ohmic behaviour begin to appear at a drift field smaller than the threshold field for amplification for longitudinal waves because the velocity of off axis shear waves is smaller than that of longitudinal wave. Therefore if a value of the velocity of sound of $2{\cdot}0 \times 10^5$ cm sec^{-1} was used the electron drift mobility μ_d obtained would agree well with the Hall mobility data in the conductivity range between 10^{-4} to 10^{-2} mho cm^{-1}.

Using off axis shear wave velocity of $2{\cdot}2 \times 10^5$ cm sec^{-1}, in the case of unoriented sample D78(1) (about 20^o off from c-axis), the

estimated drift mobility and Hall mobility were found to be in reasonably good agreement. The drift mobility varied between 300 and 220 $cm^2 v^{-1} sec^{-1}$ over a range of conductivities from 3×10^{-3} to 10^{-4} mho cm^{-1}. Over the same range of conductivities the Hall mobility varied between 360 and 300 $cm^2\ v^{-1} sec^{-1}$. The lower values of drift mobility can be ascribed to trapping effects.[8] The effect of traps in reducing the drift mobility at different temperatures forms the subject of Chapter V.

4.10 Discussion

The measured values of electron drift mobility in CdS showed good agreement with the values of Hall mobility. The electron mobility in semiconductors is usually measured experimentally by determining the Hall coefficient. However, strong acoustoelectric interactions in piezoelectric semiconductors like CdS, makes it possible to determine the drift mobility of carriers. The current voltage characteristics can be used as a practical method of determining the mobility in photo conducting CdS crystals. The technique can be used in the range of conductivities between 10^{-4} to 10^{-2} mho cm^{-1}. Irrespective of the orientation of a crystal $\mu_d = v_s/E_c$, when v_s is the appropriate velocity of sound. The drift mobility has been measured along the c axis (D116(1)), perpendicular to the c axis (D111) and at an angle ($\sim 20^\circ$ off from the c-axis) to the c-axis (D78(1)).

No acoustic contacts are required by the method and therefore, it is convenient to use this technique in the investigation of the temperature dependence of drift mobility (see Chapter V).

References

1. J.H. McFee, J. Appl. Phys., 34, 1548, 1963.

2. A.R. Hutson, Phys. Rev. Letters, 9, 296, 1962.

3. D.L. White, J. Appl. Phys., 33, 2547, 1962.

4. A.R. Hutson, J.H. McFee and D.L. White, Phys. Rev. Letters, 7, 237, 1961.

5. W.C. Wang, Phys. Rev. Letters, 9, 443, 1962.

6. H.J. McSkimin, IRE Trans. PGUE-5,25, 1957.

7. R.W. Smith, Phys. Rev. Letters, 9, 87, 1962.

8. A. Ishida, C. Hamaguchi and Y. Inuishi, J. Phys. Soc. Japan, 20, 1946, 1965.

9. R.H. Bube and R.E. Macdonald, Phys. Rev., 121, 473, 1961.

10. J.H. McFee and P.K. Tien, J. Appl. Phys., 37, 2754, 1966.

11. E.H. Putley "The Hall effect and semiconductor physics", Dover Publications, N.Y. p.26.

12. T. Ishiguro, I. Uchida, T. Suzuki and Y. Sasaki, IEEE Transactions on Sonics and Ultrasonics, March 9, 1965.

CHAPTER V

TEMPERATURE DEPENDENCE OF THE DRIFT MOBILITY AND THE EFFECT OF TRAPS

INTRODUCTION

At room temperature the electron drift mobilities calculated from equating the drift velocity and the velocity of sound ($v_d = v_s$) agreed with the measured Hall mobilities. (Chapter IV). Since the velocity of sound is independent of temperature[1] ($< 77^{o}K$), the temperature dependences of the critical field E_c and the reciprocal of the drift mobility, which are related to the sound velocity by the equation $v_s = E_c/\mu_d$, should be similar. The electron mobility in CdS changes rapidly with temperature,[2] so that the critical drift field E_c should vary with temperature. The observation of the temperature dependence of E_c should therefore provide another check on the interpretation of the saturation effect.

The mobility obtained from the current saturation break point will be low if the electrons spend an appreciable time in traps during their transit through the crystal. In this circumstance the mobility will be trap controlled. On the other hand the Hall mobility μ_H is a thermal equilibrium quantity and is unaffected by trapping processes.

It was decided, therefore, to investigate the low temperature variations of the Hall and drift mobilities to gain some information about the effect of traps on the drift mobility.

Measurements were made over the range 100-300^{o}K and are reported in this Chapter. Several intensities of illumination were used since the threshold field and Hall mobility might depend on the level of photoexcitation.

5.1 Threshold field at low temperature

The threshold field for current saturation in crystal D78(1) was measured at different temperatures between 100^{o} and $300^{o}K$ using the cryostatdescribed in Chapter III. The crystal was flooded with illumination from a tungsten lamp filtered through a 0·54 μm, wide band, interference filter and 1·5 cm path of 10% solution of copper sulphate.

Some typical current-voltage characteristics obtained in crystal D78(1) at various temperatures are shown in Fig.5.1. These measuresments were made using μ 20 μsec pulses at a repetition frequency of 25 cps, and with a constant intensity of illumination of 15% of the maximum (120 ft-c). The corresponding conductivity at room temperature was $\sim 1{\cdot}34 \times 10^{-3}$ mho cm^{-1}. Each curve in Fig.5.1 is marked with the temperature at which the current-voltage characteristic was measured.

Although the current at which saturation occurred remained fairly constant between 300^{o} and $200^{o}K$, the threshold field for current saturation decreased rapidly as the temperature was lowered. The threshold field, E_c, determined from the knee of the current-voltage characteristics, as a function of temperature is shown in curve 1, Fig.5.2. E_c decreased from 720 $v.cm^{-1}$ at $300^{o}K$ to 170 $v.cm^{-1}$ at $120^{o}K$. As the temperature was decreased below $200^{o}K$ the magnitude of the current saturation also decreased.

A plot of the saturated current I_{sat}, obtained from the I-V characteristics, as a function of temperature is shown in curve 2, Fig. 5.2 at a fixed intensity of illumination (15% of the maximum).

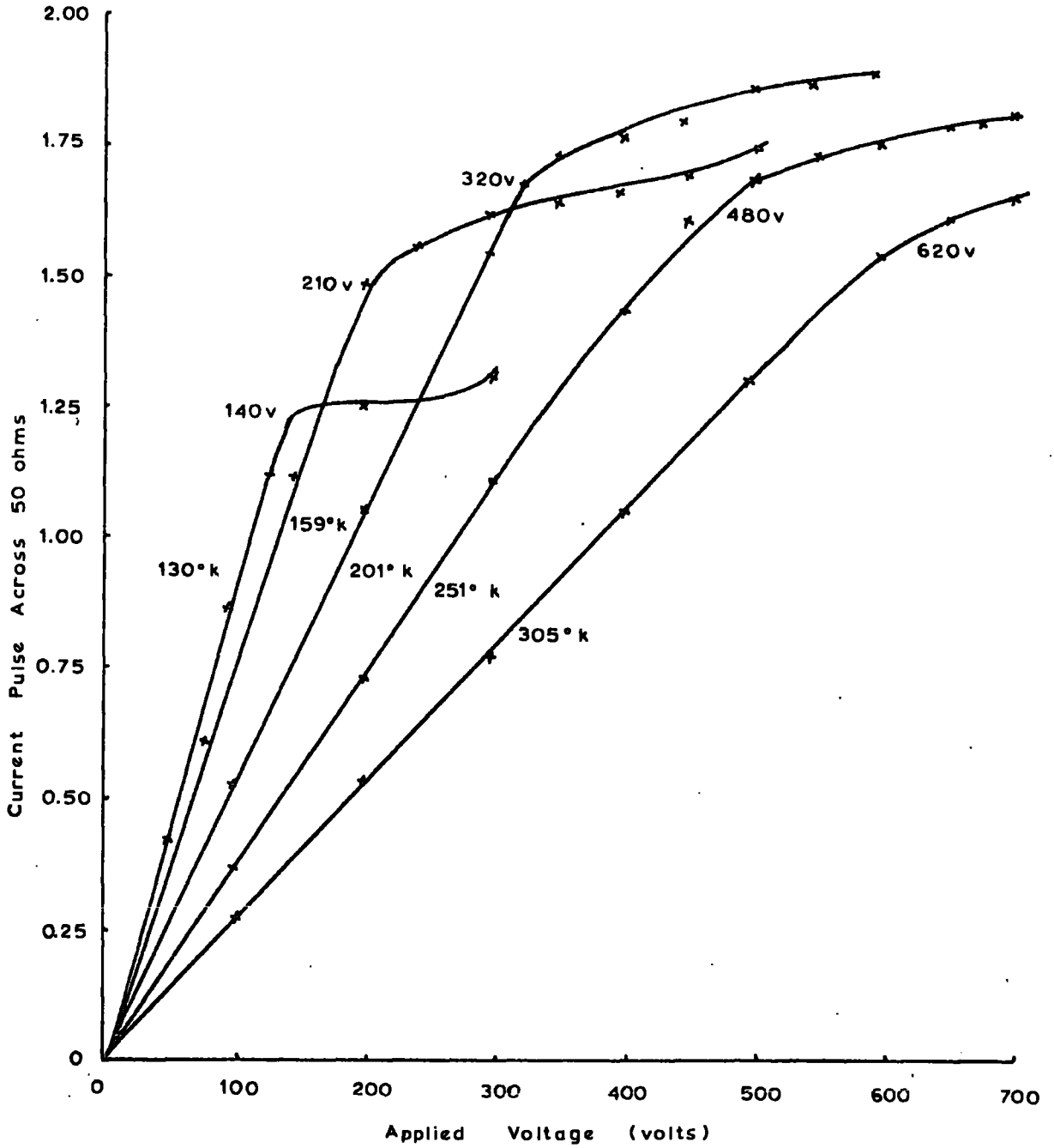

Fig.5.1. Current-voltage characteristics for crystal D78(1) as a function of temperature. Light 15%; Conductivity at room temperature $1{\cdot}34 \times 10^{-3}$ mho cm^{-1}.

The current density J_{sat} at the knee of the I-V curve can be written as

$$J_{sat} = n'e\mu_d E_c = n'ev_d$$

$$= n'ev_s \qquad 5.1$$

where n' is the electron concentration (defined later in Eqn.5.9). A quantitative estimate of the carrier concentration, n', can therefore be obtained from a measurement of J_{sat} and E_c provided the appropriate velocity of sound is used in Eq.5.1. Curve 3, Fig.5.2 shows such estimated values of n' as a function of temperature. Using the off-axis shear wave velocity $v_s = 2{\cdot}2 \times 10^5$ cm sec^{-1}, n' was found to be $2{\cdot}3 \times 10^{13}$ cm^{-3} at 300^oK and remained fairly constant down to 200^oK before decreasing gradually to $1{\cdot}7 \times 10^{13}$ cm^{-3} at 120^oK.

It is to be expected that, the carrier concentration measured from J_{sat} should have the same temperature dependence as the free carrier concentration in a trap free material. The temperature dependence of the free carrier concentration, n, as deduced from the Hall coefficieint ($n = -\frac{1}{Re}$) is presented in curve 4, Fig.5.2. Both n and n' were measured with the same intensity of illumination (15%). The magnitude of the carrier concentration n and n' are in reasonably good agreement (n' slightly bigger than n) with one another at the higher temperatures (240-300^oK). However, at lower temperatures the carrier concentration, n, deduced from the Hall measurements decreases more rapidly than n' as

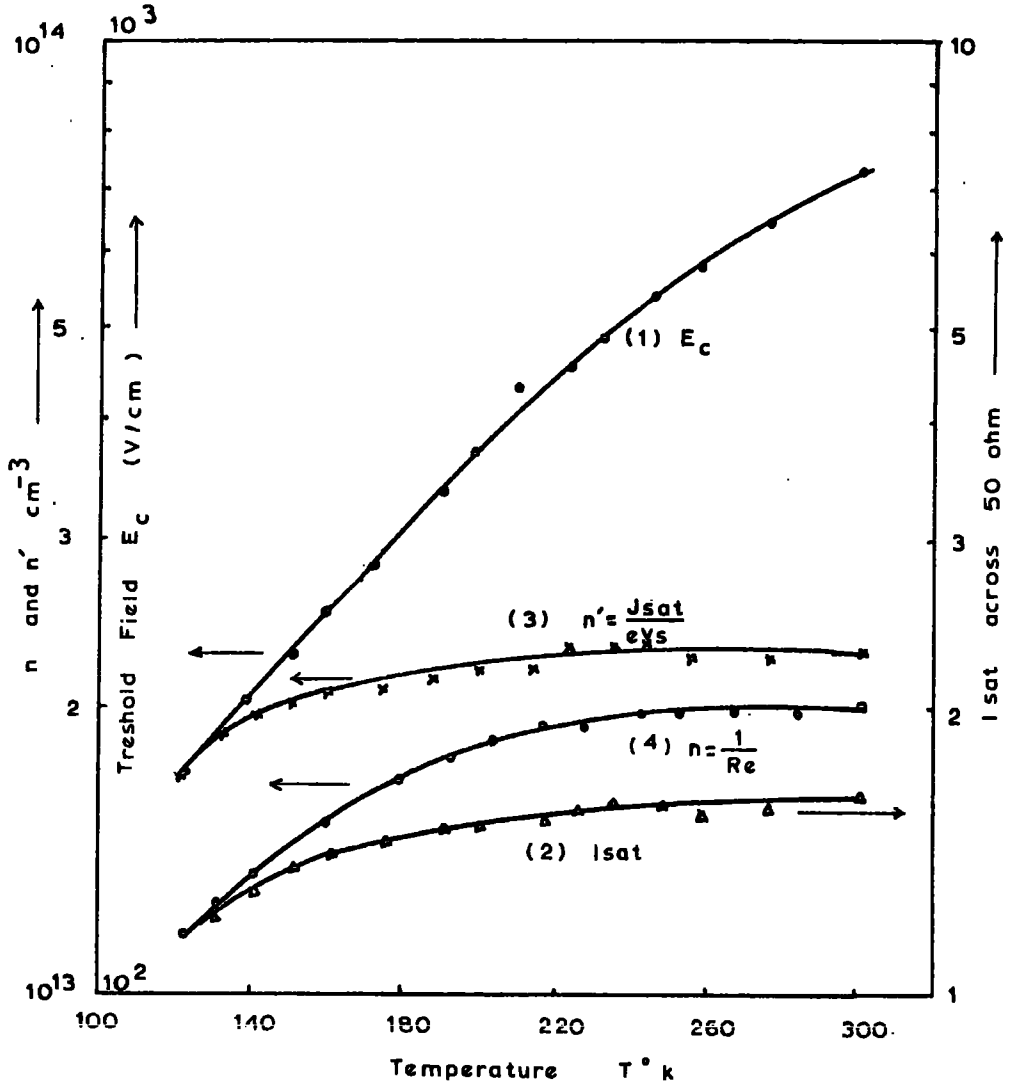

Fig.5.2. Data obtained from current saturation (I-V curves) as a function of temperature for crystal D78(1), at a fixed light intensity of 15% (room temperature $\sigma = 1{\cdot}34 \times 10^{-3}$ mho cm^{-1})

Curve (1) Threshold field E_c; curve (2) magnitude of the saturated current I_{sat}; curve (3) electron concentration n' measured from $J_{sat} = n'ev_s$; curve (4) free electron concentration n from Hall coefficient ($n = -\frac{1}{Re}$).

the temperature is reduced. This suggests that some trapping process becomes progressively more predominant as the temperature is lowered. The higher values of n' can be accounted for if the contribution of both free and trapped carriers ($n + n_t$) towards the mechanism of current saturation is considered.

[At temperatures above 240°K $n' = n + n_t$ (according to eqn.5.9) when the trapping time $\tau \ll 1/\omega$. $n' = (n + n_t)/b$ (according to Eqn. 5.10) at temperatures below about 220°K when $\tau \geq 1/\omega$, where ω is the dominant acoustic frequency and b is a temperature dependent trapping factor defined in Eqn.5.6].

5.2 Current Saturation and Trap-Controlled Electron Drift Mobility

The drift mobility obtained from the break point for current saturation is a measure of the velocity under unit electric field of the carriers which are bunched in the local piezoelectric field of the internally generated and amplified acoustic flux. These bunched carriers are in excess of the local thermal equilibrium concentration and as such may be considered as excited or injected carriers. Their mobility will be reduced if they spend appreciable time in traps during their transit through the crystal.

On the other hand the Hall mobility, $\mu_H = R_H\gamma$ and the corresponding velocity $v_{dH} = R_H J$, are microscopic quantities determined by the action of the electric and magnetic fields on the free carriers. The Hall

mobility, therefore, is a thermal equilibrium measurement not affected by the presence of traps.

In the presence of a set of traps with density N_t, at a depth E_t below the conduction band, the trap controlled drift mobility μ_d is derived as follows:

If μ_H is the Hall mobility (i.e. lattice mobility) and n and n_t are the electron densities in the conduction band and trap level respectively, then

$$\mu_d(n + n_t) = \mu_H n$$

$$\text{or} \qquad \mu_d/\mu_H = \frac{n}{n + n_t} \qquad 5.1$$

If the crystal is in thermal equilibrium

$$n_t/n = \frac{N_t}{N_c} \exp E_t/kT \qquad 5.2$$

where N_c is the effective density of states $2\left(\frac{2\pi m^* kT}{h^2}\right)^{3/2} = 4{\cdot}24 \times 10^{14} T^{3/2}$ for CdS with $m^*/m = 0{\cdot}2$.

From equations (5.1) and (5.2)

$$\mu_d/\mu_H = \left[1 + \frac{N_t}{N_c} \exp \frac{E_t}{kT}\right]^{-1} \qquad 5.3$$

If additional traps are active further terms of the form $\frac{N_{tn}}{N_c} \exp \frac{E_{tn}}{kT}$ must be added to the denominator.

For a number of trapping levels Eq.(5.3) can be written as

$$\left(\mu_H/\mu_d - 1\right) = \sum_t \frac{N_t}{N_c} \exp \frac{E_t}{k}\left(\frac{1}{T}\right) \qquad 5.4$$

With a single set of traps a plot of $\log(\mu_H/\mu_d-1)T^{3/2}$ versus $\frac{1}{T}$ should yield the parameters of the trapping system E_t and N_t as the slope and intercept respectively of a straight line. With more than one set of traps the corresponding number of straight lines should be observed.

Fraction of free space charge, f_o

The periodic space charge which is produced acoustically and which is responsible for current saturation can be thought of as two streams of bunched charge, one mobile, the other bound to electron-trapping centres. According to Hutson and White[6] a fraction f_o of the total space charge is mobile in the conduction band and hence the factor f_o is just μ_d/μ_H (from Eqn.5.1),

$$\therefore \quad f_o = \mu_d/\mu_H \qquad 5.5$$

As long as the relaxation time τ for trapping is such that $\tau \ll 1/\omega$, where ω is the dominant acoustic frequency the two streams will be coincident in space and time and are in phase and the ratio of the free charge to the total charge will be given by f_o. However, when $\tau \geq 1/\omega$ a phase difference develops which is best expressed by considering the two streams as in dynamical equilibrium. In this situation f_o becomes a complex quantity f given by[7]

$$f = \frac{bf_o}{(1-ia)}$$

where the function a is simply the ratio of the imaginary to the real part of f and measures the phase shift, and

$$b = \frac{f_o^2 + \omega^2\tau^2}{f_o(f_o + \omega^2\tau^2)} \qquad 5.6$$

The value bf_o is related to the effective drift mobility μ_d^* as follows.

The current saturation of the I-V characteristic occurs at a critical field E_c such that

$$f_o \mu_H E_c = \mu_d E_c = v_s \qquad (\text{when } \omega\tau << 1) \qquad 5.7$$

As long as the trapping time τ is less than $1/\omega$ Eqn.5.7 holds. When τ is equal to or greater than $1/\omega$ the drift mobility is modified by bf_o and

$$v_d = bf_o\mu_H E_c = v_s$$

so that

$$\mu_d = bf_o\mu_H = \frac{v_s}{E_c} \qquad 5.7(i)$$

Thus at $\omega\tau \approx 1$

$$f_o\mu_H = \mu_d/b = \mu_d^* \qquad 5.8$$

Current Saturation

The saturated current density at $\omega\tau \ll 1$, J_{sat_o} is given by

$$\begin{aligned} J_{sat_o} &= ne\mu_H E_c \\ &= ne\mu_d E_c / f_o \quad \text{[using Eqn.(5.5)]} \\ &= nev_s / f_o \\ &= (n + n_t)ev_s \quad \text{[from Eqn.(5.1)]} \qquad 5.9 \\ &= (n'ev_s) \end{aligned}$$

At $\omega\tau \geq 1$ the saturated current density can be obtained simply by replacing f_o by bf_o in Eqn.5.9, and[8]

$$\begin{aligned} J_{sat} &= \frac{nev_s}{bf_o} \\ &= \left(\frac{nev_s}{f_o}\right)\frac{1}{b} \\ &= J_{sat_o}/b \qquad 5.10 \end{aligned}$$

The modified drift mobility μ_d^* can then simply be written as

$$\begin{aligned} \mu_d^* &= \mu_d / b \\ &= \mu_d (J_{sat_o} / J_{sat}) \qquad 5.11 \end{aligned}$$

5.3 Variation of electron Drift mobility with Temperature

Fig.5.3 shows the measured electron drift mobility $\mu_d (= v_s/E_c)$ as a function of temperature from 100^o to 300^oK for crystal D78(1). μ_d was calculated from the data shown in curve 1, Fig.5.2. Also shown in Fig.5.3 are the experimentally determined values of Hall mobility $\mu_H = R_H\sigma$ over the same range of temperature and the same fixed intensity of illumination of 15%.

At higher temperatures μ_d almost coincides with μ_H and leads to an average value of mobility of 300 $cm^2v^{-1}sec^{-1}$ at room temperature. With decreasing temperature μ_d diverges from μ_H.

The decreased drift mobility μ_d at lower temperature can be explained in terms of a transition from a lattice controlled to a trap controlled drift mobility.

For a number of trapping levels Eqn.5.4 can be rewritten

$$(\mu_H/\mu_d - 1) = \frac{N_{t_1}}{N_c} \exp \frac{E_{t_1}}{kT} + \frac{N_{t_2}}{N_c} \exp \frac{E_{t_2}}{kT} + \ldots\ldots$$

$$\text{or} \quad (\mu_H/\mu_d - 1)T^{3/2} = \frac{N_{t_1}}{4{\cdot}24 \times 10^{14}} \exp \frac{E_{t_1}}{k} \cdot \frac{1}{T}$$

$$+ \frac{N_{t_2}}{4{\cdot}24 \times 10^{14}} \exp \frac{E_{t_2}}{k} \cdot \frac{1}{T} + \ldots\ldots$$

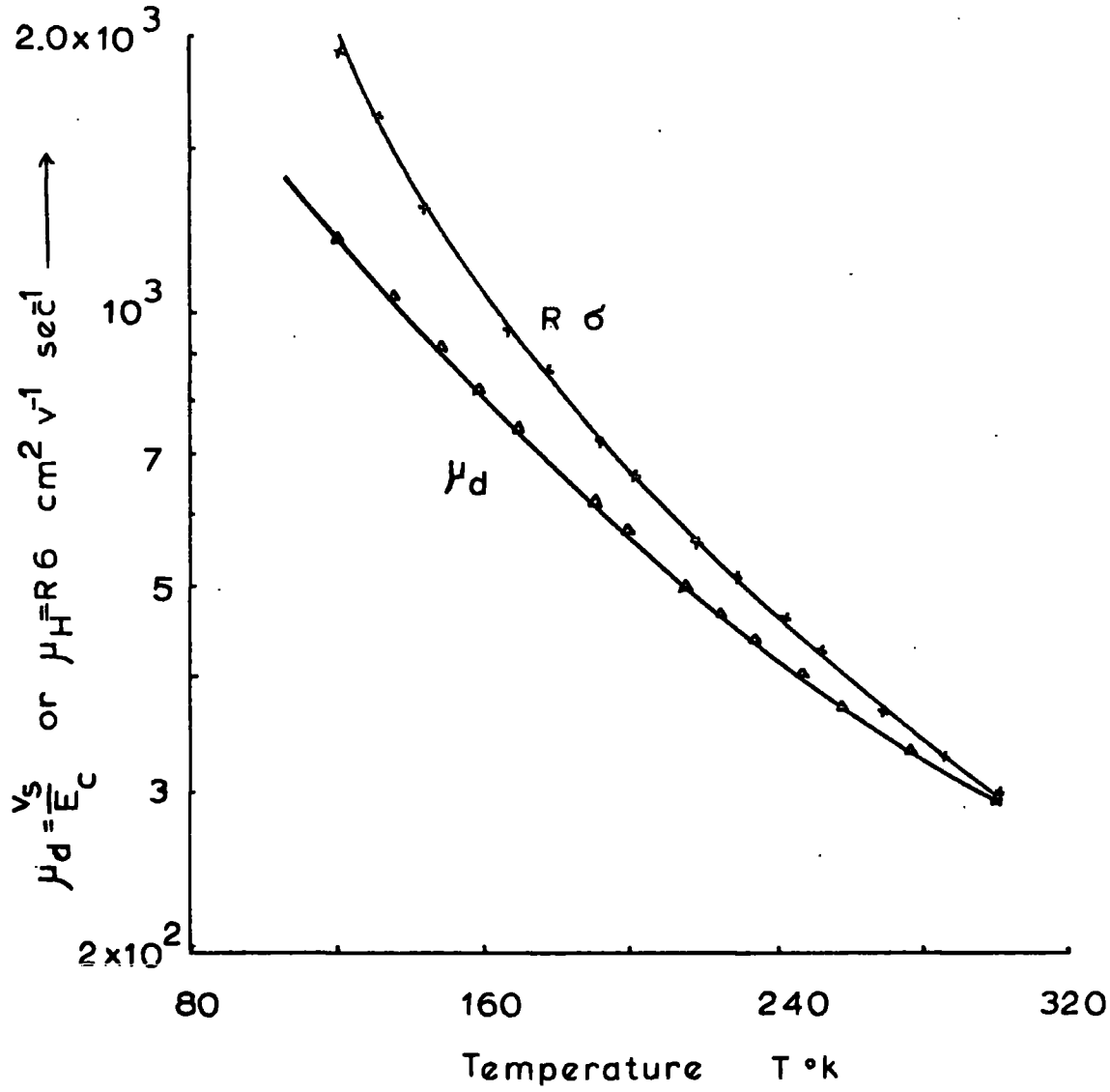

Fig.5.3. Drift mobility $\mu_d = \frac{v_s}{E_c}$, and $\mu_H = R\sigma$ as a function of T for crystal D78(1) at a fixed intensity of illumination of 15% of maximum (120 ft-c). Room Temp. $\sigma \sim 1{\cdot}34 \times 10^{-3}$ mho cm^{-1}.

$N_c = 4{\cdot}24 \times 10^{14} T^{3/2}$ for CdS with $m^*/m = 0{\cdot}2$.

A plot of $\log(\mu_H/\mu_d - 1)T^{3/2}$ versus $\frac{1}{T}$ should yield the parameters of the trapping system E_t and N_t as the slope and intercept respectively.

In order to facilitate the calculation of the trapping parameters (N_t, E_t), the results of Fig.5.3 are better represented by a plot of μ_H and μ_d versus $\frac{1}{T}$ as shown in Fig.5.4. The three sets of curves (a), (b) and (c) were obtained at three intensities of irradiation i.e. 1·5, 5, and 15% respectively.

The solid lines in Fig.5.5(a), (b) and (c) are the corresponding plots of $\log (\mu_H/\mu_d^{-1})T^{3/2}$ vs. $\frac{1}{T}$ calculated from curves (1) and (2) in Fig.5.4(a), (b) and (c) respectively. Values of E_t of 0·0115 eV, 0·01 eV and 0·008 eV and a density N_t of $1{\cdot}3 \times 10^{17} cm^{-3}$ were obtained for 1·5, 5 and 15% of the maximum light intensity. The apparent decrease of the trap depth with increasing illumination indicates that the elementary considerations which require f_o to be real are probably inadequate. It was necessary to determine whether the apparent variation in E_t was associated with f becoming complex or whether some other factor was operative.

The above results were calculated on the basis that Eqn.5.7 ($\mu_d' = v_s/E_c$) is valid. This is true as long as the trapping time τ is less than $1/\omega$, where ω is the dominant amplified frequency. In the experiment under discussion the temperature was varied and hence the

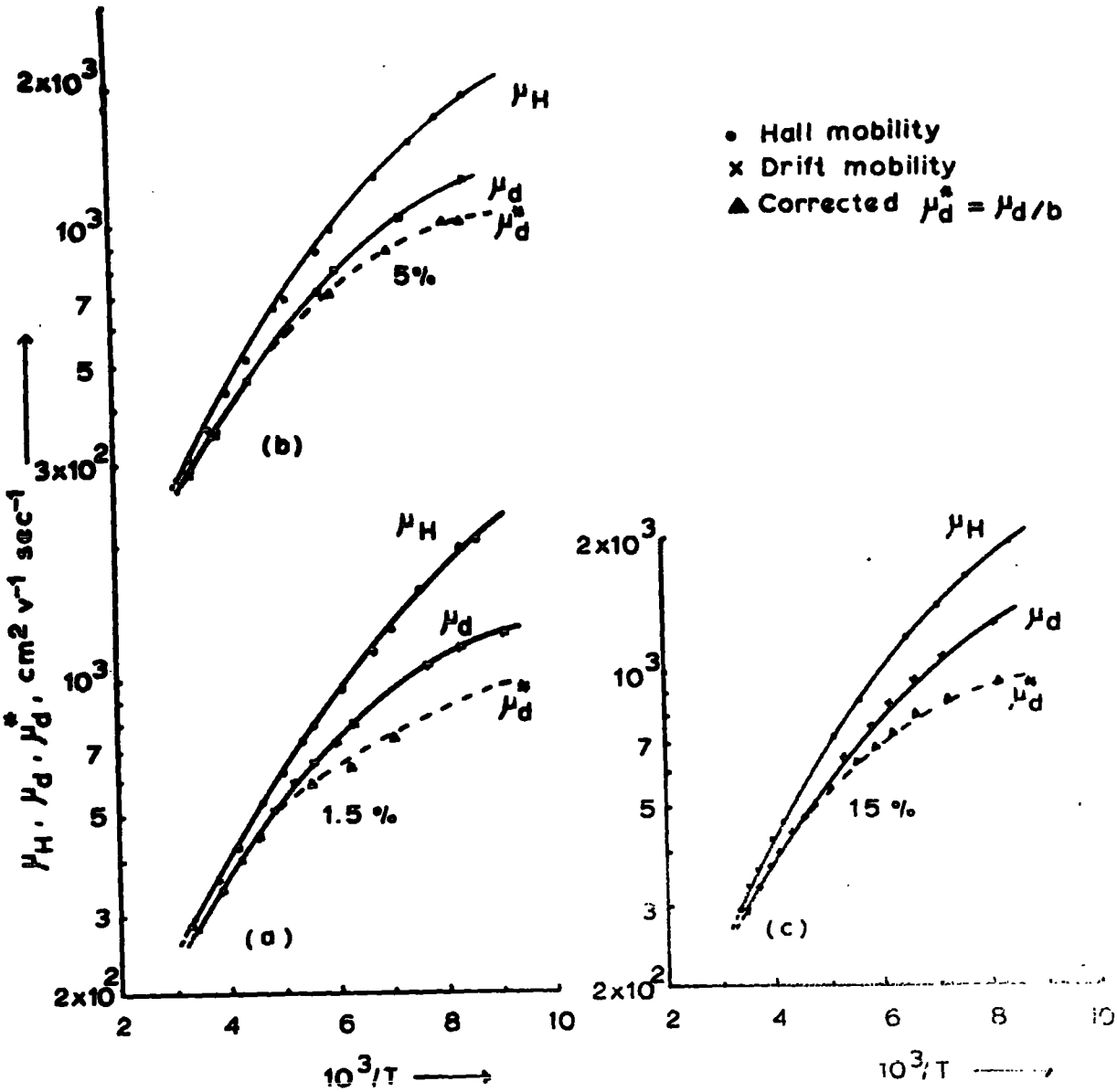

Fig. 5.4 Graph comparing the temperature dependence of the electron drift mobility with Hall mobility μ_H for crystal D78(1). (a) measurements were taken at 15% light intensity, $\mu_d = {}^{v}s/E_c$, and $\mu_d^* = \mu_d/b$ where $b = J_{sat_o}/J_{sat}$; (b) and (c) are as (a) but at 5% and 15% light intensity respectively.

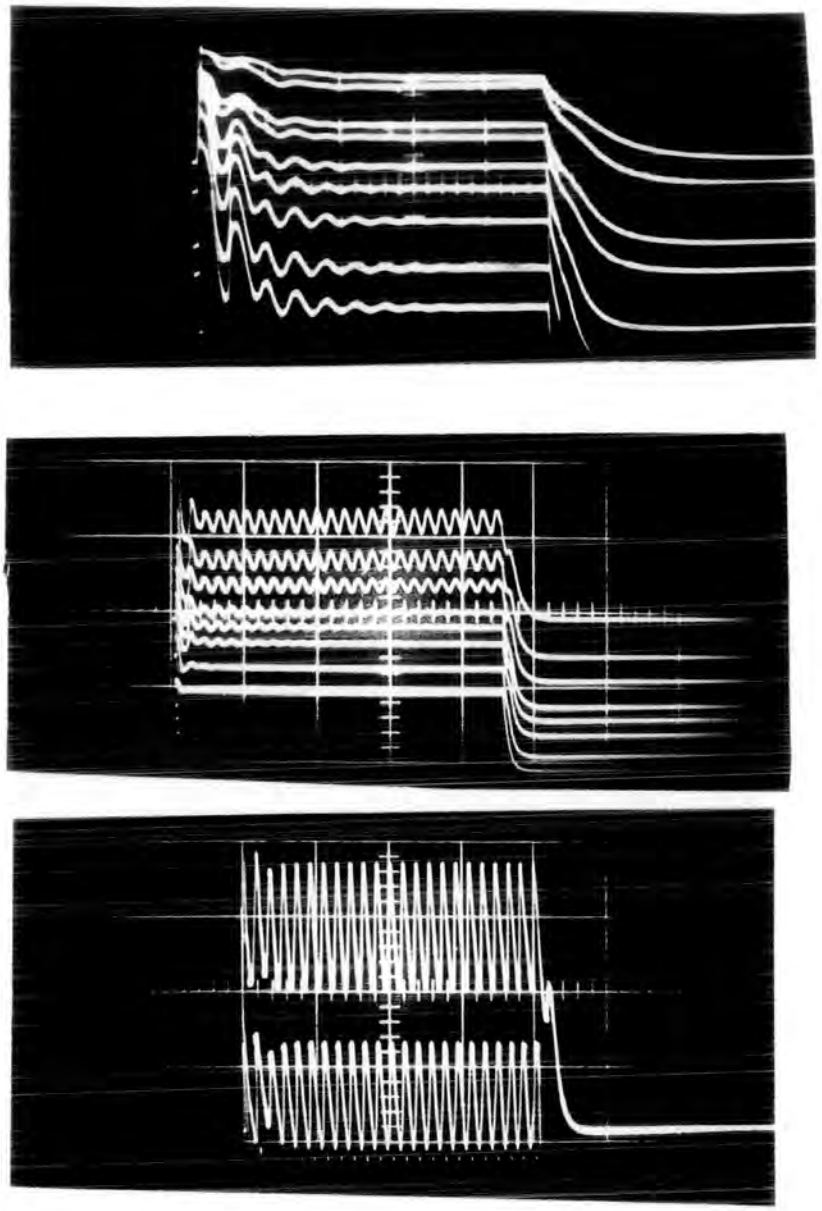

(a)

(b)

(c)

Fig.4.2 (a) Current saturation with damped oscillations in crystal D116(2). Upper traces are for decreasing conductivities (from $3{\cdot}0 \times 10^{-4}$ to $1{\cdot}0 \times 10^{-4}$ mho cm^{-1}). The period of oscillations changed from 2 μsec to 4 μsec. Hor. scale 5 μsec p. large div.

(b) Continuous current oscillations in crystal D116(3). Dimensions $6{\cdot}7 \times 2{\cdot}2 \times 1{\cdot}2$ mm^3. $\perp$ r c-axis. Upper traces for applied voltage increasing from 500 to 600 volts at $\sigma = 4{\cdot}0 \times 10^{-4}$ mho cm^{-1}. Hor. scale 20 μsec.

(c) Same as (a) with applied voltage increasing to 800 volts. Vertical scale 10 volts per large div. across 1 K Ω.

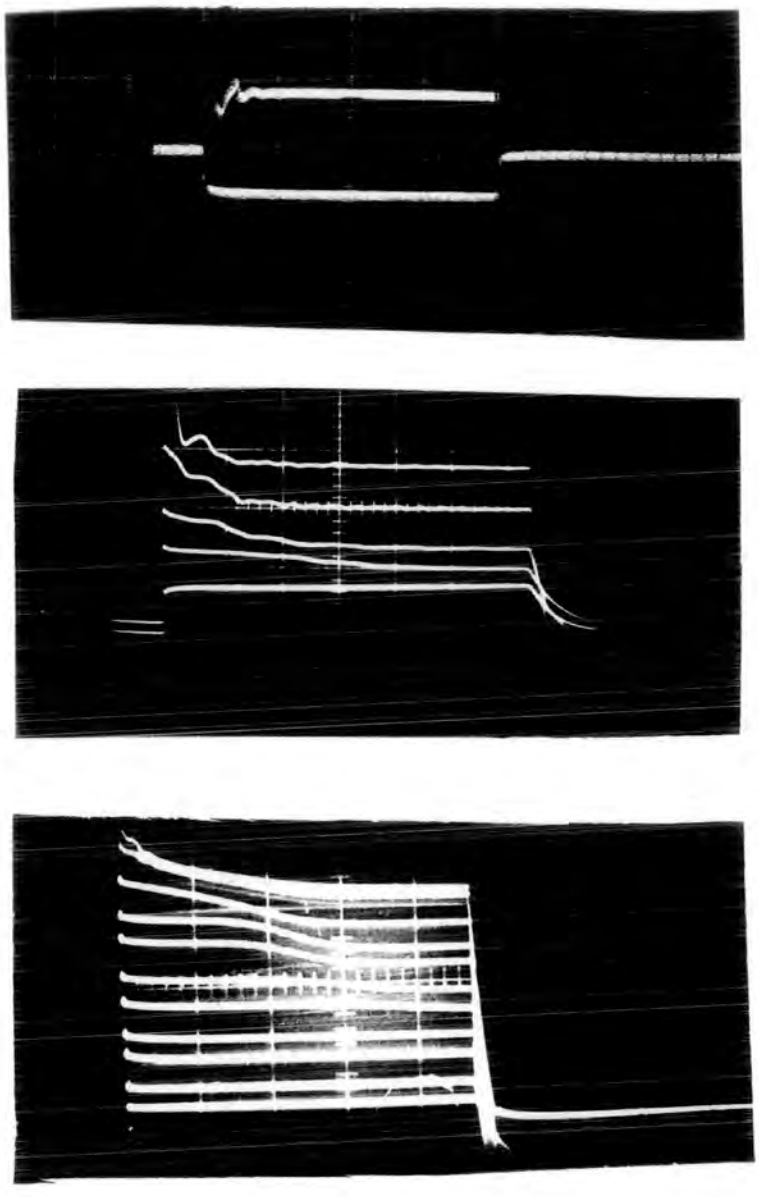

(a)

(b)

(c)

Fig.4.1 (a) Current saturation in crystal D116(2). Sample dimensions 3·35 x 2·25 x 1·65 mm^3, perpendicular to c-axis. Lower trace voltage pulse 500 volts per large div., 5 μsec per large div. Upper trace, current pulse $\sigma \sim 4 \cdot 0 \times 10^{-3}$ mho cm^{-1}.

(b) Same as (a). Upper traces are for increasing conductivity from $6 \cdot 0 \times 10^{-5}$ to $3 \cdot 0 \times 10^{-4}$ mho cm^{-1}. The build-up time decreased from 40 μsec to 15 μsec. Hor. scale 10 μsec p. large div. Upper trace, current pulse $\sigma \sim 4 \cdot 0 \times 10^{-3}$ mho cm^{-1}.

(c) Same as (a). Exaggerated build-up time (from 70 μsec to 10 sec) at $\sigma \sim 10^{-5}$ mho cm^{-1}. Upper traces show decreased build-up time with increased applied voltage (from 400 volts to 600 volts). Hor. scale 20 μsec p. large div.

a)

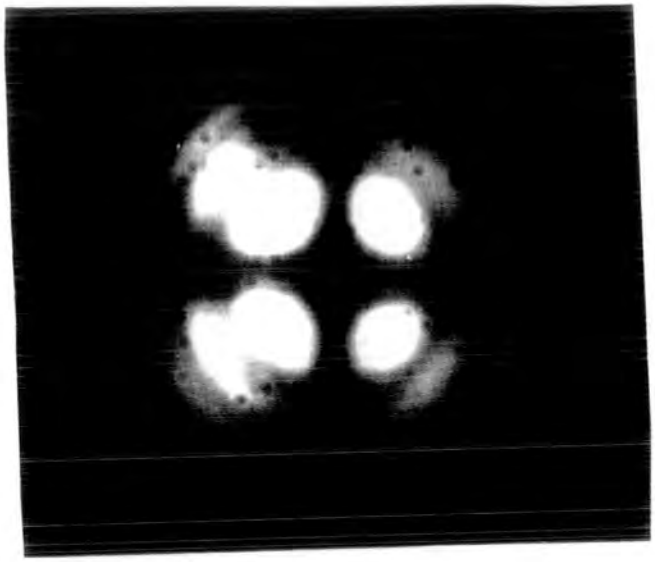

b)

Fig.3.2 (a) A uniaxial interference figure looking down the optic (hexagonal) axis of a CdS crystal,
(b) optic axis inclined to the axis of the microscope.

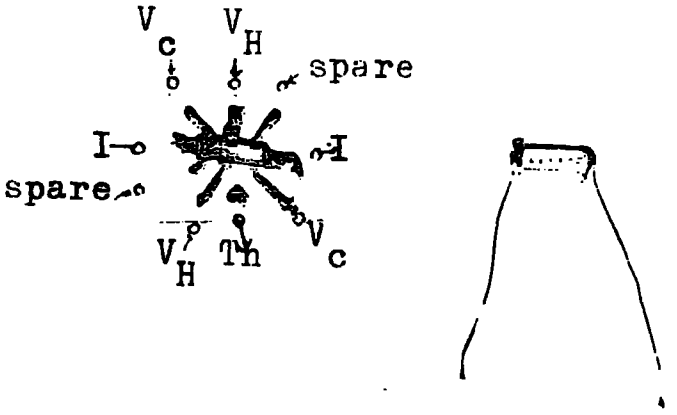

Fig.3.3 (a) Photograph of a mounted CdS Hall sample. I-I are current contacts; V_c-V_c are for conductivity and V_H-V_H for Hall voltage measurements.

(b) Shows large area contacts covering the ends for I-V characteristics and evaporated dots along the length (1 mm apart) for potential distribution measurements.

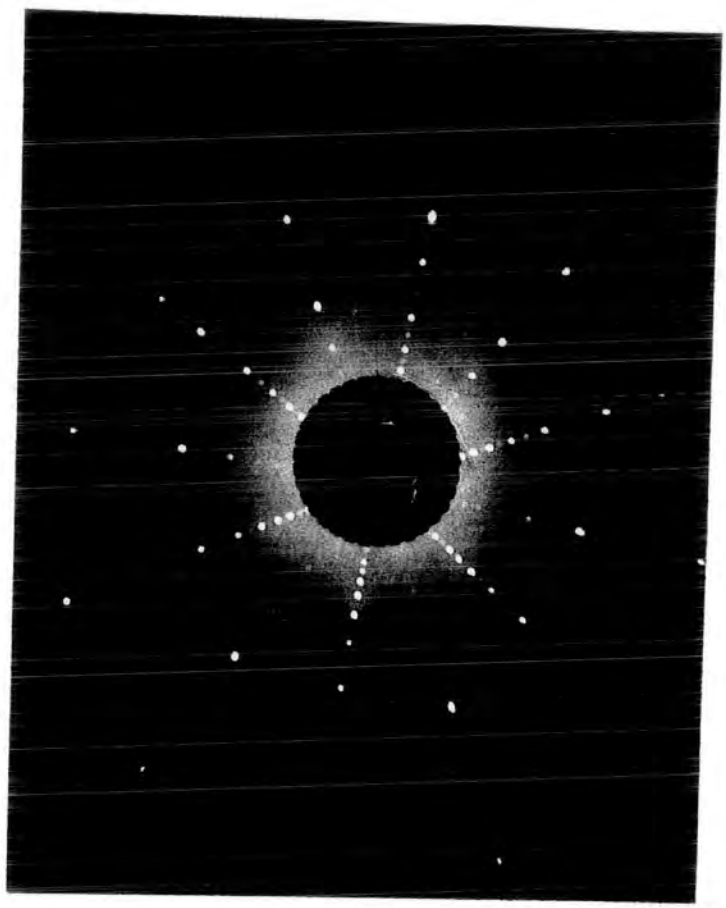

Fig.3.1 Back reflection X-ray photograph of a CdS crystal with incident beam parallel to the hexagonal axis.

temperature dependence of τ must be considered in calculating the drift mobility.

It was observed (see curve 2, Fig.5.2) that at temperatures below about 200°K the saturated current J_{sat} was less than J_{sat_o} (the room temperature value), which indicates a transition from $\omega\tau < 1$ to $\omega\tau > 1$. According to Eqn.5.10, at this point the value of b (J_{sat_o}/J_{sat}) changes from b = 1 to b > 1, and hence the values of μ_d in curve (2) Fig.5.4 should be modified further to $\mu_d^* = \mu_d/b$ according to Eqn.5.11. The dashed curves (3), Fig.5.4 show such corrected drift mobility values $\mu_d^* = \mu_d/b$. The drift mobility μ_d decreased (below 200°K) in the same ratio as the saturation current J_{sat} decreased from J_{sat_o}.

Finally when the corrected drift mobility values (the dashed curves (3), Fig.5.4) are utilised, a plot of $\log(\mu_H/\mu_d^* - 1)T^{3/2}$ versus $\frac{1}{T}$ displays two straight lines as shown by the dashed curves in Fig.5.5. Fig.5.5(a), (b) and (c) show the plots for the data obtained from Figs. 4(a), (b) and (c) respectively.

From the slope of the higher temperature line an average value of $E_{t_1} = 0{\cdot}037 \pm 0{\cdot}002$ eV was obtained. The calculated trap density was $N_{t_1} = 3{\cdot}1 \times 10^{16}$ cm^{-3}. From the lower temperature line average values of $E_{t_2} = 0{\cdot}015 \pm 0{\cdot}001$ eV and $N_{t_2} = 1{\cdot}35 \times 10^{17}$ cm^{-3} were obtained. Thus the differences between the measured values of μ_d and μ_H can be accounted for in terms of the presence of two sets of shallow traps.

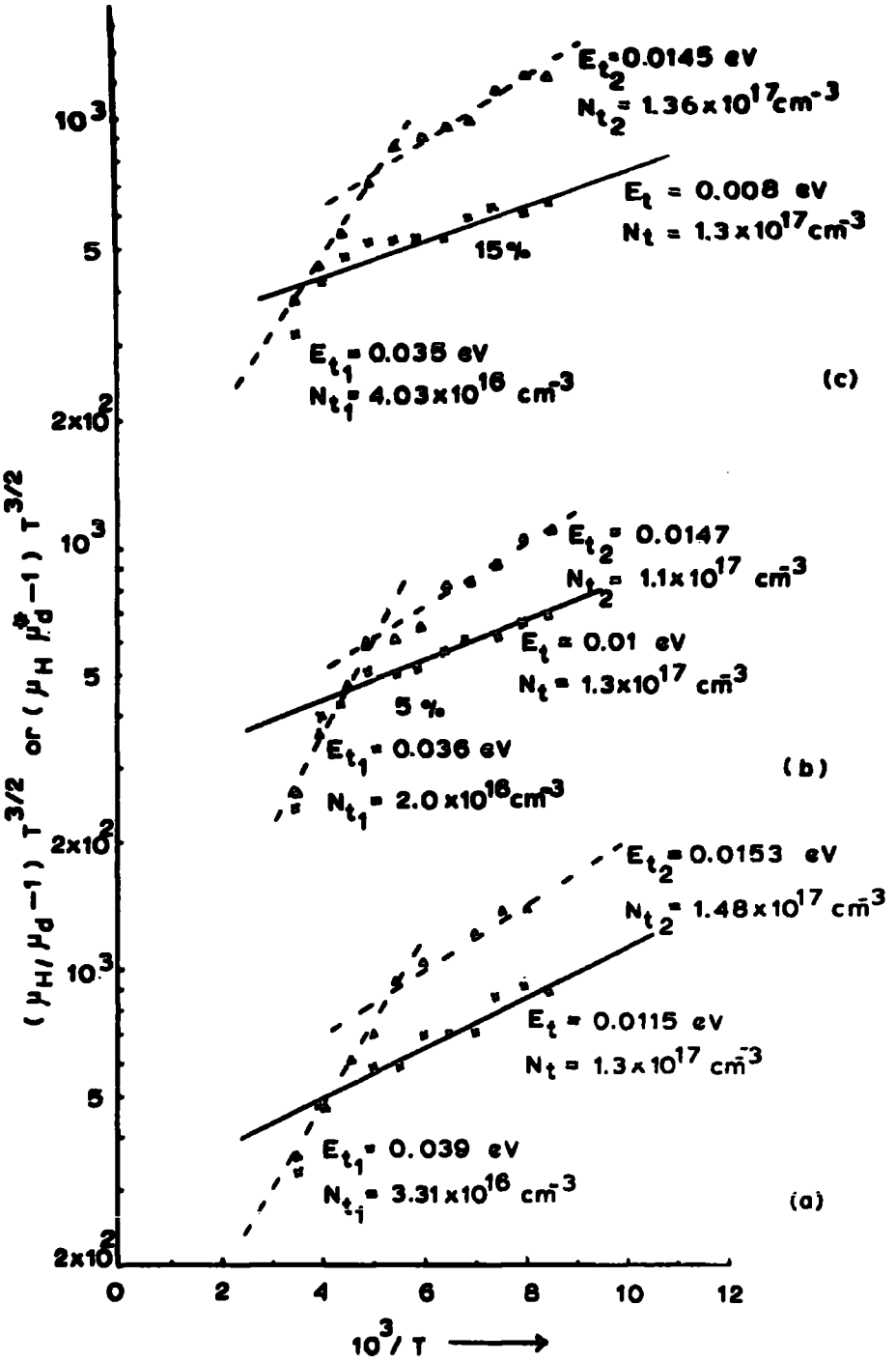

Fig. 5.5 $(\mu_H/\mu_d-1)T^{3/2}$ vs. $\frac{1}{T}$ for sample D78(1) as shown by solid line; (a) 1.5%, (b) 5% and (c) 15% intensity of illumination respectively. Also shown by broken line $(\mu_H/\mu_d^*-1)\,T^{3/2}$ vs. $\frac{1}{T}$. The trapping parameters E_t and N_t are shown in each curve. The broken line demonstrates two sets of trapping parameters E_{t_1}, E_{t_2} and N_{t_1}, N_{t_2} in each case.

(i) Capture cross section for electrons

The following procedure is adopted to estimate the capture cross section S of the shallower trapping level.

The equilibrium of the conduction band electrons in the presence of a given type of trapping centre will depend upon the capture cross section S of the centres, the density of states N_c and the mean thermal velocity of the electrons v_{th}. The trapping time τ can be expressed as

$$\frac{1}{\tau} = N_c v_{th} S \exp(-E_t/kT) \qquad 5.13$$

when b deviates from unity it can be assumed that $\omega\tau \simeq 1$. This occurs at ~200°K. ω is the dominant acoustic frequency and is given by[6] $\omega = (\omega_c \omega_D)^{\frac{1}{2}}$. ω_c (= σ/ϵ), ω_D (= v_s^2/D), σ, ϵ and D (= $\frac{\mu_d kT}{e}$) are the dielectric relaxation frequency, diffusion frequency, electrical conductivity, dielectric constant and diffusion constant respectively.

For the CdS sample D78(1) the following numerical values were used to calculate S.

$v_s = 2{\cdot}2 \times 10^5$ cm sec^{-1} (off axis shear wave)

$\omega_c = 1{\cdot}25 \times 10^{12} \times \sigma = 3{\cdot}75 \times 10^9$ sec^{-1} (at $\sigma = 3 \times 10^{-3}$ mho cm^{-1})

$\omega_D = 7{\cdot}6 \times 10^9$ sec^{-1}

Thus

$$\omega = \frac{1}{\tau} = (\omega_c \omega_D)^{\frac{1}{2}} = 5{\cdot}34 \times 10^9 \text{ sec}^{-1}$$

$$v_{th} \text{ (at } 200^\circ\text{K)} = \sqrt{\frac{2kT}{m^*}} = 1{\cdot}74 \times 10^7 \text{ cm sec}^{-1}$$

$$N_c = 4{\cdot}24 \times 10^{14}\ T^{3/2} = 1{\cdot}2 \times 10^{18}\ cm^{-3} \text{ (at } 200^{\circ}K)$$

$$\exp(-E_t/kT) = 0{\cdot}427 \text{ at } 200^{\circ}K \text{ and } E_t = 0{\cdot}015 \text{ eV}$$

The capture cross section, S, therefore becomes

$$S = \omega/N_e\ v_{th} \exp(-E_t/kT)$$

$$= 6{\cdot}0 \times 10^{-16}\ cm^2$$

This is of the order of magnitude to be expected for a centre which is singly positively charged when empty.

5.4 Discussion

Current voltage characteristics have been measured over a range of temperature between 300°K and 110°K in crystal D78(1). With decreasing temperatures down to 200°K although the saturated current changed very little the critical field for saturation E_c changed very rapidly (Fig.5.1). The value of E_c as a function of temperature is shown in curve 1, Fig.5.2

The carrier concentration estimated from the saturated current density $n' (= ev_s/J_{sat}$, curve 3, Fig.5.2) does not follow the free carrier concentration n (curve 4, Fig.5.2) obtained from the Hall coefficient (at temperatures below $\sim 200^{\circ}K$). The essential point of this difference between n and n' is that both trapped and free carriers are involved in current saturation. At lower temperatures (according to

Eqns. 5.9 and 5.10) both free and bound electrons ($n + n_t$) contribute to the current saturation. As long as the trapping time $\tau < \frac{1}{\omega}$, Eq.5.9 is effective, this is true in our experiments for temperatures down to 200°K. However at still lower temperature τ becomes greater than $\frac{1}{\omega}$ and saturated current is modified by the factor b (Eqn.5.10) when the free and trapped chatge is bunched out of phase.

The value of drift mobility obtained from current saturation due to the acoustoelectric effect does not agree with the Hall mobility measured at lower temperatures (110-300°K). The smaller values of drift mobility show that at lower temperature the charge transport is controlled by trapping states close to the conduction band. Initially when the temperature variation of $\omega\tau$ was neglected the depth of the dominant trap appeared to vary from 0·0115 to 0·008 eV when the intensity of illumination was increased by one order of magnitude. However using the corrected values of drift mobility $\mu_d^* = \mu_d/b$ according to Eqn.5.10, two trapping levels of E_{t_1} = 0·037 eV and E_{t_2} = 0·015 eV at densities $N_{t_1} = 3{\cdot}1 \times 10^{16}$ cm^{-3} and $N_{t_2} = 1{\cdot}35 \times 10^{17}$ cm^{-3} were clearly demonstrated to be responsible for the effects observed.

Smith and Moore[8] have made similar measurements on a photoconducting CdS crystal. They analysed their results in terms of a single trapping level at 0·025 eV with a density of $3{\cdot}4 \times 10^{17}$ cm^{-3}. However they did not consider the variation of the factor b (Eqn.5.10) in their calculation.

It has been shown by Kroger et al[9] who measured the conductivity and Hall coefficient that the activation energies associated both with donor impurities and with shallow defect centres in CdS are at about 0·03 eV. Using the simple hydrogen model approximation Kroger et al[10] estimated that the ionisation energy of the shallow donors should be 0·04 eV.

In an experiment involving time resolved photoluminescence spectra of green emission in CdS Colbow[11] obtained a value of the donor binding energy of 0·03 eV at donor concentration of 10^{16} cm^{-3}.

Spear and Mort[12] measured the electron drift mobility by studying charge transport in CdS crystals and found that high mobility (~ 265 cm^2 $v^{-1}sec^{-1}$) CdS crystals have a shallow trapping level with activation energy that decreases with increasing trap density. The energy is given by[12]

$$E_t = E_{t_o} - a\, N_t^{1/3}$$

where $E_{t_o} = 0{\cdot}049$ eV and $a = 4{\cdot}2 \times 10^{-8}$ eV cm.

Inserting the present experimental values of N_{t_1} and N_{t_2} in the above equation ionisation energies of the two shallow traps in our sample become $E_{t_1} = 0{\cdot}0358$ eV and $E_{t_2} = 0{\cdot}027$ eV.

Further in order to provide a test for the trap theory, we have estimated directly the magnitude of the capture cross section for recombination of an electron with the trapping centre. The value of

$S = 6 \times 10^{-16}$ cm^2 was obtained for the 0·015 eV trap. This suggests that ionised donors are responsible for these shallow trapping levels. The drift mobility experiments performed at lower temperatures, therefore, can clearly provide a sensitive means of studying shallow centres.

Photo-Hall measurements made on the same crystal D78(1) indicated the presence of two deeper trapping levels with activation energies of 0·281 eV and 0·362 eV (see Chapter IV). These deeper traps would have such larger values of τ that the electrons captured in them would be unable to bunch in the acoustoelectric field in the time available (i.e. $\frac{1}{\omega}$). With such traps $\omega\tau >> 1$, and under this condition $\mu_d = \mu_H$. Thus the current saturation experiment can not provide information about deep traps. The drift mobility technique, therefore, complements the photo-Hall effect[13] and TSC[14] methods as a means of determining trap parameters.

References

1. D. Gerlich, J. Phys. Chem. Solids, 28, 2575, 1967.

2. H. Fujita, K. Kobayashi, T. Kawai and K. Shiga, J. Phys. Soc. Japan, 20, 109, 1965.

3. A.R. Hutson, Phys. Rev. Letters, 9, 296, 1962.

4. R.H. Bube, "Photoconductivity", John Wiley and Sons, N.Y. 1960, p.68.

5. A.R. Smith, "Semiconductors", Cambridge University Press, London, 1959.

6. A.R. Hutson and D.L. White, J. Appl. Phys. 33, 40, 1962.

7. I. Uchida, T. Ishiguro, Y. Sasaki and T. Suzuki, J. Phys. Soc. Japan, 19, 674, 1964.

8. A.R. Moore and R.W. Smith, Phys. Rev., 138, A1250, 1965.

9. F.A. Kroger, H.J. Vink and J. van der Boomgraard, Z. Phys. Chem., B203, 1, 1954.

10. F.A. Kroger, H.J. Vink and J. Volger, Physica, 20, 1095, 1954.

11. K. Colbow, Phys. Rev., 141, 742, 1966.

12. W.E. Spear and J. Mort, Proc. Phys. Soc. (London), 81, 130, 1963.

13. R.H. Bube and H.E. Macdonald, Phys. Rev., 121, 473, 1961.

14. K.H. Nicholas and J. Woods, Brit. J. Appl. Phys., 15, 783, 1964.

CHAPTER VI

EFFECT OF INFRA-RED QUENCHING ON THE THRESHOLD FIELD FOR CURRENT SATURATION

INTRODUCTION

Cadmium sulphide crystals have always been found to be n-type at room temperature.[1,2] It is not yet possible to dope CdS in such a way that it becomes p-type. However, it is possible to excite free carriers and obtain a majority of free holes[3] by simultaneous irradiation with band gap and infra-red radiation at room temperature. The effect of the infra-red quenching radiation, on the one hand, is to reduce the density of free electrons, and on the other hand, is to increase the hole population. In view of this dual effect of infra-red radiation, it seemed worthwhile to examine the effect on the threshold field for current saturation as the relative population of holes in the free carrier concentration was increased.

6.1 Optical Quenching in CdS

Optical quenching measurements were made on crystal D116(1). The sample was selected because of its very high photosensitivity and uniform potential distribution (Chapter IV, Section 4.5).

The sample with dimensions 7·3 x 2·1 x 1·25 mm^3, was such that its long dimension coincided with the c-axis. It was provided with its cathode by melting indium on to an evaporated layer of indium. The anode contact was of silver paste (Johnson Matthey grade FSP43) on evaporated gold. The purpose of the gold contact was to promote reasonable hole injection at the anode.[4]

To make the measurements under quenching conditions, the sample was placed in a Tufnol box (5" x 4" x $2\frac{1}{2}$"), which contained a window ($1\frac{1}{2}$" x 1") through which the crystal could be simultaneously irradiated with band gap and infra-red radiation.

The band gap illumination was provided by light from a 48W tungsten lamp passing through an 0·52 μm, wide band interference filter and a 1·5 cm path of a 10% solution of copper sulphate. The intensity of illumination was varied using neutral density filters.

The infra-red radiation was provided by a second 48W tungsten lamp which passed through an OX2 Chance glass filter (transmission 0·75 to 4·5 μm). Both the lamp transformers were powered from stabilised 240 vac supplies. The OX2 Chance glass filter spans the wavelength

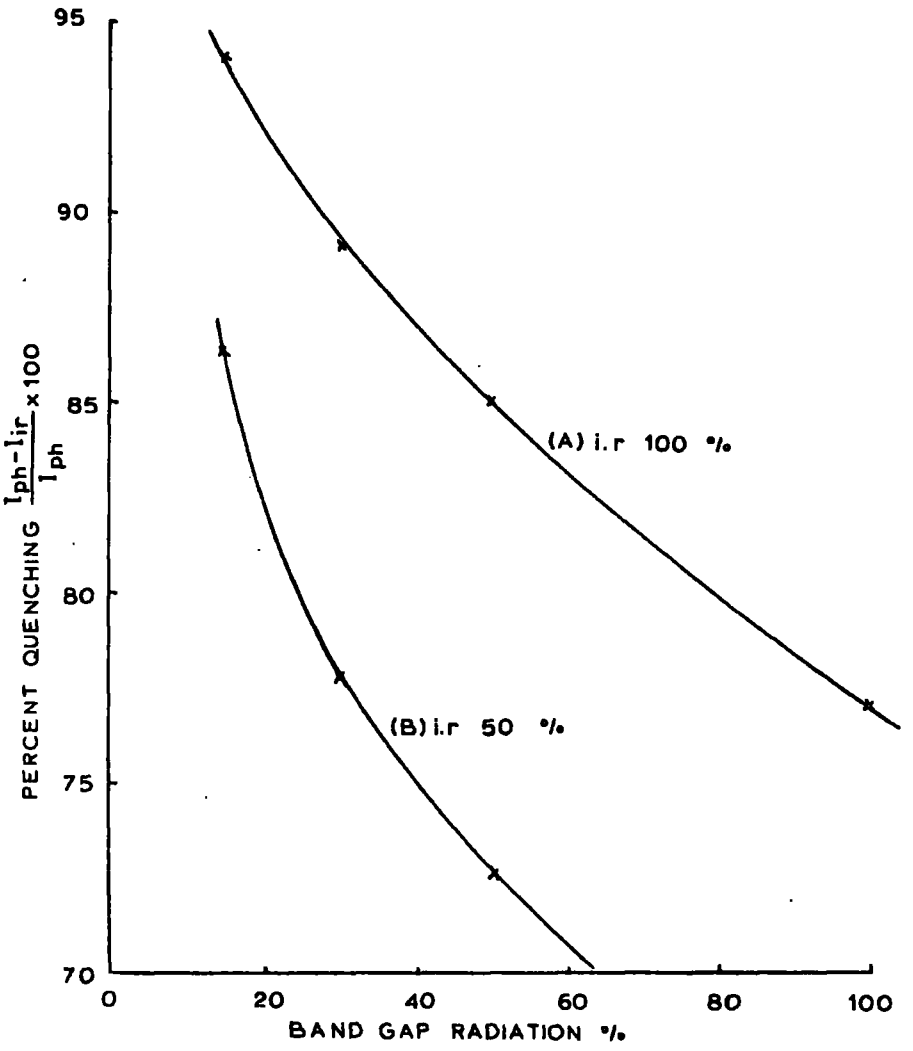

Fig.6.1. Per cent quenching as a function of primary (5200Å) radiation in crystal D116(1). Curve A was obtained at fixed maximum intensity of i.r. (O x 2 filter) radiation; curve B with half the maximum i.r. radiation. Per cent quenching decreases with decreasing infra-red and/or increasing primary radiation.

range of the quenching spectrum of photoconductivity in CdS which has two maxima at 0·9 and 1·45 μm[5] at room temperature.

As a measure of the quenched photo current, the quantity 'per cent quenching' Q is used. Per cent quenching refers to the ratio of the difference between the quenched equilibrium current, I_{ir}, and the maximum unquenched current, I_{ph},

$$Q = \frac{I_{ph} - I_{ir}}{I_{ph}} \times 100 \qquad 6.1$$

The magnitude of the quenching effect as a function of the intensity of the primary radiation (0·52 μm) at two fixed intensities of the infra-red radiation is shown in Fig.6.1.

The ratio of the currents (I_{ph}/I_{ir}) is the inverse ratio of the sample resistances (R_{ph}/R_{ir}). Curve A, Fig.6.1, shows that the per cent quenching decreased from 94% to 77% as the intensity of primary radiation was increased from 15% to the maximum available. The magnitude of the quenching, however, decreased from 86% to 61% (curve B), over the same range of primary radiation, but with half the intensity of infra-red intensity used to obtain curve A.

There are, therefore, two ways to decrease the effective per cent quenching in CdS: (1) to decrease the intensity of infra-red radiation and (2) to increase the intensity of primary radiation.

6.2 Effect of infra-red quenching on photo-Hall mobility

It is well known that there are negatively charged sensitizing centres in CdS, with levels which lie about 1·0 eV above the top of the valence band.[5] Under photoexcitation these centres capture excited holes and become neutral. In CdS these captured holes are thermally stable at room temperature, but they can be ionised by the optical excitation of electrons from the valence band, i.e., by initiating infra-red quenching of photo conductivity.

The Hall mobility for two carrier conductivity can be expressed as[6]

$$\mu_H = (p\mu_p^2 - n\mu_n^2)/(p\mu_p + n\mu_n) \qquad 6.2$$

where p and n are the concentrations of holes and electrons, and μ_p and μ_n are the hole and electron mobilities. There is therefore a strong possibility of observing a change in the Hall mobility under quenching conditions as holes play a progressively more important role in the conduction process as the per cent quenching increases.

In order to gain some information about the effects of infra-red quenching the mobility of sample D116(1) was measured under quenching conditions. The results are shown in Table 6.1. The magnitude of the quenching was varied by changing the intensity of primary radiation only while the intensity of the infra-red was maintained at a maximum.

The table shows the Hall data obtained at three different levels of quenching.

TABLE 6.1

Hall mobility data under quenching radiation

Crystal - D116(1). Dimensions 7·3 x 2·1 x 1·25 mm^3

I		II	III		IV	V	
Conductivity σ mho cm^{-1}		P.C. Quenching	Hall mobility μ_H $cm^2\ v^{-1} sec^{-1}$		Free electron concentration cm^{-3} before quenching	Free electron and free hole concentration with quenching n cm^{-3}	
			without quenching	with quenching			
(a)	(b)		(a)	(b)		(n)	(p)
$2·3 \times 10^{-3}$	$4·6 \times 10^{-4}$	80	300	160·3	$4·8 \times 10^{14}$	$5·57 \times 10^{12}$	$2·5 \times 10^{13}$
$1·39 \times 10^{-3}$	$2·3 \times 10^{-4}$	85	300	105·9	$2·89 \times 10^{14}$	$2·1 \times 10^{12}$	$1·68 \times 10^{13}$
$5·56 \times 10^{-4}$	$2·83 \times 10^{-5}$	95	300	88	$1·16 \times 10^{14}$	$2·33 \times 10^{11}$	$2·2 \times 10^{12}$

The Hall mobility under infra-red quenching (two carrier mobility) is shown in column III(b). The following method was used to calculate the electron and hole concentrations shown in column V(a) and V(b).

(1) The ratio of p/n was first estimated from eqn.6.2 ~~assuming~~ assuming values of $\mu_n = 300$ $cm^2 v^{-1} sec^{-1}$ and $\mu_p = 48$ $cm^2 v^{-1} sec^{-1}$ (see Section 6.4).

(2) The concentrations of electrons and holes were then obtained by considering the contributions of both electrons and holes towards the conductivity under quenching conditions (column I(b)).

The data in column V(a) and V(b) indeed show that the infra-red quenching radiation on the one hand reduced the density of free electrons, and on the other hand increased the hole population. With 95% quenching the hole population was roughly ten times that of the free electrons.

6.3 Current-voltage characteristics under quenching conditions

In order to extend the information about the effect of infra-red excitation (increased hole population) on the threshold field for current saturation, current-voltage characteristics were obtained under quenching conditions.

The data presented here were obtained from crystal D116(1). The c-axis was parallel to the long dimension of the sample. The sample contacts and the method of illumination were the same as those described in Section 6.1.

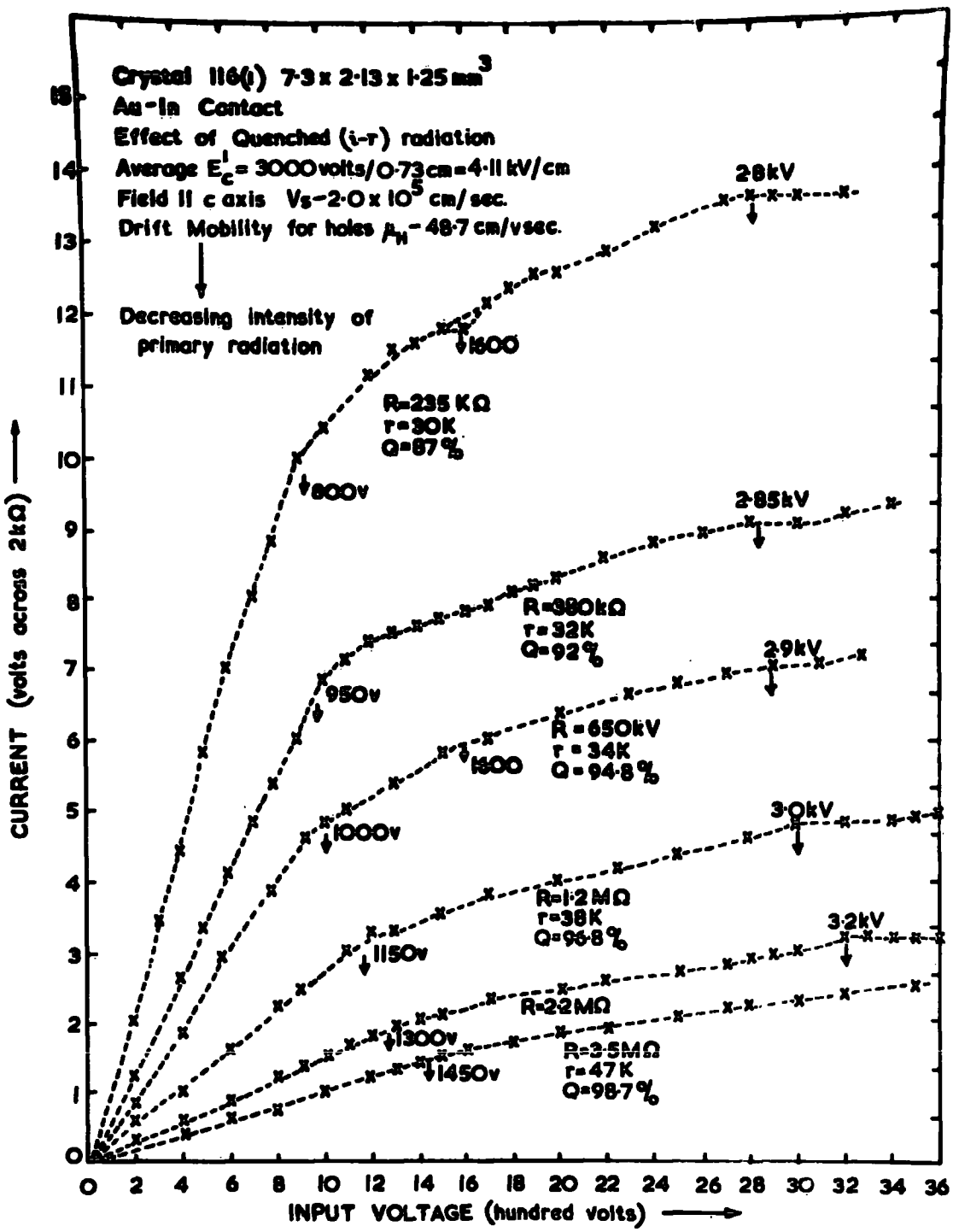

Fig.6.2 Current-voltage characteristics of the crystal D116(1) under i.r. quenching conditions. The intensity of the i.r. radiation was held at a maximum. The intensity of the band gap radiation was increased to reduce the resistance of the sample. R = resistance of the sample under quenching condition; r = resistance with band gap radiation only; Q = percent quenching as defined in the text.

The current-voltage characteristics were measured at room temperature with 30 μsec pulses at a repetition frequency of 25 counts/sec and are shown in Fig.6.2. The characteristics were obtained with the fixed maximum intensity of i.r. and different intensities of band gap irradiation. The lower curves correspond to lower intensities of primary radiation. Beside each curve in Fig.6.2 the sample resistance with quenching, R, and without quenching, r, is shown as well as the per cent quenching Q. Each I-V characteristic shows departures from linearity at two different field strengths.

In a second experiment the quenching radiation was turned off and current voltage characteristics were measured with band gap illumination only. The current-voltage characteristics obtained are shown in Fig.6.3. These curves show that as the resistivity of the sample was reduced by increasing the excitation intensity, the saturation became more pronounced. The critical field is denoted by the arrow on each curve and can be seen to have remained substantially unchanged while the resistance of the sample was reduced from 1•2 MΩ - 4•2 KΩ However, the lower four curves obtained at low conductivities show that the current returned to the ohmic value (with an accompanying increase in build up time) at field intensities more than about twice the critical field for saturation (1400 v cm^{-1}). Current saturation could not be detected when the conductivity was reduced below 10^{-5} mho cm^{-1}.

At the lower conductivities the acoustic wave amplification would be low because of the weak acoustoelectric interaction.[11] At the critical field for current saturation, however, the amplification (at $\sigma > 10^{-5}$ mho cm^{-1}) of the acoustic wave was large enough to obtain a net round trip gain and flux build up was possible with large build up times. However, at field intensities more than twice the critical field, the amplification failed to produce a net gain due to the lower acoustic wave amplification[18] and on further increase in applied field the current gradually returned to ohmic value. The shape of the characteristics in Fig.6.3 is entirely in agreement with the prediction of the small signal theory of Hutson and White.[11]

(i) Comparison of Fig.6.2 and Fig.6.3

It is immediately apparent that the curves shown in Fig.6.2 are substantially different from those shown in Fig.6.3. For example, the magnitude of the critical field E_c at which the characteristics first departed from linearity under quenching conditions increased by a factor of two (from 1100 v/cm to 2000 v/cm) as the per cent quenching was increased from 87 to 98·7%. In contrast when primary radiation only was used, Fig.6.3, the threshold field remained substantially constant.

The interesting point to note in Fig.6.2 is that the characteristics under the quenching conditions exhibit a second saturation at about 3·0 kv which it totally absent from curves of Fig.6.3.

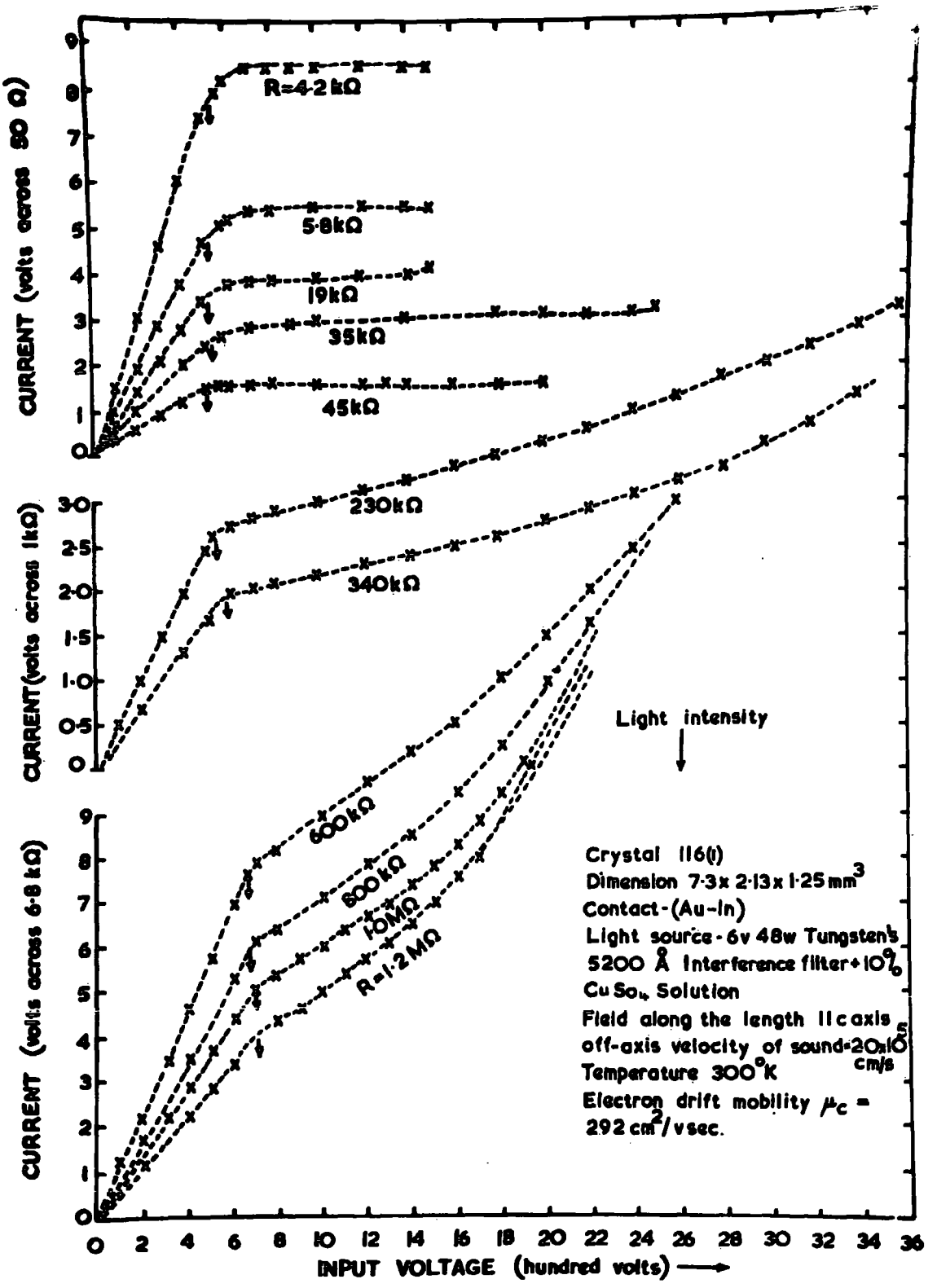

Fig.6.3 Current-voltage characteristics for crystal D116(1) under illumination with various intensities of band gap (5200 Å) light. Each curve is marked with the ohmic resistance.

(ii) The drift mobility of electrons

Assuming that the acoustoelectric interaction occurred via the off axis shear modes,[7] then $v_s = 2{\cdot}0 \times 10^5$ cm sec^{-1} and the value of the electron drift mobility calculated from the curves of Fig.6.3 lies between 295 and 303 $cm^2\ v^{-1} sec^{-1}$ (i.e. E_c lies between 650 and 700 v/cm). The measured Hall mobility was found to have a similar value of 300 $cm^2\ v^{-1} sec^{-1}$ (see surve 2, Fig.4.8).

This method of calculating drift mobilities depends on the uniformity of the sample (Section 4.4(i)). The distribution of potential (uniformity) was checked under pulsed conditions in both the ohmic and the saturation regions of the I-V characteristic with band gap radiation (see Fig.4.7, Chapter IV). No appreciable non-uniformity was apparent in the ohmic region.

(iii) The drift mobility of holes

The drift mobility under quenching conditions calculated from the curves of Fig.6.2 was smaller than the value found when band gap irradiation only was used. The drift mobility obtained from the first saturation lay between 185 $cm^2\ v^{-1} sec^{-1}$ and 100 $cm^2\ v^{-1} sec^{-1}$ (corresponding to fields between 1080 and 2000 v cm^{-1}, $v_s = 2{\cdot}0 \times 10^5$ cm sec^{-1}). The apparent decrease in the electron drift mobility by a factor of 2~3, demonstrates an increased participation of holes in the mechanism of current saturation as a result of i.r. quenching. The

mobility measured is in fact an ambipolar mobility[15] (see Section 6.5).

Not only did the optical freeing of holes have a distinct effect on the first saturation, but a second saturation at a field E_c', much greater than E_c, was produced. This second saturation was totally absent from the curves of Fig.6.3. The second saturation is probably due to an acoustoelectric interaction with holes (discussed below), which occurs when the drift velocity of holes equals the velocity of sound. If this is correct, a measurement of E_c' will provide a simple method of determining the drift mobility of holes.

The characteristics of Fig.6.2 exhibit a second saturation at about 3·0 kv, i.e. a field of 4·1 kv cm^{-1} which corresponds to a carrier mobility of 48 $cm^2\ v^{-1}\ sec^{-1}$ ($v_s = 2{\cdot}0 \times 10^5$ cm sec^{-1}), which is close to values reported previously for holes in CdS.[8,9]

Using a crystal of CdS with a sufficiently long hole life time. Le Comber et al[8] have observed interaction between holes and piezo-electric lattice modes in a modified Haynes-Shockley photo-injection time of flight experiment.[10] Using a velocity of sound $v_s = 1{\cdot}8 \times 10^5$ cm sec^{-1}, which is appropriate for a crystal oriented perpendicular to the c-axis, Le Comber et al obtained a hole mobility of 23 $cm^2\ v^{-1} sec^{-1}$ at room temperature.

While measuring the photo-Hall mobility of electrons in CdS Onuki and Hase[9] calculated the hole mobility to be 38 $cm^2\ v^{-1} sec^{-1}$, the

electron mobility was 235 $cm^2\ v^{-1}sec^{-1}$. They[9] also estimated a hole mobility of 48 $cm^2\ v^{-1}sec^{-1}$ for a sample with an electron mobility of 290 $cm^2\ v^{-1}sec^{-1}$.

The value of hole mobility determined from the second saturation of Fig.6.2 was 48 $cm^2\ v^{-1}sec^{-1}$ (using an off axis shear wave velocity $v_s = 2{\cdot}0 \times 10^5$ cm sec^{-1}) while the electron Hall and drift mobility at room temperature lay between 295 and 303 $cm^2\ v^{-1}sec^{-1}$ (see Section 4.8).

6.4 Discussion

Hutson and White[11] have demonstrated that ultrasonic travelling wave amplification is possible in piezoelectric semiconductors by drifting majority carriers (either electrons or holes) in the same direction as the sound waves.

Ultrasonic amplification and non-ohmic behaviour have been observed by drifting holes in tellurium[12,13] (the sample was cooled to $77^{o}K$, when conduction became p-type). Ishiguro et al[12] estimated the hole mobility in tellurium from the onset of current saturation and found good agreement with the Hall mobility.

Sommers et al[14] have reported positive evidence for significant minority carrier drift in insulating crystals of CdS from the measurements of the short circuited photoelectro magnetic (PEM) current.

Recently Greebe[15] (1968) has shown that over a restricted range of electric field, minority carriers can amplify ultrasound as effectively as majority carriers.

[Greebe[15] has discussed the theoretical contribution of minority carriers to the interaction between ultrasound and charge carriers in piezoelectric semiconductors. He has deduced an expression for the amplification factor α (for details see ref.5) with the aid of a some what more general formulation of the small signal theory of Hutson and White.[11]]

From the above discussion it appears most likely that the second saturation observed in Fig.6.2 is due to the amplification of ultrasound and the accompanying acoustoelectric interaction with drifting holes. The nature of the curves may be explained as follows:

(1) The second saturation, E_c' , occurs at a critical field about six times greater than the critical field for saturation with the band gap irradiation only E_c.

(2) Amplification of ultrasound occurs when the electron drift velocity exceeds the velocity of sound ($v_d \geq v_s$) in CdS.[11] When the drift field increases beyond the critical value ($v_d = v_s$), the amplification decreases after reaching a maximum[17] and becomes negligible at electron drift velocities more than three times the velocity of sound ($v > 3v_s$).

(3) At a field intensity greater than six times the critical field for saturation (the second saturation E_c' in Fig.6.2), the electrons contribute very little for the amplification of acoustic flux generated in the crystal.

(4) Carriers responsible for acoustoelectric interaction and current saturation at such a high field therefore can only be holes moving with a velocity equal to the velocity of sound (i.e. $E_c' = v_s/\mu_{dh}$, where μ_{dh} is the drift mobility of holes).

On ambipolar drift velocity

The change in the field at the first saturation in Fig.6.2 and the apparent decrease in the electron drift mobility under increased quenching would appear to be due to ambipolar effects.[16]

Under quenching conditions comparable numbers of electrons and holes are present in a CdS crystal (see Section 6.2). It is therefore possible to produce appreciable spatial 'bunching' of carriers without affecting the net space charge as both signs of carriers are present. Due to the strong piezoelectric property of the crystal the electrons and holes bunch in potential minima and maxima producing a conductivity modulation along the crystal.

The total field, E_t, in a crystal can be expressed as the sum of applied field E_a and the internal field E_i. The internal field arises in CdS as the bunched electrons and holes try to diffuse away with significantly different diffusion coefficients D, $D = \mu KT/e$. If the electrons and holes could move entirely independently of each other, the electrons would tend to move faster than the holes, leaving the holes behind altogether. When this actually begins to happen, however, since they are oppositely charged, their separation creates an internal electric field E_i which begins to retard the faster moving electrons and drags the slower moving holes more strongly. Eventually the internal field becomes large enough to counteract any tendency for the

charges to separate further. Under this condition the electrons and holes diffuse together and the effective diffusion coefficient becomes larger than that for holes, but smaller than that for electrons. When an external field is applied this phenomenon is known as "ambipolar diffusion", consequently in an external field an ambipolar[19] drift velocity must be used. The ambipolar mobility is defined by the expression:

$$\mu_a = \frac{(n_o - p_o)\mu_n\mu_p}{n\mu_n + p\mu_p}$$

$$= \frac{(n_o - p_o)\mu_n\mu_p}{(n_o + \delta_p)\mu_n + (p_o + \delta_p)\mu_p} \qquad 6.3$$

where n_o and p_o are the equilibrium electron and hole concentrations, and δ_p is the excess hole concentration for an n-type crystal.

Equation 6.3 is derived from a consideration ~~of the consideration~~ of the continuity equation applied to semiconductor into which a localised concentration of minority carriers is injected. The minority carriers are accompanied by an equal concentration of majority carriers but the number of these latter is very small compared with the equilibrium density of majority carriers n_o and p_o.

In our problem the excess electrons and holes are not localised when they are created by the interaction, but they are localised by the acoustoelectric interaction in sufficiently high fields. It is this localisation which leads to the ambipolar effect. The proper expression for the ambipolar mobility in a piezoelectric semiconductor where δp is greater than the equilibrium concentration p_o would seem to present a formidable mathematical problem. This has not been attempted and it is not possible therefore to compute the value of the ambipolar mobility μ_a in terms of n, p, μ_n and μ_p. However if the expression 6.3 is used it is interesting to note that with the values $n = 3{\cdot}3 \times 10^{11}$ cm^3, $p = 2{\cdot}97 \times 10^{12}$ cm^{-3}, $\mu_n = 300$ $cm^2v^{-1}sec^{-1}$ and $\mu_p = 48$ $cm^2v^{-1}sec^{-1}$ for sample D116(1) the value of μ_a would be 157 $cm^2v^{-1}sec^{-1}$ (at 95% quenching); the measured value was 146 $cm^2v^{-1}sec^{-1}$ (from fourth curve from bottom, Fig.6.2).

References

1. J. Woods and J.A. Champion, J. Electron Control, 7, 243, 1959.

2. D.C. Reynold, L.C. Green, R.G. Wheeler and R.S. Hogan, Bull. Am. Phys. Soc., 3, 111, 1956.

3. S.O. Hemila and R.H. Bube, J. Appl. Phys., 38, 5258, 1967.

4. R.W. Smith, Phys. Rev., 105, 900, 1957.

5. R.H. Bube, Phys. Rev., 99, 1105, 1955.

6. R.A. Smith, "Semiconductors", Cambridge Univ. Press, 1961, p.103.

7. J.H. McFee, J. Appl. Phys., 34, 1548, 1963.

8. P.G. Le Comber, W.E. Spear and A. Weinmann, Brit. J. Appl. Phys., 17, 467, 1966.

9. M. Onuki and N. Hase, J. Phys. Soc. Japan, 20, 171, 1965.

10. J. Mort and W.E. Spear, Phys. Rev. Letters, 8, 314, 1962.

11. A.R. Hutson and D.L. White, J. Appl. Phys., 33, 40, 1962.
D.L. White, J. Appl. Phys., 33, 2547, 1962.

12. T. Ishiguro and T. Tanuka, J. Phys. Soc. Japan, 21, 489, 1966.

13. G. Quentin and J.M. Thuillier, Proc. Int. Conf. Sem. Phys., Paris, 1964, p.571.

14. H.S. Sommers Jr., R.E. Berry and I. Sochard, Phys. Rev., 101, 987, 1956.

15. C.A.A.J. Greebe, Phys. Letters, 28A, 455, 1968.

16. W. van Roosbroeck, Phys. Rev., 91, 282, 1953.

17. A.R. Hutson, J.H. McFee and D.L. White, Phys. Rev. Letters, 7, 237, 1961.

18. T. Ishiguro, I. Uchida, T. Suzuki and Y. Sasaki, Trans. Sonics Ultrasonics, March 9, 1965.

CHAPTER VII

SUMMARY AND CONCLUSIONS

In the last three chapters various measurements on current saturation in photoconducting cadmium sulphide crystals have been described. Attempts have been made to interpret the results of these measurements in the appropriate chapters. The purpose here is to summarise briefly the implications of the work.

Current Saturation

When crystals of CdS were subjected to pulsed electric fields with magnitudes above a critical value of the order of 10^3 v cm^{-1}, current saturation was observed. Saturation occurred in crystals with conductivities greater than $\sim 10^{-5}$ mho cm^{-1}. To observe the effect, therefore, semi-insulating crystals have to be illuminated to reduce their resistivities to the required magnitude. The onset of current saturation was found to be associated with a build-up of acoustic flux, which was detected at an output transducer.

Effect of Crystal Inhomogeneity

The method of calculating the drift mobility from current saturation requires that the potential distribution along the specimen should be reasonably uniform. Non-uniformity in the sample has been found to lead to a higher critical field E_c and lower apparent drift

mobility. Also the values of E_c in non-uniform samples varied quite strongly with the intensity of incident illumination. In a uniform crystal, however, E_c remained constant in the conductivity range from 10^{-4} to 10^{-2} mho cm^{-1}.

By removing the high resistive end of one of the non-uniform samples we have been able to demonstrate that the variation of E_c with conductivity was caused by the inhomogeneity in the sample.

The Drift Mobility

The measured values of electron drift mobility at room temperature showed good agreement with the values of Hall mobility in the conductivity range from 10^{-4} to 10^{-2} mho cm^{-1}. Irrespective of the orientation of the crystal the drift mobility μ_d was equal to v_s/E_c, where v_s is the appropriate velocity of sound.

The Effect of Traps

The drift mobility measured at lower temperatures was smaller than the Hall mobility. The smaller values of drift mobility at lower temperatures have been interpreted in terms of a trap controlled charge transport process. Information about the position and density of shallow trapping centres has been obtained.

Initially when the temperature variation of $\omega\tau$ was neglected the depth of the dominant trap appeared to vary from 0·0115 to 0·008 eV as the intensity of illumination was increased by an order of magnitude.

However, by considering the temperature dependence of the trapping time τ in the acoustoelectric theory of current saturation and by using the values of drift mobility modified by the factor b, (according to Eqn. 5.10), the existence of two trapping levels with ionisation energies of 0·037 eV and 0·015 eV at densities of $3{\cdot}1 \times 10^{16}\,cm^{-3}$ and $1{\cdot}35 \times 10^{17}\,cm^{-3}$ has been demonstrated.

Further, in order to provide a test for the trapping theory the magnitude of the capture cross-section for electrons of the shallower trap has been calculated. The value obtained namely $6 \times 10^{-16}\,cm^{2}$ verifies the validity of the assumptions used in the trapping theory. The magnitude of the cross-section suggests that singly ionised donors are responsible for these shallow centres.

In our high resistivity crystals the shallow electron traps are probably connected with an almost completely compensated set of donors. These donors could be due to impurities in the starting materials, or alternatively, they might be associated with a definite type of crystal defect caused by non-stoichiometry in the composition of the crystals. A singly ionised sulphur vacancy would be an example of this second possibility.

Photo-Hall measurements made on the same sample indicated the presence of two deeper trapping levels with activation energies of 0·281 eV and 0·362 eV. These deeper traps would have such large values of τ that electrons captured in them would be unable to bunch in the

acoustoelectric field in the time available (i.e. $\frac{1}{\omega}$). With such traps $\omega\tau >> 1$, and under this condition $\mu_d = \mu_H$. The current saturation method, therefore is unable to provide information about deep traps.

The drift mobility experiment at lower temperatures which provides a sensitive means of studying shallow centres, should be used, therefore, as a method complementary to the photo-Hall technique and the TSC method as a means of determining trap parameters.

The Hole Mobility

Cadmium sulphide has always been found to be n-type at room temperature. However the photo-Hall measurements under quenching conditions have demonstrated that the free hole concentration can exceed the free electron concentration under these conditions.

The current voltage characteristics measured under the same conditions have exhibited a second saturation at a field E_c' much higher than E_c. Assuming that the second saturation was due to acoustoelectric interaction with holes a value of the hole drift mobility of 48 $cm^2 v^{-1} sec^{-1}$ was obtained. This is in reasonable agreement with previously published values.

Suggestions for Further Work

In the light of the above results, the following suggestions for future work are made.

As drift mobility experiments at low temperatures provide a sensitive means for studying shallow centres, it would be interesting to extend these measurements to doped specimens or to crystals grown under conditions which produce a known type of defect. Further measurements of similar nature can be extended to other II-VI piezoelectric crystals like CdSe, ZnSe, etc.

As the current saturation experiment under quenching conditions provide the first experimental evidence of the acoustoelectric interaction with minority carriers (holes in CdS), it would be interesting to measure hole mobility in normally n-type II-VI piezoelectric crystals. These measurements could also be performed at different temperatures. (This should provide information concerning the mechanism of hole scattering and information about hole traps).